

University of Alberta

2-D Hydraulic and Ice Process Modeling at Hay River, NWT

by

Michael Gregory Brayall

A thesis submitted to the Faculty of Graduate Studies and Research in partial fulfillment of the requirements for the degree of

Master of Science

in

Water Resources Engineering

Department of Civil and Environmental Engineering

©Michael Gregory Brayall
Spring, 2011
Edmonton, Alberta

Permission is hereby granted to the University of Alberta Libraries to reproduce single copies of this thesis and to lend or sell such copies for private, scholarly or scientific research purposes only. Where the thesis is converted to, or otherwise made available in digital form, the University of Alberta will advise potential users of the thesis of these terms.

The author reserves all other publication and other rights in association with the copyright in the thesis and, except as herein before provided, neither the thesis nor any substantial portion thereof may be printed or otherwise reproduced in any material form whatsoever without the author's prior written permission.

Examining Committee

Faye Hicks, Civil and Environmental Engineering

Peter Steffler, Civil and Environmental Engineering

Carlos Lange, Mechanical Engineering

Abstract

This study was part of the development of an ice jam flood forecasting system for Hay River, NWT. 2-D numerical models were used to simulate ice processes in an effort to predict ice jam formation. A summer survey was conducted to finalize the bathymetry of the Hay River Delta. Observations were undertaken during freeze-up and the winter to better understand Hay River ice conditions. Ice jam events were surveyed during breakup in 2008 and 2009 for model testing. The data collected was used to develop CRISSP2D and River2D models to simulate observed conditions. Simple tests were conducted with CRISSP2D to better understand the model inputs. CRISSP2D modeling of Hay River was unsuccessful and its limitations were discussed. River2D was able to match observed ice jam profiles. The results were used to create an Ice Jam Profile Generator to assist the Town of Hay River with evacuation planning.

Acknowledgements

The author would like to thank Dr. Faye Hicks for all of her support and guidance. Thanks is also extended to Dr. Peter Steffler and Dr. Carlos Lange for being part of the examining committee.

The extensive field program was a joint effort between the University of Alberta and the Department of Indian Affairs and Northern Development (DIAND). A big thanks goes out to the University of Alberta team, comprised of Robyn Andrishak, Chris Krath, Joshua Maxwell, Jennifer Nafziger, Nadia Kovachis, David Watson, Liming Zhao, Janelle Morley, Brett Howard, Gareth Hanna, and Dave Keller. This research project was not possible without your assistance. A special thanks goes to Shawne Kokelj and Meg McCluskie from DIAND for their hard work during spring breakup.

The town of Hay River and the Flood Watch committee played an important role during breakup and a big thanks is in order. A special thanks goes out to the Water Survey of Canada for their hard work. Gratitude is also extended to Dr. Hung Tao Shen for his assistance with the CRISSP2D model.

Funding for this project was provided by Natural Sciences and Engineering Research Council of Canada.

For all their love and encouragement, the author would like to thank his Family and his wife Amanda. This was not possible without you.

Table of Contents

| | | |
|-----|--|----|
| 1.0 | Introduction..... | 1 |
| 1.1 | River Ice Processes | 2 |
| 1.2 | Previous Research..... | 5 |
| 1.3 | Study Objectives | 7 |
| 2.0 | Field Program and Historical Data | 9 |
| 2.1 | Open Water | 9 |
| 2.2 | Freeze-up..... | 12 |
| 2.3 | Winter | 13 |
| 2.4 | Breakup..... | 15 |
| | 2.4.1 Breakup 2008 | 16 |
| | 2.4.2 Breakup 2009 | 17 |
| | 2.4.3 Historical Breakup Data..... | 19 |
| | 2.4.4 Breakup Discharge and Water Elevations | 20 |
| 3.0 | Model Description and Testing..... | 48 |
| 3.1 | CRISSP 2-D..... | 48 |
| | 3.1.1 Hydrodynamic Module | 50 |
| | 3.1.2 Ice Dynamics Module | 53 |
| | 3.1.3 Breakup Module..... | 55 |
| | 3.1.4 Thermal Module..... | 56 |

| | | |
|---------|--|-----|
| 3.2 | River 2-D | 56 |
| 3.3 | Geometry and Computational Mesh | 59 |
| 3.4 | CRISSP2D Model Testing | 61 |
| 3.4.1 | Simple Trapezoidal Channel Model | 62 |
| 3.4.2 | Simple Trapezoidal Channel with a Constriction | 67 |
| 3.4.3 | Discussion of Results | 69 |
| 4.0 | Models' Application to Hay River, NWT | 77 |
| 4.1 | Geometry and Computational Mesh | 78 |
| 4.2 | Open Water Modeling | 79 |
| 4.3 | Ice Cover Modeling | 83 |
| 4.4 | Freeze-up Modeling | 85 |
| 4.5 | Breakup Modeling | 89 |
| 4.5.1 | CRISSP 2-D | 89 |
| 4.5.2 | River 2-D | 96 |
| 4.5.2.1 | Model Setup and Results | 96 |
| 4.5.2.2 | Analysis | 100 |
| 5.0 | Ice Jam Profile Generator | 139 |
| 6.0 | Summary and Recommendations | 157 |
| 7.0 | References | 162 |
| | Appendix A : CRISSP2D Default Model Inputs | 166 |

| | |
|--|-----|
| Appendix B : Ice Jam Profile Predictor Error Results | 171 |
|--|-----|

List of Figures

| | |
|--|----|
| Figure 1.1 Image of a typical ice jam profile (adapted from Ashton, 1986). | 8 |
| Figure 2.1 Contour map of Hay River Delta bathymetry collected during the open water field program..... | 23 |
| Figure 2.2 Map of discharge cross sections measured with an ADCP during the 2007 open water survey. | 23 |
| Figure 2.3 Velocity cross sections obtained from ADCP measurements at cross section 1 (a), 2 (b), 3 (c) and 4 (d). | 24 |
| Figure 2.4 Annotated aerial photograph of the Hay River Delta..... | 25 |
| Figure 2.5 Image showing the juxtaposed ice cover formation in the East Channel during 2008 freeze-up..... | 26 |
| Figure 2.6 Image of the beginning of ice cover formation in the West Channel delta in 2008, looking down the Fishing Village Channel. | 26 |
| Figure 2.7 Image of the East-West Channel split during the 2008 freeze-up..... | 27 |
| Figure 2.8 Image of ice jam in the East Channel on 4-May-08..... | 27 |
| Figure 2.9 Image of the ice jam in the West Channel on 4-May-08..... | 28 |
| Figure 2.10 Image of the ice jam at the mouth of the East Channel on 5-May-08. | 28 |
| Figure 2.11 The top of ice profile in the East Channel on 28-Apr-08..... | 29 |
| Figure 2.12 The top of ice profile of the ice jam in the East Channel on 5-May-08. | 29 |
| Figure 2.13 Maximum top of ice profiles measured on 6-May-08 in the (a) East and (b) Fishing Village Channels. | 30 |

| | |
|---|----|
| Figure 2.14 Image of ice jam in the West Channel on 3-May-09..... | 31 |
| Figure 2.15 Image of ice jam in the East Channel on 3-May-09..... | 31 |
| Figure 2.16 Image of ice jam in the East Channel on 4-May-09..... | 32 |
| Figure 2.17 Image of the ice jam in the West Channel delta on 4-May-09..... | 32 |
| Figure 2.18 Image of the ice jam in the East Channel on 6-May-09..... | 33 |
| Figure 2.19 Image of the ice jam in the West Channel delta on 6-May-09..... | 33 |
| Figure 2.20 The surveyed top of ice profiles from 26-Apr-09 in the (a) East, (b) Fishing Village and (c) Rudd Channels..... | 34 |
| Figure 2.21 The surveyed top of ice profiles from 30-Apr-09 in the (a) East, (b) Fishing Village and (c) Rudd Channels..... | 35 |
| Figure 2.22 The surveyed top of ice profiles from the morning of 3-May-09 in the (a) East, (b) Fishing Village and (c) Rudd Channels..... | 36 |
| Figure 2.23 The surveyed top of ice profiles from the afternoon of 3-May-09 in the (a) East, (b) Fishing Village and (c) Rudd Channels..... | 37 |
| Figure 2.24 The surveyed top of ice profiles from the evening of 3-May-09 in the East Channel..... | 38 |
| Figure 2.25 The surveyed top of ice profiles from the afternoon of 4-May-09 in the (a) East, (b) Fishing Village and (c) Rudd Channels..... | 39 |
| Figure 2.26 The surveyed top of ice profiles from the morning of 5-May-09 in the (a) East, (b) Fishing Village and (c) Rudd Channels..... | 40 |
| Figure 2.27 The surveyed maximum top of ice profiles from the night of 6-May- 09 in the (a) East, (b) Fishing Village and (c) Rudd Channels..... | 41 |

| | |
|---|----|
| Figure 2.28 The surveyed top of ice profiles from the 1963 breakup in the East Channel. | 42 |
| Figure 2.29 The surveyed top of ice profiles from the 1985 breakup in the (a) East, (b) Fishing Village and (c) Rudd Channels. | 43 |
| Figure 2.30 The surveyed top of ice profiles from the 1988 breakup in the (a) East, (b) Fishing Village and (c) Rudd Channels. | 44 |
| Figure 2.31 The surveyed top of ice profiles from the 1989 breakup in the (a) East and (b) Rudd Channels. | 45 |
| Figure 2.32 The surveyed top of ice profiles from the 1990 breakup in the (a) East and (b) Fishing Village Channels. | 46 |
| Figure 2.33 The surveyed top of ice profiles from the 1992 breakup in the (a) East and (b) Fishing Village Channels. | 47 |
| Figure 3.1 Channel cross section of the simple trapezoid channel model. | 71 |
| Figure 3.2 Variation of mean ice discharge with increasing coupling time ratios. | 71 |
| Figure 3.3 Surface ice concentration results with varying coupling time ratios at model time $t = 4800s$ | 72 |
| Figure 3.4 Variation of mean absolute mean difference of the ice discharge from the mean with the coupling time ratio. | 72 |
| Figure 3.5 Variation of average ice discharge with the initial ice parcel size ratio. | 73 |
| Figure 3.6 Variation of mean absolute mean difference of the ice discharge from the mean with the initial ice parcel size ratio. | 73 |

| | |
|--|-----|
| Figure 3.7 Variation of surface ice concentration with the initial ice parcel size ratio at model time $t = 5$ hrs..... | 74 |
| Figure 3.8 Variation of ice thickness and ice concentration with coupling time ratio..... | 75 |
| Figure 3.9: Variation of ice thickness and ice concentration with internal friction angle..... | 76 |
| Figure 4.1: The computational mesh for the River2D and CRISSP2D models of the Hay River..... | 104 |
| Figure 4.2: The computational mesh at the East-West Channel split illustrating techniques used to minimize the number of elements and nodes in the model. | 104 |
| Figure 4.3 Comparison of modeled water surface profiles with surveyed water levels for the a) East and (b) West Channels at a discharge of 160 m^3/s | 105 |
| Figure 4.4 Comparison of modeled water surface profiles with surveyed water levels for the a) East and (b) West Channels at a discharge of 258 m^3/s | 106 |
| Figure 4.5 Sensitivity analysis of bed roughness with River 2-D down the a) East and (b) West Channels..... | 107 |
| Figure 4.6 Comparison of velocity profiles measured in the field and River 2-D model results a) upstream of the split and just downstream of the split in the (b) East and (c) West Channels. | 108 |

| | |
|---|-----|
| Figure 4.7 Comparison of the open water rating curve developed by Gerard and Stanley (1988) with HEC-2 and the open water rating curves developed with River 2-D at three different bed roughness heights. | 109 |
| Figure 4.8 Comparison of channel cross section just upstream of the East-West Channel split from Gerard and Stanley (1988) and Meliefste and Hicks (2006). | 109 |
| Figure 4.9 East-West Channel flow split relationship established using River 2-D at three different bed roughness heights and compared to 2007 discharge measurements. | 110 |
| Figure 4.10 Comparison of ice survey on 28-Apr-08 and CRISSP 2-D model results. | 110 |
| Figure 4.11 Freeze-up modeling results with CRISSP2D Model after 10 minutes model time. | 111 |
| Figure 4.12 CRISSP2D Freeze-up model results after 90 minutes of model time. Ice parcels were injected after 60 minutes of modeling and shown going down the East Channel. | 112 |
| Figure 4.13 CRISSP2D freeze-up modeling results after 270 minutes of model time. | 113 |
| Figure 4.14: A comparison of the surveyed top of ice profiles from 26-Apr-08 and the CRISSP2D freeze-up model profile results in the (a) East, (b) Fishing Village and (c) Rudd Channels. | 114 |

| | |
|--|-----|
| Figure 4.15 CRISSP2D 5-May-08 ice thickness and ice concentration model results without a force ice jam toe location. | 115 |
| Figure 4.16 Comparison of top of ice survey from an ice jam in the East Channel on 5-May-08 and CRISSP 2-D model results..... | 115 |
| Figure 4.17 Comparison of top of ice survey from an ice jam in the East Channel on 3-May-09 and CRISSP 2-D model results..... | 116 |
| Figure 4.18 Comparison of top of ice survey from an ice jam in the East Channel on 4-May-09 and CRISSP 2-D model results..... | 117 |
| Figure 4.19 Comparison of top of ice survey from an ice jam in the East Channel on 5-May-09 and CRISSP 2-D model results..... | 118 |
| Figure 4.20 A comparison of the modeled ice profiles from 5-May-09 for two maximum Manning's n ice roughnesses in the (a) East and (b) Fishing Village Channels..... | 119 |
| Figure 4.21 A comparison of the modeled ice profiles from 5-May-09 for two initial ice parcel sizes in the (a) East and (b) Fishing Village Channels. | 120 |
| Figure 4.22 A comparison of the modeled ice profiles from 5-May-09 for two model coupling times in the (a) East and (b) Fishing Village Channels. | 121 |
| Figure 4.23 A comparison of the modeled ice profiles from 5-May-09 for two internal angles of friction in the (a) East and (b) Fishing Village Channels. | 122 |

| | |
|--|-----|
| Figure 4.24 A comparison of the surveyed top of ice profiles from 1985 and the River 2-D model ice jam profile results in the (a) East, (b) Fishing Village and (c) Rudd Channels..... | 123 |
| Figure 4.25 A comparison of the surveyed top of ice profiles from 1988 and the River 2-D model ice jam profile results in the (a) East, (b) Fishing Village and (c) Rudd Channels..... | 124 |
| Figure 4.26 A comparison of the surveyed top of ice profiles from 1989 and the River 2-D model ice jam profile results in the (a) East, (b) Fishing Village and (c) Rudd Channels..... | 125 |
| Figure 4.27 A comparison of the surveyed top of ice profiles from 1990 and the River 2-D model ice jam profile results in the (a) East, (b) Fishing Village and (c) Rudd Channels..... | 126 |
| Figure 4.28 A comparison of the surveyed top of ice profiles from 1992 and the River 2-D model ice jam profile results in the (a) East, (b) Fishing Village and (c) Rudd Channels..... | 127 |
| Figure 4.29 A comparison of the surveyed top of ice profiles from 5-May-08 and the River 2-D model ice jam profile results in the (a) East, (b) Fishing Village and (c) Rudd Channels..... | 128 |
| Figure 4.30 A comparison of the surveyed top of ice profiles from 6-May-08 and the River 2-D model ice jam profile results in the (a) East, (b) Fishing Village and (c) Rudd Channels..... | 129 |

| | |
|--|-----|
| Figure 4.31 A comparison of the surveyed top of ice profiles from 3-May-09 and the River 2-D model ice jam profile results in the (a) East, (b) Fishing Village and (c) Rudd Channels..... | 130 |
| Figure 4.32 A comparison of the surveyed top of ice profiles from 4-May-09 and the River 2-D model ice jam profile results in the (a) East, (b) Fishing Village and (c) Rudd Channels..... | 131 |
| Figure 4.33 A comparison of the surveyed top of ice profiles from 5-May-09 and the River 2-D model ice jam profile results in the (a) East, (b) Fishing Village and (c) Rudd Channels..... | 132 |
| Figure 4.34 A comparison of the surveyed top of ice profiles from 7-May-09 and the River 2-D model ice jam profile results in the (a) East, (b) Fishing Village and (c) Rudd Channels..... | 133 |
| Figure 4.35 Comparison of the rating curve in Stanley (1988) at the West Channel split (river km 1111.0) and the River2D model results. | 134 |
| Figure 4.36 Comparison of the rating curve in Gerard and Stanley (1988) and discharge measurements in Jasek (1993) to the River2D model results..... | 134 |
| Figure 4.37 Comparisons of rating curve at Island A (river km 1113) from Stanley (1988) for an ice jam at the East Channel mouth and the 2008 and 2009 final ice elevations. | 135 |
| Figure 4.38 Relationship between the total discharge and the percentage going down the East Channel under open water and ice jam conditions. . | 135 |

| | |
|---|-----|
| Figure 4.39 Relationship between the total discharge and the East Channel discharge under open water and ice jam conditions. | 136 |
| Figure 4.40 Relationship between the discharge and the most downstream extent of ice movement in the East Channel. | 136 |
| Figure 4.41 Relationship between the discharge and the most downstream extent of ice movement in the West Channel. | 137 |
| Figure 4.42 Comparison of ice volume estimates on the Hay River before breakup and the ice volume in the final ice jam configuration. | 137 |
| Figure 4.43 An example of stranded ice on an Island from the 2009 breakup of the Hay River. | 138 |
| Figure 5.1 An ice jam rating curve developed from River 2-D modeling results at river km 1107.5. | 144 |
| Figure 5.2 An ice jam rating curve developed from River 2-D modeling results at river km 1108.0. | 144 |
| Figure 5.3 An ice jam rating curve developed from River 2-D modeling results at river km 1108.5 in the East Channel. | 145 |
| Figure 5.4 An ice jam rating curve developed from River 2-D modeling results at river km 1109.0 in the East Channel. | 145 |
| Figure 5.5 An ice jam rating curve developed from River 2-D modeling results at river km 1109.5 in the East Channel. | 145 |
| Figure 5.6 An ice jam rating curve developed from River 2-D modeling results at river km 1110.0 in the East Channel. | 146 |

| | |
|---|-----|
| Figure 5.7 An ice jam rating curve developed from River 2-D modeling results at river km 1110.5 in the East Channel. | 146 |
| Figure 5.8 An ice jam rating curve developed from River 2-D modeling results at river km 1111.0 in the East Channel. | 146 |
| Figure 5.9 An ice jam rating curve developed from River 2-D modeling results at river km 1111.5 in the East Channel. | 147 |
| Figure 5.10 An ice jam rating curve developed from River 2-D modeling results at river km 1112.0 in the East Channel. | 147 |
| Figure 5.11 An ice jam rating curve developed from River 2-D modeling results at river km 1112.5 in the East Channel. | 147 |
| Figure 5.12 An ice jam rating curve developed from River 2-D modeling results at river km 1113.0 in the East Channel. | 148 |
| Figure 5.13 An ice jam rating curve developed from River 2-D modeling results at river km 1113.5 in the East Channel. | 148 |
| Figure 5.14 An ice jam rating curve developed from River 2-D modeling results at river km 1108.5 in the West Channel. | 148 |
| Figure 5.15 An ice jam rating curve developed from River 2-D modeling results at river km 1109.0 in the West Channel. | 149 |
| Figure 5.16 An ice jam rating curve developed from River 2-D modeling results at river km 1109.5 in the West Channel. | 149 |
| Figure 5.17 An ice jam rating curve developed from River 2-D modeling results at river km 1110.0 in the West Channel. | 149 |

| | |
|--|-----|
| Figure 5.18 An ice jam rating curve developed from River 2-D modeling results at river km 1110.5 in the West Channel. | 150 |
| Figure 5.19 An ice jam rating curve developed from River 2-D modeling results at river km 1111.0 in the West Channel. | 150 |
| Figure 5.20 An ice jam rating curve developed from River 2-D modeling results at river km 1111.5 in the West Channel. | 150 |
| Figure 4.64 An ice jam rating curve developed from River 2-D modeling results at river km 1112.0 in the West Channel. | 151 |
| Figure 5.22 An ice jam rating curve developed from River 2-D modeling results at river km 1112.5 in the West Channel. | 151 |
| Figure 5.23 Comparison of ice jam survey data from 1985 and the ice surface profile from the Ice Jam Profile Generator in the (a) East and (b) West Channels. | 152 |
| Figure 4.24 Comparison of ice jam survey data from 1990 and the ice surface profile from the Ice Jam Profile Generator in the (a) East and (b) West Channels. | 153 |
| Figure 5.25 Comparison of ice jam survey data from 6-May-08 and the ice surface profile from the Ice Jam Profile Generator in the (a) East and (b) West Channels. | 154 |
| Figure 5.26 Ice jam profile plot at a discharge of 600 m ³ /s highlighting key elevations in the (a) East and (b) West Channels. | 155 |
| Figure 5.27 Ice jam profile plot at a discharge of 600 m ³ /s highlighting key elevations in the mouth of the East Channel. | 156 |

List of Tables

| | |
|--|----|
| Table 2.1 ADCP measurements from 27-Jul-2007 in the Hay River delta. | 12 |
| Table 2.2 Upstream and downstream boundary conditions for the two dimensional model runs. | 22 |
| Table 3.1 Summary of the analyzed simple trapezoidal channel tests. | 64 |
| Table 3.2 Summary of the simple trapezoidal channel with a constriction model tests. | 68 |
| Table 4.1 Intact ice cover results for a range of inflow discharges and ice roughness values. | 85 |
| Table 4.2 CRISSP2D model input values for freeze-up modeling. | 87 |
| Table 4.3 CRISSP2D model input values for breakup modeling. | 90 |
| Table 4.4 Summary of CRISSP2D ice input conditions and model run results. .. | 94 |
| Table 4.5 Summary of River2D model run ice inputs and the corresponding top of ice profile figure numbers. | 99 |

List of Symbols

H = total water depth (m)

η = water surface elevation (m)

q_{tx} = total unit discharge in x direction (m^2/s)

q_{ty} = total unit discharge in y direction (m^2/s)

N = ice concentration

t_s = submerged ice thickness (m)

H_t = water depth underneath ice water interface, adjusted from the real ice-water interface to include water flow between particles (m)

ρ = water density (kg/m^3)

τ_{sx} = shear stress in the x-direction at the ice-water interface (N/m^2)

τ_{sy} = shear stress in the y-direction at the ice-water interface (N/m^2)

τ_{bx} = shear stress in the x-direction at the water-bed interface (N/m^2)

τ_{by} = shear stress in the y-direction at the water-bed interface (N/m^2)

g = acceleration due to gravity (m^2/s)

$\frac{D\vec{V}_i}{Dt}$ = acceleration of ice parcels (m^2/s)

\vec{V}_i = ice velocity (m/s)

M_i = ice mass per unit area (kg/m^2)

\vec{R} = internal ice resistance (Pa)

\vec{F}_a = wind drag force (Pa)

\vec{F}_w = water drag force (Pa)

\vec{G} = gravitational force (Pa)

q_{lx} = unit discharge in x direction beneath the ice (m^2/s)

q_{ly} = unit discharge in y direction beneath the ice (m^2/s)

D = flow depth beneath the ice (m)

t_s = submerged ice thickness (m)

S_{0x} = bed slope in the x direction (m/m)

S_{0y} = bed slope in the y direction (m/m)

S_{fx} = friction slope in the x direction (m/m)

S_{fy} = friction slope in the y direction (m/m)

ρ = water density (kg/m^3)

τ_{lxx} = xx component of turbulent stress tensor ()

τ_{lxy} = xy component of turbulent stress tensor ()

τ_{lyy} = yy component of turbulent stress tensor ()

1.0 Introduction¹

Each spring, rivers in northern latitudes experience ice breakup as daylight hours lengthen and temperatures increase. River ice removal can vary from the gradual deterioration of the ice cover in a thermal breakup, to a rapid release of the intact ice during a dynamic breakup. Dynamic ice breakup can happen very quickly and can involve the formation and release of ice jams resulting in rapidly rising water levels. For instance, Hutchison and Hicks (2007) documented a 4.3 m water level increase during an ice jam release event on the Athabasca River, with a maximum rate of rise above 0.8 m/min. For populated areas along rivers that experience dynamic ice breakup, this poses a major challenge to local officials developing evacuation protocols. Residents have very little notice to evacuate and the risk of property damage and loss of life can be very high.

The town of Hay River is an example of a community threatened by ice jam flooding each spring. It is located along the banks of the Hay River as it enters Great Slave Lake, forming a delta with two main channels. Each spring, breakup upstream is comprised of a series of ice jam formation and release events. The ice runs bring significant volumes of ice into the delta that stops against the intact ice of Great Slave Lake. In the past, this has caused large ice jams and flooded portions of the community. Recent examples of this were observed in 2003 and 2008 and illustrate the importance of a flood evacuation plan for the community.

¹ A version of this chapter describing the town of Hay River has been published as a conference paper entitled "2-D Modeling of Ice Processes on the Hay River NWT" by Michael Brayall and Faye Hicks for the 15th Workshop on River Ice in St. John's Newfoundland and Labrador, June 15-17, 2009.

Extensive research of the river ice breakup on the Hay River has been done to assist the community with understanding the breakup process. A key component of an evacuation plan is the ability to predict where an ice jam could form and the maximum water elevation expected. Numerical models have been developed to assist with ice jam prediction. One dimensional ice jam models have been used in past research to determine the potential maximum water elevation. These models have limitations in the Hay River delta though because they are unable to resolve the flow split between the East and West Channels. In recent years, two dimensional ice models have been developed and offer the potential to more accurately model past ice jams and to predict the occurrence of future ice jams.

1.1 River Ice Processes

An understanding of river ice processes is important to accurately predict ice jam formation. Generally, there are three phases to the ice regime of rivers in northern climates. The phases are ice cover formation, ice cover growth and ice cover removal. This section provides a general overview of each phase.

Ice cover formation begins each year when air temperatures decrease and supercool the water temperature a few hundredths of degrees below zero. Two types of ice begin to form: border ice and frazil ice. Border ice grows horizontally out from the banks in regions with very low vertical turbulence. Once the surface is covered in border ice no additional supercooling occurs. The thickness increases as it is cooled by the air and the banks. The second type of ice are tiny ice particles, known as frazil ice, that form in the fast flow of the river

where the turbulence is high and the water column is well mixed. They are usually shaped as small discs, but needles have also been observed. Frazil particles readily adhere to each other and form frazil flocs. Frazil flocs remain in suspension until they grow large enough for buoyancy to overcome the vertical turbulence of the flow. The flocs rise to the water surface and form frazil pans. Frazil pans increase in size and thickness as additional frazil flocs rise and adhere to the edges and bottom. As the surface ice concentration increases, frazil pans come into contact, freeze together and form ice rafts.

Surface ice concentration increases from both border ice and frazil pans until bridging occurs. Bridging is when ice movement stops due to congestion of surface ice. It typically occurs in areas where the open water area constricts either due to the natural channel shape or due to border ice growth. Incoming ice pans can accumulate at the upstream edge and form a stationary ice cover. This is called a juxtaposed ice cover. If the velocity is high enough, ice pans are swept beneath the stationary cover in a process called hydraulic thickening. As the length of the accumulation increases, the force acting on it does as well. If the combination of the force of the accumulated mass and the drag of the water underneath overcome the internal strength of the cover, it can collapse. This is known as a hummocky ice cover and is thicker than a juxtaposed cover.

Once a stable ice cover forms during freeze-up, ice growth will continue throughout the winter. Subzero air temperatures cause the ice sheet to thermally thicken downward. Growth on the top of the ice sheet can occur in several manners. Snow ice is formed when snow collects on the surface and the snow

mass causes the ice surface to be inundated, flooding the ice sheet. Aufeis is another type of ice accumulation that forms when water flows on top of the ice. This occurs when the main flow channel becomes obstructed by the ice sheet or when there is a ground water spring. The ice freezes in successive layers and can form substantial accumulations.

In the spring the ice cover begins to deteriorate due to above zero temperatures and increased solar radiation. The ice cover can either undergo a thermal or a dynamic breakup. A thermal breakup is when the ice cover deteriorates in place. It generally happens when the air temperature rises gradually and snowmelt runoff takes place over a drawn out timeframe. A dynamic breakup occurs when the ice sheet is fractured into distinct sheets by an increase in water level. The water level increase can be triggered by a rapid increase in river flow or by an ice jam release event upstream or a combination of both. Dynamic breakup is generally associated with rapid increases in air temperature and a steep runoff hydrograph. Spring rainfall can also contribute to a dynamic breakup.

Eventually, through a combination of increasing water levels and decreasing discrete ice sheet dimensions, the ice cover breaks free from the geometric constraints of the channel banks and moves downstream with the flow. The ice run will continue downstream until it encounters a new geometric constraint or a strong intact ice cover. The ice run will then accumulate into an ice jam, reducing the flow capacity of the channel and raises water levels upstream. Ice runs from upstream collect in the ice jam, increasing its length and mass. If the combination of ice mass and water mass overcomes internal strength of the ice jam, it

collapses. The thicker ice jam reduces the channel flow capacity and increases the upstream water level. Often the geometric constraints holding the jam in place will fail beneath the mass of water and ice and the jam will release into an ice run again. This process continues until all ice has been melted to a point where it has no internal strength and collapses.

An ice jam is composed of three regions. Figure 1.1 shows the typical ice jam profile and labels the three regions. The ice jam toe is the most downstream region of the ice jam and develops when an ice run encounters a strong intact ice cover or a geometric constraint. Ice accumulations are typically the thickest in the jam toe. The ice jam toe can either be floating, grounded to the bed, or a blend of both. The water surface slope is highest in the ice jam toe region. If the ice jam is long enough to develop uniform flow underneath, it transitions upstream from the toe region to the equilibrium region. The ice thickness in the equilibrium region is constant and the water surface slope is equal to the bed slope. The region upstream of the equilibrium region is the transition to the jam head. The ice jam thickness gradually decreases to a minimum defined by the ice floe sizes and the flow hydraulics. If the ice jam is not long enough to develop the equilibrium region, the ice jam proceeds gradually from the toe region to the head region.

1.2 Previous Research

The breakup of the Hay River has always been an important event and has been documented since 1893 (Stanley et al., 1959). The first report was Stanley et al.

(1959) and documented the several breakups in the 1950s and presenting flood mitigation concepts. Numerous breakup reports were completed through the years, generally in response to major flood events. Major break events are documented in Stanley et al. (1963), UMA (1978), Jasper (1983), Wedel (1985), Gerard and Stanley (1988), Gerard and Jasek (1990) and Jasek et al. (1993). No breakup reports have been published since. Monitoring was continued by the University of Alberta from 2003 – 2010.

The ability to forecast an ice jam flood has been a key area of research. Wedel (1985) discussed the need for flood forecasting and discussed the challenges of the task. The factors that contribute to breakup flooding were discussed and several indicators were identified for measurement to assist with forecasting. Gerard and Stanley (1988) presented a flood forecasting algorithm and tested it on the breakup from 1988. The algorithm was used in 1989 and its effectiveness was evaluated in Gerard and Jasek (1990). One of the major flaws present in the algorithm was the inability to predict when an ice jam would push to the mouth of the East Channel. This was identified by Gerard and Jasek to be the worst ice jam configurations, as seen in 1963 (Stanley, 1963). Breakup monitoring by the University of Alberta since 2003 was aimed at improving the accuracy and the usability of the flood forecasting algorithm.

Ice jam computer models have been developed in the past and used to assist the town of Hay River with ice jam flood forecasting. Wiens (1983) used HEC-2 to model a 1:100 yr ice jam event at the mouth of the East and West Channels. The model was used to define the flood lines and the floodway for the town council.

Flato and Gerard (1986) developed a new river ice jam model called ICEJAM and it was used by Stanley (1988) to model ice jams from 1987 and 1988. The model results were used by Gerard and Stanley (1988) to develop the first flood forecasting algorithm. Gerard et al. (1990) identified that surge waves from upstream ice jam releases had an effect on ice jam stability in the delta and should be included in the forecasting algorithm. Research on surges was continued by Hicks et al. (1992). An error was found in the discharge measurements from 1985-1989 by the Water Survey of Canada in 1993. Jasek (1993) presented this error and compared it to the work in Stanley (1988) and found that the models would have to be re-calibrated with the updated discharge measurements.

1.3 Study Objectives

The primary objective of the study was to determine whether two dimensional numerical models could be used as an evacuation planning tool to predict ice jam formation, ice movement and subsequent water elevations in the Hay River delta. It was part of a larger study aimed at developing a flood forecasting system for the town of Hay River. An extensive field monitoring program was undertaken to gather data to develop the models and to document breakup of the Hay River. Two dimensional model runs of the Hay River delta were developed using River2D and CRISSP2D modeling programs. The models were used to simulate measured ice jams in the delta. The results were compared and the applicability of each model for ice jam flood forecasting was discussed.

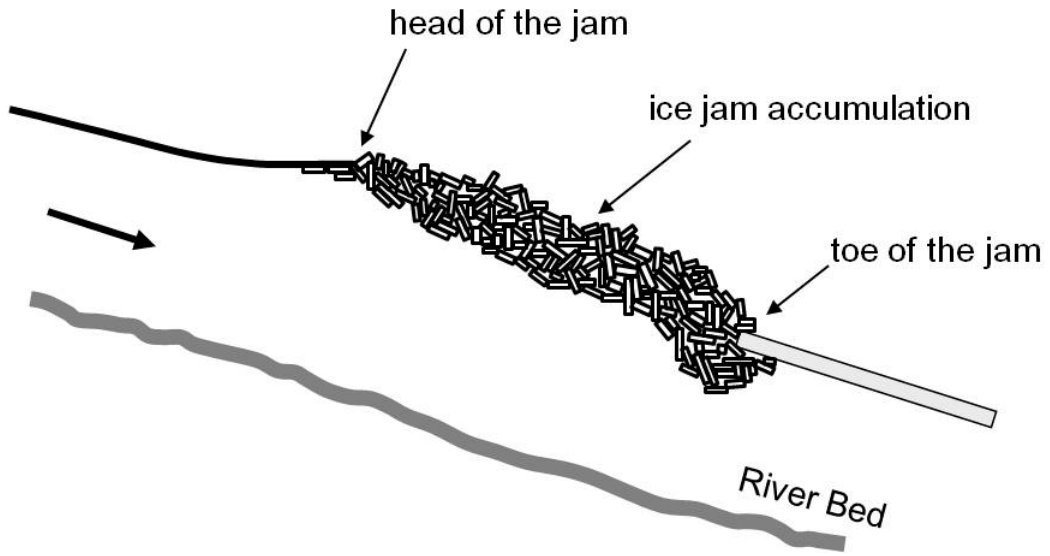


Figure 1.1 Image of a typical ice jam profile (adapted from Ashton, 1986).

2.0 Field Program and Historical Data

The development of a two dimensional hydraulic model required a large quantity of field data. Data collected for the study was obtained as part of an ice jam flood forecasting system being developed for the town of Hay River. Three open water field programs were undertaken to measure the bathymetry of the Hay River delta and to obtain water level data for the calibration of the bed roughness. Freeze-up observations were conducted in the fall of 2008 to better understand ice cover formation and gather qualitative data for model validation. In 2009, a winter survey was conducted to measure ice thicknesses and to measure the winter discharge. Breakup data was available from two sources. Breakup monitoring programs were conducted in 2008 and 2009. The progression of breakup was documented with aerial photography and top of ice profiles. Additional historic breakup data was compiled from past research reports. This chapter documents the results for each field program and summarizes the important historical data.

2.1 Open Water

Summer research programs were conducted in 2005, 2007 and 2008 to measure data under open water flow conditions. The important data that was obtained from the summer research program were water flow velocities, discharge measurements, water levels and bathymetry data. Each piece of data is important for understanding the flow regime and for developing two dimensional flow models under both open water and ice affected scenarios. A good understanding of the flow regime is important for interpreting results and aids in model calibration.

To develop a two dimensional hydraulic model a river bathymetry survey was conducted in three phases. Figure 2.1 shows the river bathymetry obtained from the summer research programs and displays the river distance down both the East and West Channels. Phase 1 of the survey program was documented in Meliefste and Hicks (2006). In phase 1 (August 2005), bed and bank data was collected from river kilometer 1107.0 to 1112.2 in the East Channel and to 1111.0 in the West Channel. The remaining stretches of each channel out to Great Slave Lake were surveyed in phase 2 (July 2007). Additional bathymetry data was collected in the area around the West Channel Bridge (km 1108.1 to 1108.6) in phase 3 (September 2008).

Different survey equipment was used during phase 1 and phase 2 and 3. An OHMEX SonarLite 2000 depth sounder was used to collect water depths for each phase of the survey. Two different positing methods were used during the bathymetric surveys. For Phase 1, a Lecia TPS 1200 robotic total station was employed to track a boat mounted prism. In Phase 2 and 3, a Trimble Real Time Kinematic Global Positioning System (RTK GPS) was used to track the boat's coordinate. The river bank survey was completed using a Sokkia Powerset Series total station in Phase 1 and the RTK GPS in Phase 2 and 3. The water surface profile was obtained from the vertical position of the boat.

There were three reasons for the switch from a total station based survey to a RTK GPS survey. Both systems require a base point over a known location, but the RTK GPS has a larger operational radius. The robotic total station also requires visual sight lines from the total station while the RTK GPS uses a radio

signal for communication. Therefore the RTK GPS is a more flexible survey tool. The last reason for the switch is that the RTK GPS was found to have better vertical accuracy than the robotic total station.

Discharge measurements and velocity cross sections were obtained during the 2007 summer survey to understand the flow distribution through the Hay River delta. The measurements were done using an Acoustic Doppler Current Profiler (ADCP). An ADCP measures the water velocity using a physical principle called the Doppler shift. It has the ability to take single panel velocities or to measure continuous velocity profiles across the channel width. From the velocity profile measurements, the ADCP software is able to calculate the discharge across the section. A total of six ADCP passes were done at each site to ensure the accuracy of the discharge measurement. Six cross sections were completed and the locations are shown in Figure 2.2. The discharge in the Hay River on July 27, 2007 was measured by Water Survey of Canada and was $254 \text{ m}^3/\text{s}$. The river discharge, based on the WSC measurements on July 26, 27, and 28, was decreasing an average of $0.3 \text{ m}^3/\text{s}$ every hour. Such a small change in the discharge is imperceptible over the twelve hours of ADCP measurements.

Each ADCP pass provided a velocity cross section that was important for calibration of the model. Figure 2.3 shows the average velocity cross section measurements at sites 1 through 4. Velocity cross sections were not available at site 5 and 6 because the signal from the RTK GPS was lost. The measured discharges at each site are provided in Table 2.1. The main channel discharge from cross section 1 is than the WSC measurement by 4%. The discharge

measurements have good closure when comparing cross section 1 with the sum of cross sections 2 and 3. The closure is also good when comparing cross section 3 with the sum of cross sections 5 and 6. The closure is not quite as good when comparing cross section 2 with cross section 4. This error is most likely caused by the low velocities experienced at cross section 4 caused by its proximity to Great Slave Lake. ADCPs have difficulty resolving velocities near to zero.

Table 2.1 ADCP measurements from 27-Jul-2007 in the Hay River delta.

| ADCP Measurement Cross Sections | Discharge (m ³ /s) |
|---------------------------------|-------------------------------|
| 1 | 245 |
| 2 | 195 |
| 3 | 49 |
| 4 | 180 |
| 5 | 24 |
| 6 | 25 |

2.2 Freeze-up

Freeze-up monitoring was conducted on 28-Oct-08 to better understand the ice cover formation process to assist with model development, calibration and interpretation. Observations were conducted from several key sites on the ground and with aerial observations. The discharge of the Hay River on the day of freeze-up observations was obtained from the Water Survey of Canada gauge located upstream and it was 140 m³/s. The water surface elevation of Great Slave Lake was 156.834m, also obtained from a Water Survey of Canada gauge.

Freeze-up began with the formation of thermal ice across the channel width in the downstream reaches of both the East and West Channels. Figure 2.5 shows

border ice began at approximately river km 1111 in the East Channel and it extended downstream to Great Slave Lake. Also shown in Figure 2.5 is the development of a juxtaposed ice cover from ice pans generated upstream. The ice pans can be identified by the white colour, while the thermal ice is much darker. The ice pans lose momentum and are stopped by the thermal ice. Thermal ice in the West Channel was observed starting at around river km 1112, shown in Figure 2.6, past the West Channel Fishing Village to Great Slave Lake. Incoming ice pans in the West Channel fill the Fishing Village Channel first, forming a juxtaposed cover and then pans are forced down the Rudd Channel onto Great Slave Lake. Figure 2.7 shows the East-West Channel split. Incoming ice pans fill the East Channel first and are forced down the West Channel. Targets were setup at the East-West Channel split to facilitate an ice pan particle tracking analysis from the air. No analysis has been completed at this time, but this technique could be used in the future to calculate ice pan velocities from the air.

2.3 Winter

To document winter ice conditions in the Hay River delta, a survey was conducted in March 2008. The two objectives were to measure ice and snow thickness and measure the winter discharge in the East and West Channels. The plan was to measure several discharge cross sections, similar to the summer measurements. Problems were encountered measuring each discharge cross section. The air temperature was below -20°C , making the ice very strong and difficult to drill through, limiting the speed of work. As well, a large percentage of the ice is grounded to the bed in March due to low discharge. Water survey of

Canada reported that the discharge was less than $10 \text{ m}^3/\text{s}$. The bed material is composed of sand and gravel and allows subsurface flow. As a result it was very difficult to find holes that contained enough water depth for velocity measurements.

The cross section that was completed was located in the East Channel, approximately 100 m downstream of the East-West Channel split. A total of 16 holes were drilled. The data that was collected in each hole included the water depth below the ice, the ice thickness, the snow depth and the velocity profile. Water depth was measured using a survey rod. Some difficulty was encountered at this site differentiating between the ice and snow due to heavy snowmobile traffic and they were measured together. The velocity profile was measured with an Acoustic Doppler Profiler (ADP). It operates in the same manner as an ADCP but can only do single panel measurements. The reason an ADP was used instead of the ADCP was because the ADP does not require a continuous computer connection to operate in the field. This is one of the draw backs of the ADCP for winter field work as battery life of a laptop can be an issue in the cold. A precise discharge was difficult to deduce from the ADP measurements as the measured velocities were near zero.

An attempt was made to measure a velocity cross section in the West Channel. Two attempts were made to drill holes through the ice at different locations in the cross section but were unable to break through the ice to water. The holes drilled in the ice were greater than one meter deep. Due to time constraints of the survey and the difficulty encountered with drilling the holes, this cross section was

abandoned. The depth of the drilled holes matches observations by University of Alberta researchers in 2007. They found that the ice in the West Channel freezes to the bed during the winter months. As a result, water typically flows overtop of ice in the West Channel in the early days of each breakup.

2.4 Breakup

Breakup monitoring programs were conducted in 2008 and 2009 to obtain data for ice jam modeling. Generally speaking, the data required to model an ice jam is the inflow discharge, the ice surface elevation profile along the model reach and the ice jam thickness. The inflow discharge is required as the upstream boundary condition and the water elevation is required as the downstream boundary condition. Discharge measurements at breakup were available at two sites, depending on the local ice conditions. The ice surface profiles are required to calibrate the ice roughness and to validate the model results. Ice surface profiles were measured using an RTK GPS. Aerial observations were conducted to document the locations of ice jams in the delta for modeling and to identify incoming ice runs from upstream. These observations helped to locate ice jam toe locations when access was either impossible or unsafe and helped document the extent of flooding. Figure 2.4 is an annotated aerial photograph of the Hay River delta and assists with describing the events that occurred during the 2008 and 2009 breakups.

Ice jam thickness is also a data requirement for an ice jam model. Measuring the thickness of an ice jam is very difficult though. For a breakup ice jam, two

methods are available to estimate the ice jam thickness. The first is to measure the height of the shear wall after the ice jam has cleared. The shear wall is the cliff of grounded ice rubble left stranded in shallow flow areas after the ice jam has cleared and water levels have receded. Shear wall measurements can be very dangerous though as it requires a person to walk out onto the unstable ice rubble. As well, it only provides an estimate of the ice jam thickness along the banks and does not necessarily provide the ice jam thickness in the main channel. A second method to measure the ice jam thickness is documented in Beltaos et al. (1996). A remote probe was used to measure a profile of the bottom of the ice relative to the water surface. This method is very cost prohibitive because the odds of recovering the probe are very low. The difficulty encountered when determining the ice jam thickness means it is often estimated iteratively until the model results match the observed top of ice profile.

2.4.1 Breakup 2008

Ice movement was first observed in the delta in the evening of 4-May and continued until the next morning when a jam formed in the East Channel at river km 1111 (Figure 2.8). An ice jam formed in the West Channel at approximately the same time up against the intact lake ice (Figure 2.9). At 20:10 on 5-May, the intact ice downstream of the jam at river km 1111 in the East Channel released, creating a jam at the mouth of the East Channel (Figure 2.10). The ice jam resulted in severe flooding for residents and businesses on both Vale Island, as well as in the Old Village on the Kátl`odeeche First Nation reserve. Large ice pieces knocked down power lines and the Anglican Church was pushed off of its

foundation. Local residents of the reserve were stranded for several hours and a state of emergency was called by Hay River officials.

Three top of ice profile surveys were completed in 2008. The first was done on 28-Apr before appreciable runoff had occurred. It is shown in Figure 2.11 and is a good indicator of the freeze-up stage. It was also very important for calibrating the intact ice roughness for modeling. On 5-May, an ice jam profile was measured down the East Channel and is shown in Figure 2.12. The second ice jam profile was done on 6-May and included the East and Fishing Village Channels. The profile is shown in Figure 2.13. These profiles assisted with both CRISSP 2-D and River 2-D modeling of the events.

2.4.2 Breakup 2009

Ice began moving in the Hay River at around 02:00 on 3-May and quickly formed an ice jam. The ice jam experienced several brief consolidation events during the early morning lasting no longer than ten minutes but remained in place. The ice jam released at 11:35 and the majority of the ice travelled down the West Channel and stopped at 12:55. The ice jam toe in the West Channel, seen in Figure 2.14, was just beyond river km 1110. The East Channel jam had toed out at river km 1110.5 shown in Figure 2.15. Ice movement began again at 21:02 in the West Channel and the head of the ice jam passed the East-West Channel split at 21:35. The ice jam consolidation came to a stop soon after. 4-May saw several consolidation events down both the East and West Channels. A flight was conducted on 4-May in the afternoon to document the ice jams in the delta and to

identify ice conditions upstream. Figure 2.16 shows the ice jam toe in the East Channel on 4-May. Comparing Figure 2.16 to Figure 2.15 from 3-May, the toe location has moved very little. Figure 2.17 shows the extent of ice movement in the West Channel delta. The jam toe in the Rudd Channel was at river km 1111.7 and at river km 1112.5 in the Fishing Village Channel. A large volume of the ice went out the Island Channel onto Great Slave Lake. Intermittent ice movement continued into the morning of 5-May and stopped at around 06:00. No more movement occurred that day. Figure 2.18 shows how the ice movement on 5-May pushed down the west side of Island B in the East Channel and toed out at river km 1112.0. Ice jam toes in the Rudd and Fishing Village Channel remained in place on 5-May. Ice movement began again in the delta at around 05:00 on 6-May with intermittent starting and stopping all day. Figure 2.19 shows the final location of the jam toe in the Fishing Village Channel at river km 1112.8. The final position of the jam toe in the East Channel was at the river mouth. This caused moderate flooding along the west banks of the East Channel in the Old Town.

Eight top of ice jam profiles were measured, documenting the breakup progression in the East, Fishing Village and Rudd Channels. The first profile was measured on 26-Apr and is shown in Figure 2.20. Very little runoff had occurred at the time of the first measurement and the top of ice levels were indicative of the freeze-up stage. Figure 2.21 shows the profile taken on 30-Apr before breakup had begun. Three profiles were measured on 3-May in the morning, afternoon and evening. They are shown in Figure 2.22 to Figure 2.24. Figure 2.22 and

Figure 2.23 contain profiles of all three channels while the third profile in Figure 2.24 was limited to only the ice jam toe in the East Channel due to ice movement. The next profile was completed in the afternoon of 4-May and is shown in Figure 2.25. Figure 2.26 shows the profile that was collected in the morning of 5-May. The final profile was collected on 7-May and documented maximum water and ice levels achieved the night of 6-May. It is shown in Figure 2.27.

2.4.3 Historical Breakup Data

The long record of observation of Hay River provides knowledge of common ice jam locations for modeling. In the East Channel, runs push to approximately river km 1111 before stopping and forming an ice jam. This is because at this location the channel depth increases and the flow velocity subsequently decreases.

Without the drag force from the water velocity, ice runs are unable to push further downstream. Severe flooding has historically occurred when East Channel ice jams form downstream of river km 1111. Examples of this were seen in 1963, 2008, and 2009; however, there is currently no model for predicting when this might be expected. Ice jams in the West Channel typically form in the Fishing Village and the Rudd Channels. Ice jams in the Fishing Village Channel can cause flooding; although there is a dike along this channel, flow can escape around the end and run along the “oxbow” channel flooding areas in behind the dike. If ice pushes through to the lake directly, or escapes across the Island Channel, then flooding is mitigated.

The historical record of ice jam events was an important source for model inputs. A record of ice jam profiles was compiled in Jasek et al. (1993). Figure 2.28 through Figure 2.33 present the documented breakup top of ice profiles for 1963, 1985, 1988, 1989, 1990, and 1992 respectively.

2.4.4 Breakup Discharge and Water Elevations

Each ice jam model run requires an upstream and a downstream boundary condition corresponding to the time of the surveyed top of ice profile. The upstream boundary condition is the river discharge. Two gauges are available for discharge measurements during breakup. They are the WSC gauge at Hay River and the Emergency Measures Organization (EMO) gauge at Alexandra Falls. If the WSC gauge was free of ice effects, then it was used to determine the discharge at the time of the survey. If the WSC gauge was experiencing ice effects, the EMO gauge was used. River 1-D modeling done by Watson (2011) determined a travel time of approximately 9 hours between the gauge and town.

The discharge for the historical ice jams was obtained from Jasek (1993) who corrected an apparent error in discharge measurements from 1985-1989. The discharge measurements were reduced by almost 20%. WSC has recently disputed the correction in Jasek (1993). Unfortunately, at the time of the work in this thesis, an answer to the dispute had not been found yet. Table 2.2 documents the discharge for each top of ice profile and how it was determined.

The delta has four outflow channels into Great Slave Lake that make up the downstream boundary conditions. They are the Fishing Village, Rudd and Island

Channels in the West Channel Delta and the East Channel. Water elevation measurements are impossible to conduct in the Island Channel during breakup so it was assumed to have the same elevation as the Rudd Channel. The water elevation was estimated at each outflow boundary from the most downstream survey point in each channel. Several different downstream boundary condition scenarios were used, depending on available data. Ideally, ice profile data existed in the East, Rudd and Fishing Village Channels. Unfortunately, in some years, profile data was only available in either the Rudd Channel or the Fishing Village Channel. In this scenario, the water level was assumed to be the same in both channels. Table 2.2 presents the downstream boundary elevations and how they were determined.

Table 2.2 Upstream and downstream boundary conditions for the two dimensional model runs.

| # | Date | Discharge (m ³ /s) | Discharge Type ² | Downstream Boundary Elevation (m) | | | Boundary Condition Type ³ |
|----|-----------|----------------------------------|--------------------------------|-----------------------------------|-----------------|--------|---|
| | | | | East | Fishing Village | Rudd | |
| 1 | 1985 | 1000 | 1 | 158.05 | 159.85 | 160.37 | 1 |
| 2 | 27-Apr-88 | 605 | 1 | 156.68 | 157.012 | | 1 |
| 3 | 6-May-89 | 900 | 1 | 157.288 | 159.259 | | 3 |
| 4 | 28-Apr-90 | 560 | 1 | 156.8 | 156.93 | | 2 |
| 5 | 28-Apr-92 | 900 | 1 | 157.1 | 158.21 | | 2 |
| 6 | 5-May-08 | 500 | 2 | 156.62 | 158.61 | | 2 |
| 7 | 6-May-08 | 893 | 1 | 158.65 | 158.61 | | 2 |
| 8 | 3-May-09 | 268 | 2 | 156.52 | | | 1 |
| 9 | 4-May-09 | 500 | 2 | 156.56 | 156.82 | 157.6 | 1 |
| 10 | 5-May-09 | 670 | 1 | 156.73 | 156.97 | 157.6 | 2 |
| 11 | 7-May-09 | 900 | 1 | 158.5 | 158.06 | 159.32 | 1 |

22

² Type 1 discharges are from the Water Survey of Canada gauge

Type 2 discharges are from the Alexandra Falls gauge, lagged by 9 hours

³ Boundary Condition Type 1 is when profile data was available in the East, Rudd and Fishing Village Channels

Boundary Condition Type 2 is when profile data was available in the East and Fishing Village Channels

Boundary Condition Type 3 is when profile data was available in the East and Rudd Channel

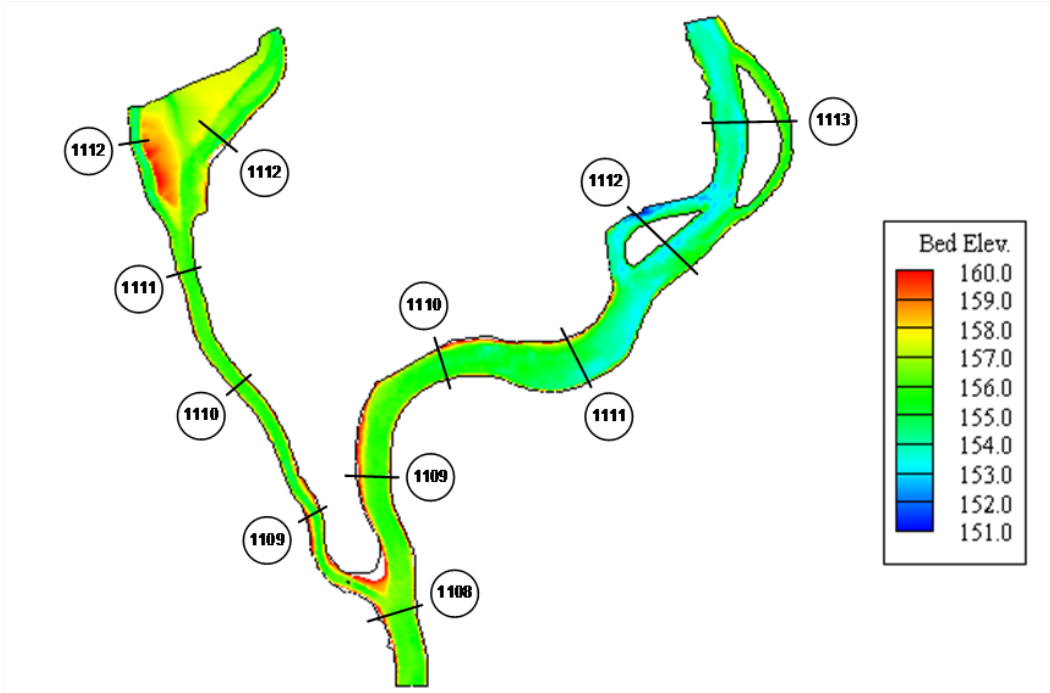


Figure 2.1 Contour map of Hay River Delta bathymetry collected during the open water field program.

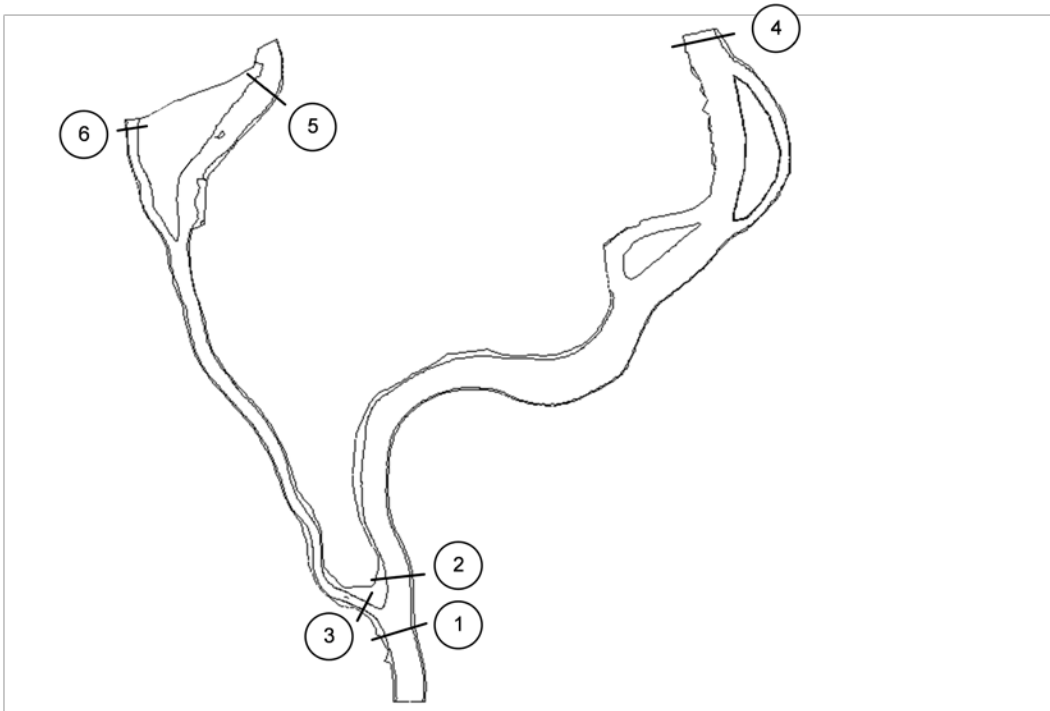


Figure 2.2 Map of discharge cross sections measured with an ADCP during the 2007 open water survey.

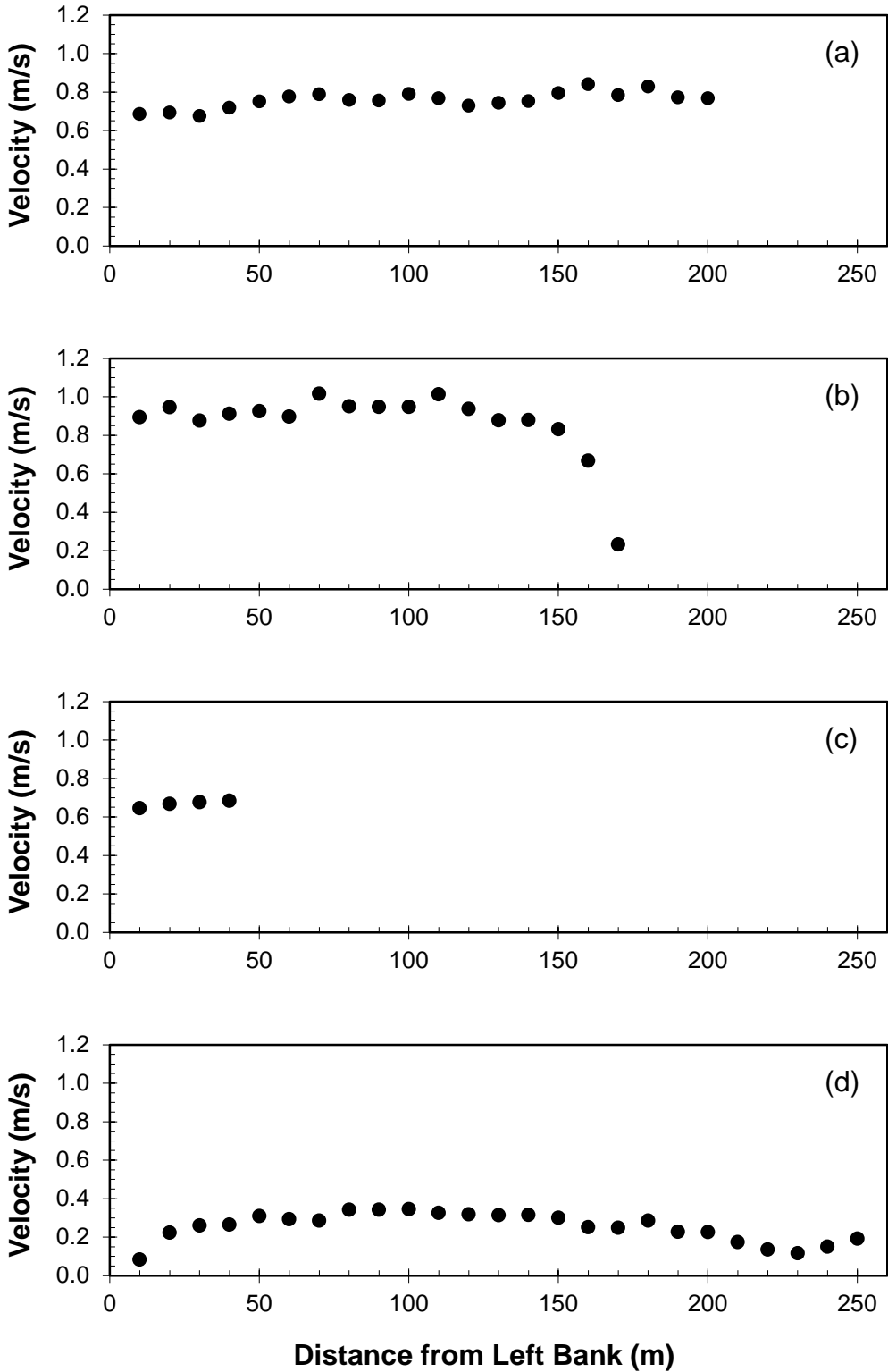


Figure 2.3 Velocity cross sections obtained from ADCP measurements at cross section 1 (a), 2 (b), 3 (c) and 4 (d).

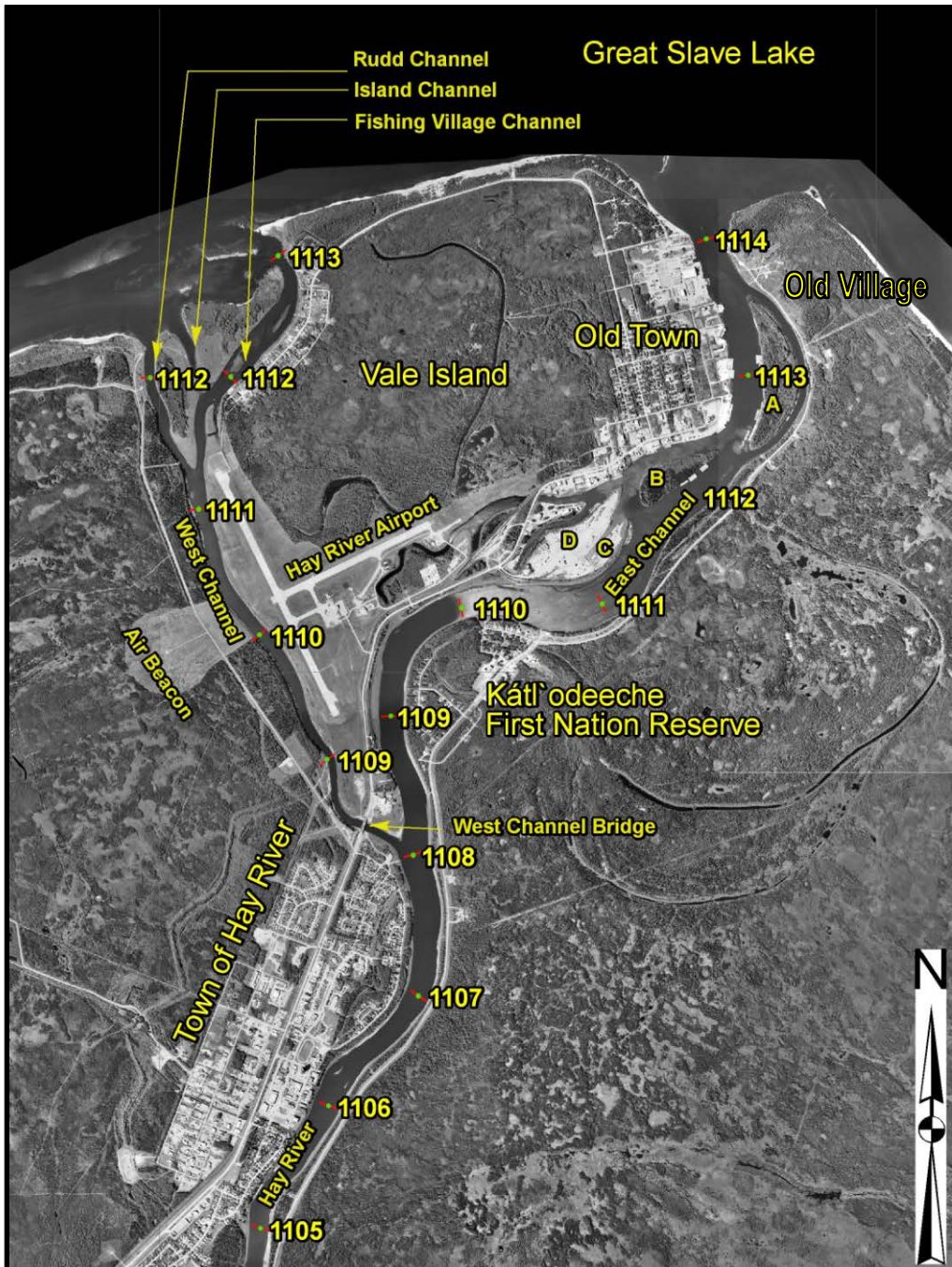


Figure 2.4 Annotated aerial photograph of the Hay River Delta



Figure 2.5 Image showing the juxtaposed ice cover formation in the East Channel during 2008 freeze-up.



Figure 2.6 Image of the beginning of ice cover formation in the West Channel delta in 2008, looking down the Fishing Village Channel.

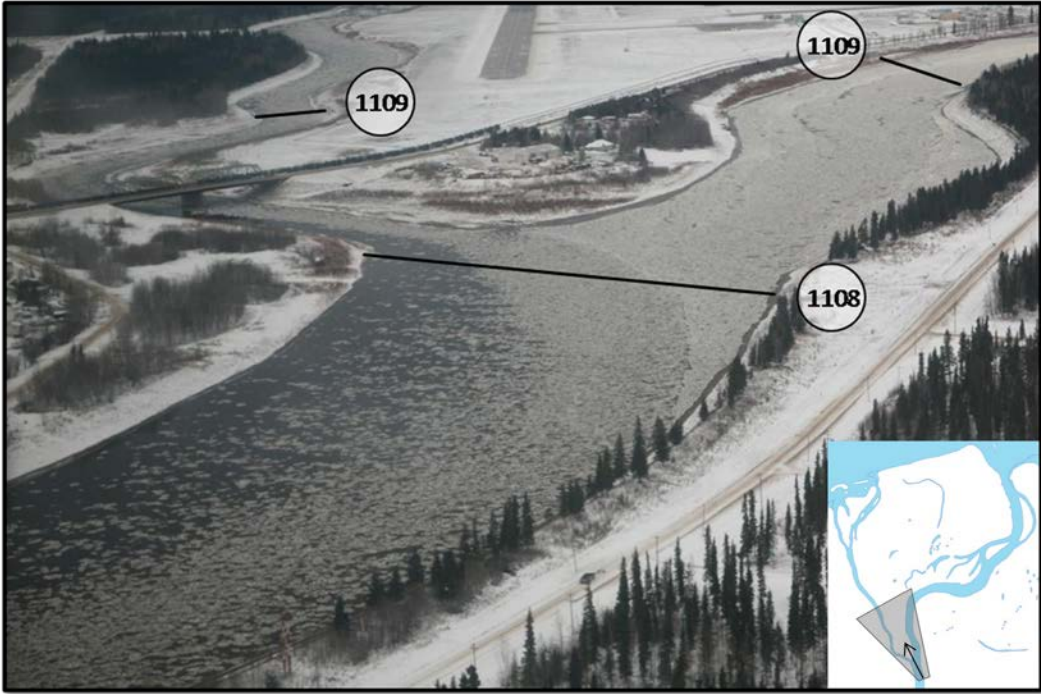


Figure 2.7 Image of the East-West Channel split during the 2008 freeze-up.

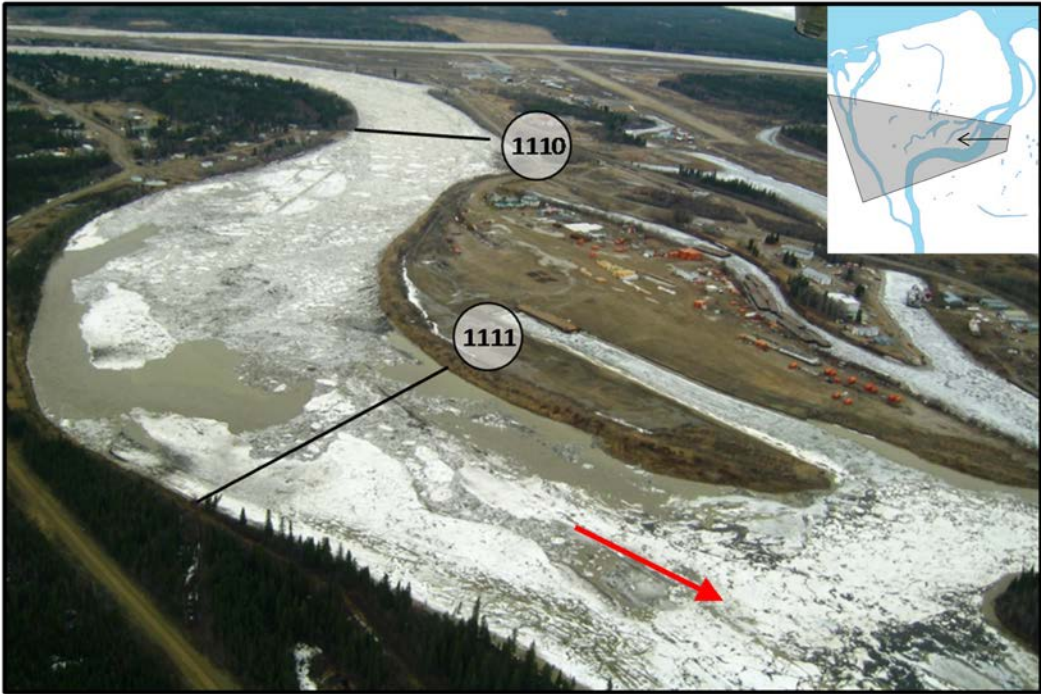


Figure 2.8 Image of ice jam in the East Channel on 4-May-08.



Figure 2.9 Image of the ice jam in the West Channel on 4-May-08.



Figure 2.10 Image of the ice jam at the mouth of the East Channel on 5-May-08.

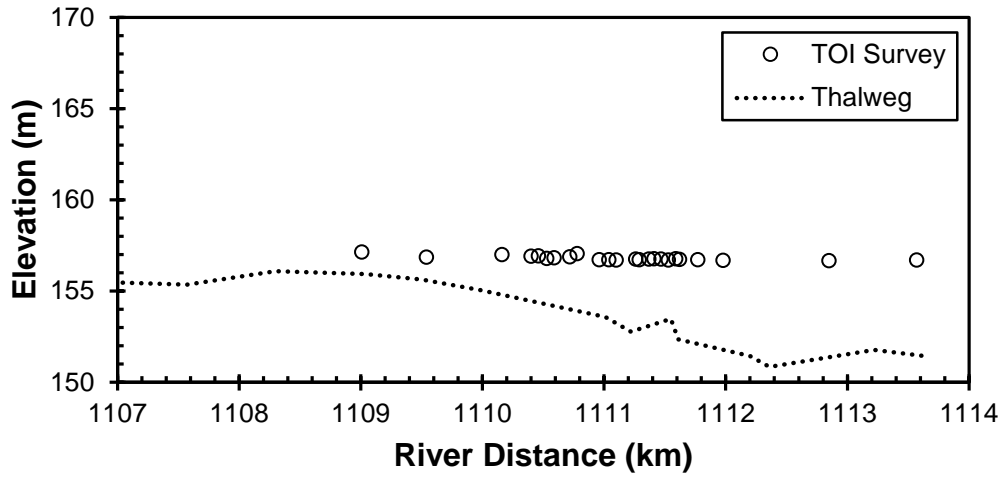


Figure 2.11 The top of ice profile in the East Channel on 28-Apr-08.

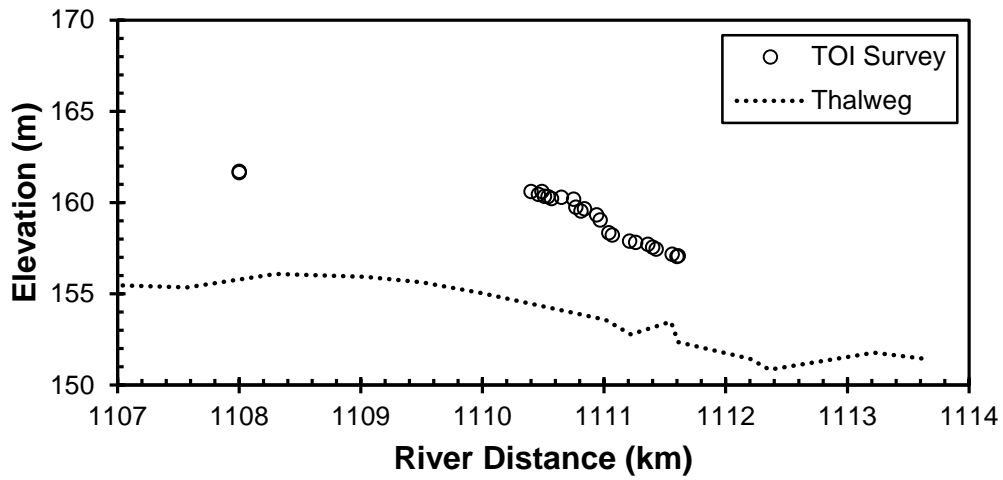
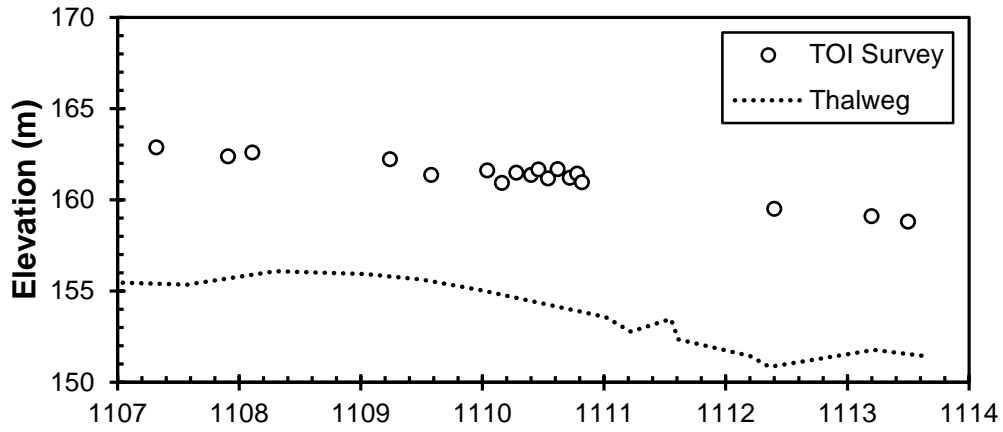
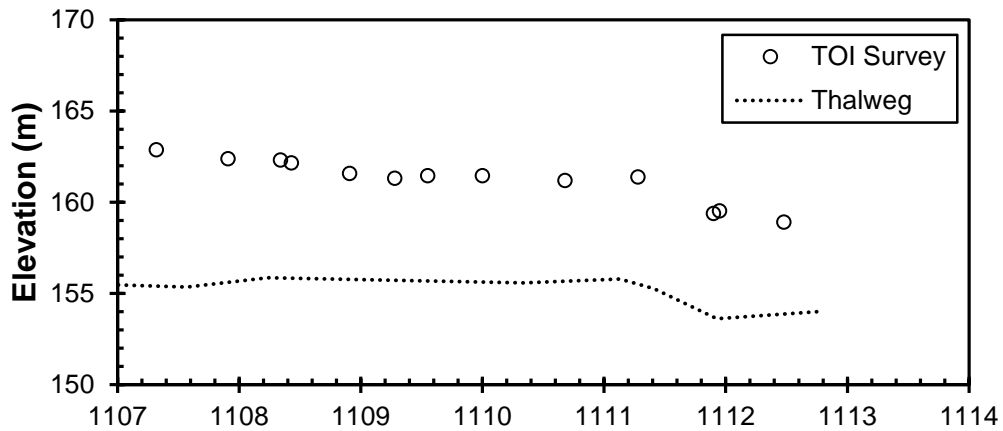


Figure 2.12 The top of ice profile of the ice jam in the East Channel on 5-May-08.



(a)



(b)

River Distance (km)

Figure 2.13 Maximum top of ice profiles measured on 6-May-08 in the (a) East and (b) Fishing Village Channels.



Figure 2.14 Image of ice jam in the West Channel on 3-May-09.



Figure 2.15 Image of ice jam in the East Channel on 3-May-09.



Figure 2.16 Image of ice jam in the East Channel on 4-May-09.



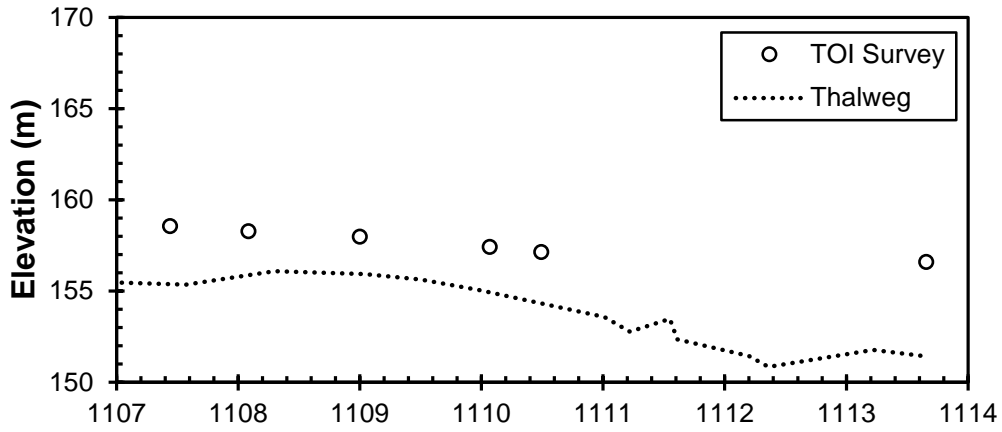
Figure 2.17 Image of the ice jam in the West Channel delta on 4-May-09.



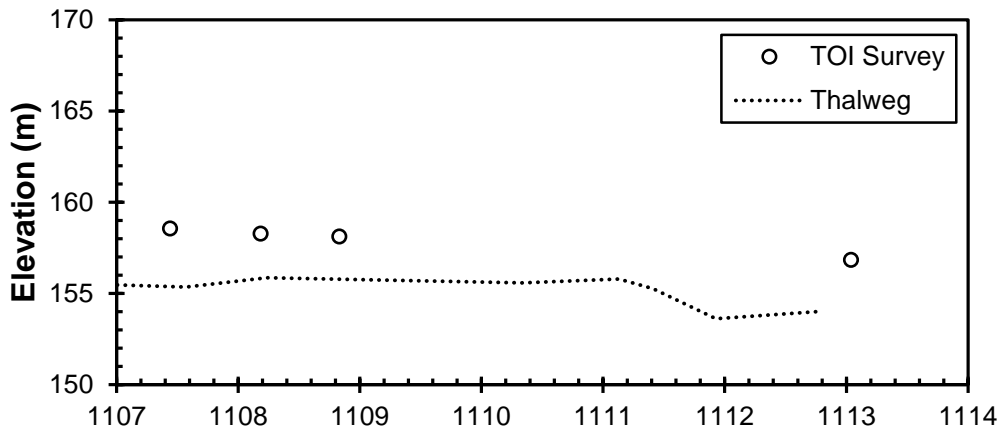
Figure 2.18 Image of the ice jam in the East Channel on 6-May-09.



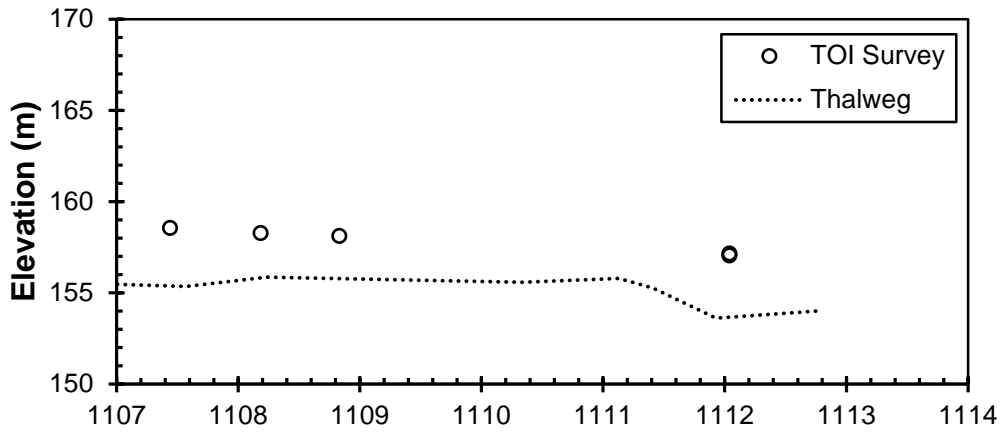
Figure 2.19 Image of the ice jam in the West Channel delta on 6-May-09.



(a)

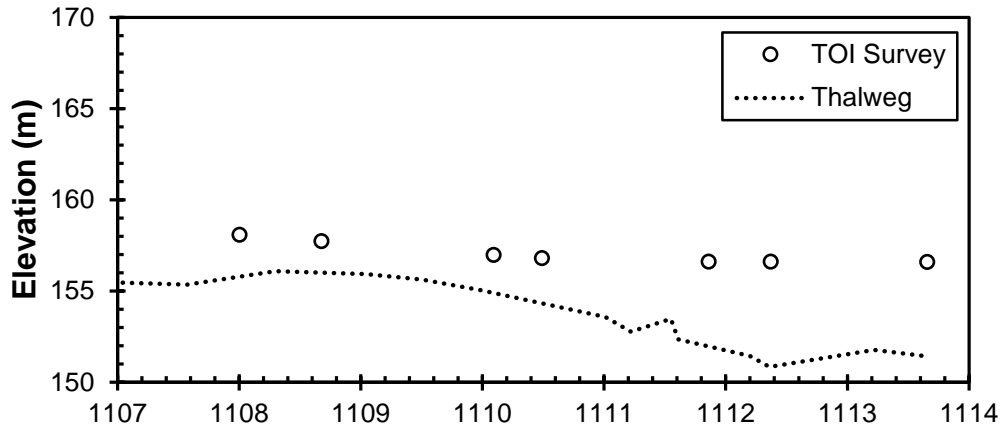


(b)

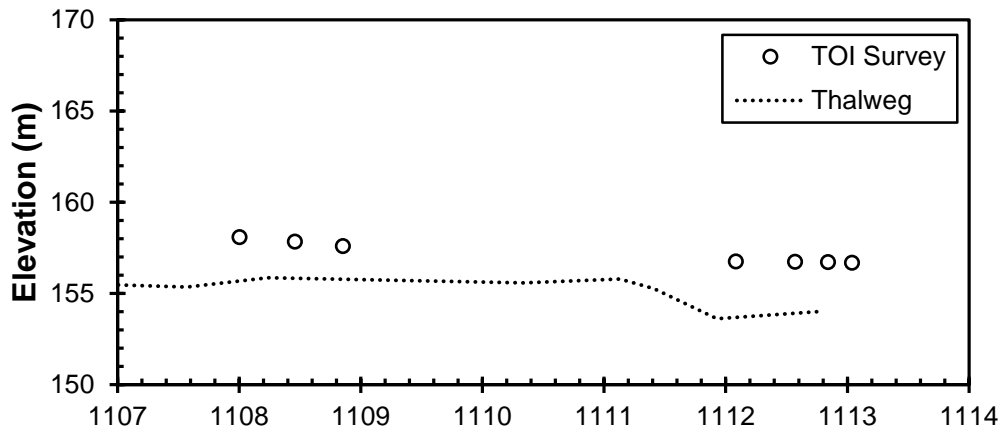


(c)

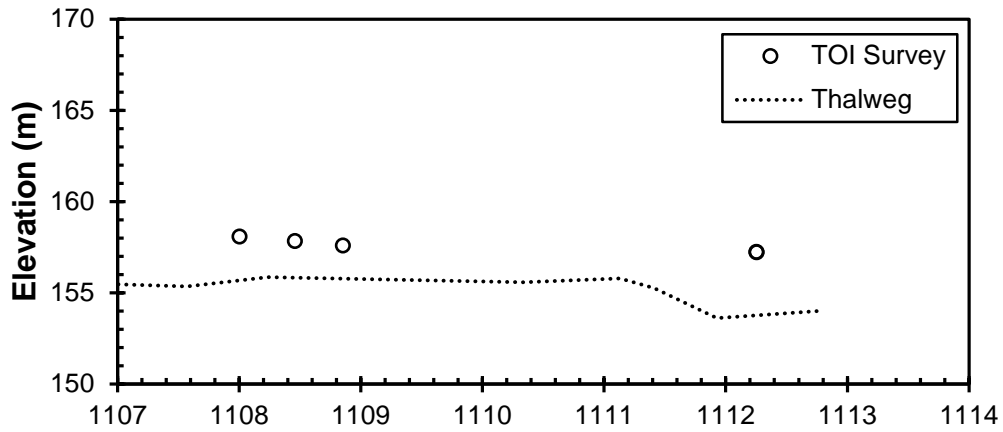
Figure 2.20 The surveyed top of ice profiles from 26-Apr-09 in the (a) East, (b) Fishing Village and (c) Rudd Channels.



(a)

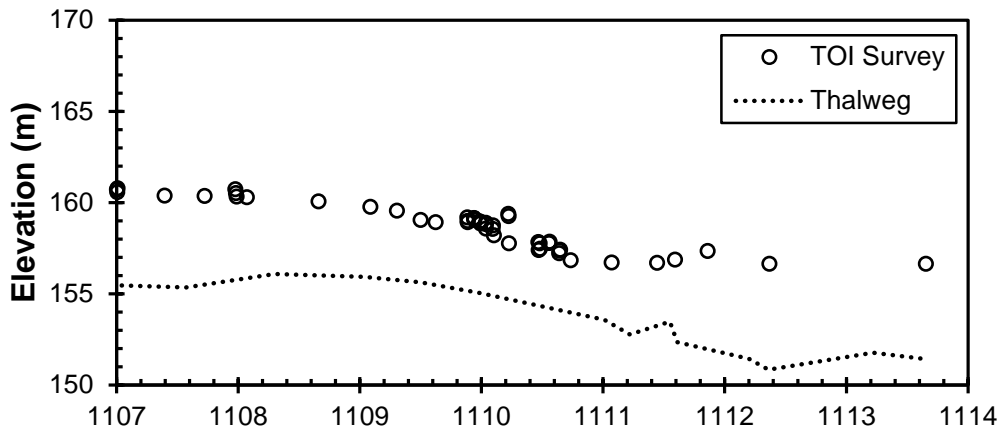


(b)

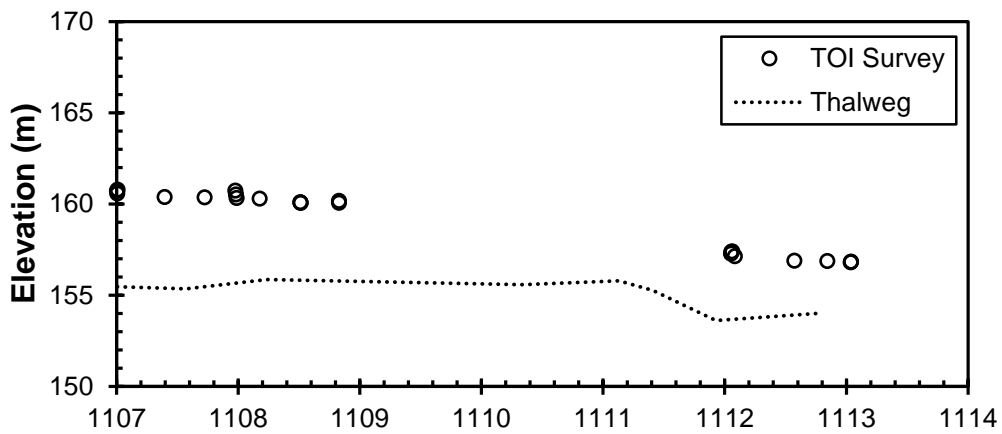


(c)

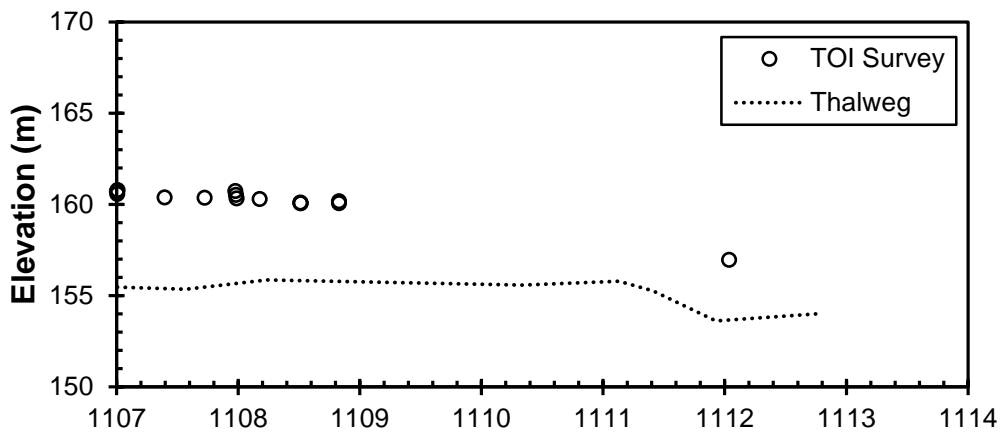
Figure 2.21 The surveyed top of ice profiles from 30-Apr-09 in the (a) East, (b) Fishing Village and (c) Rudd Channels.



(a)



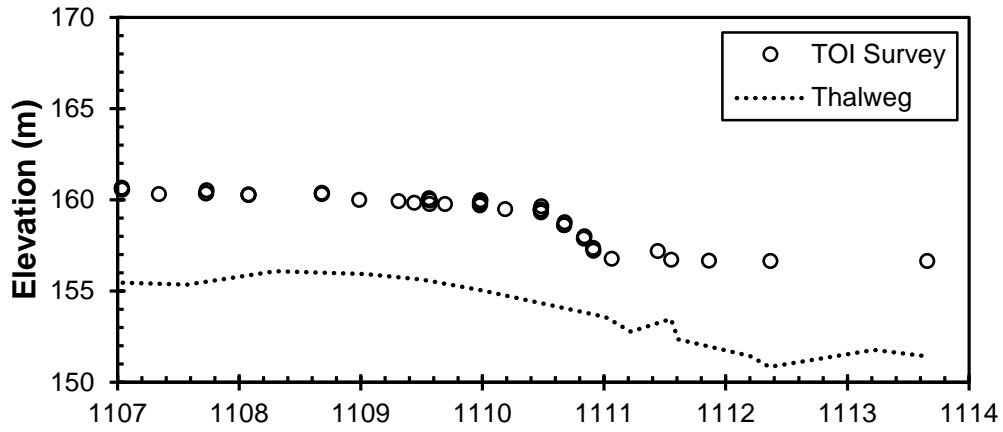
(b)



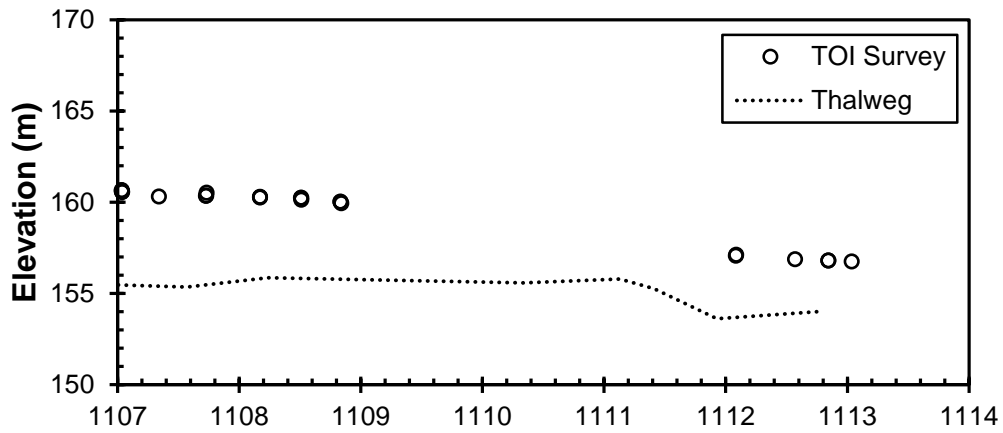
(c)

River Distance (km)

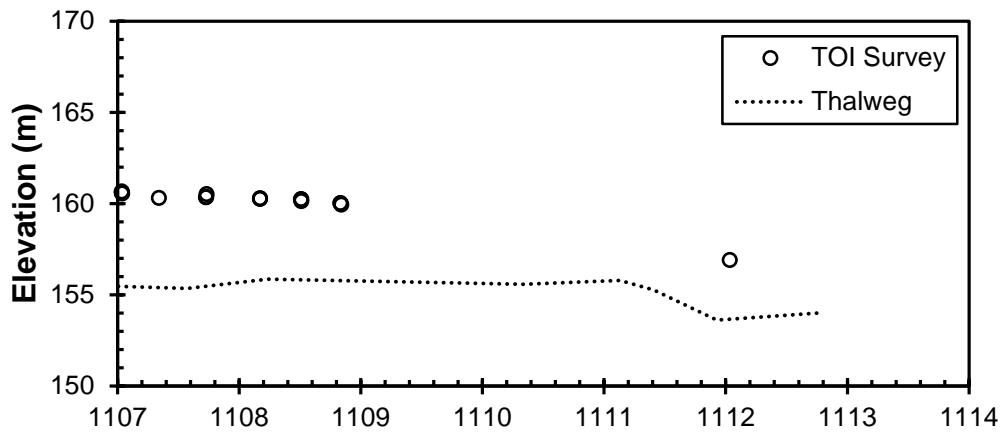
Figure 2.22 The surveyed top of ice profiles from the morning of 3-May-09 in the (a) East, (b) Fishing Village and (c) Rudd Channels.



(a)



(b)



(c)

River Distance (km)

Figure 2.23 The surveyed top of ice profiles from the afternoon of 3-May-09 in the (a) East, (b) Fishing Village and (c) Rudd Channels.

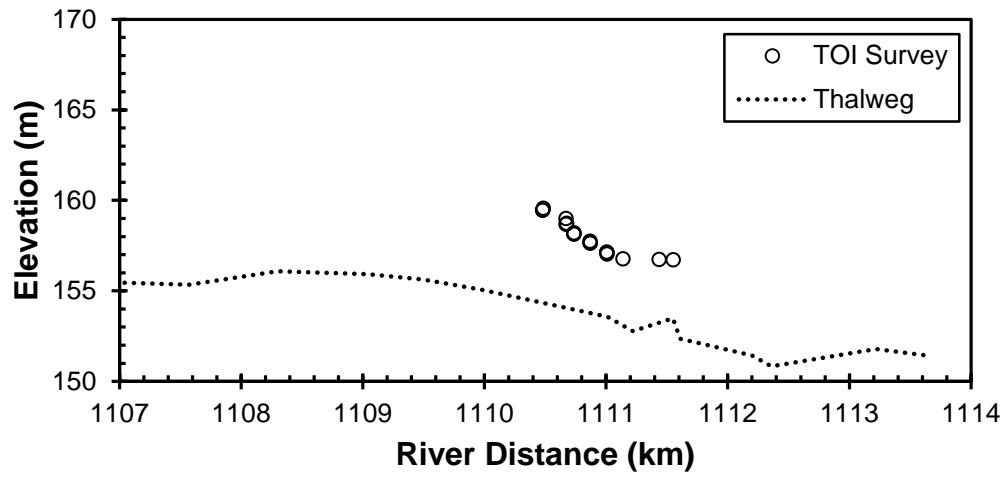
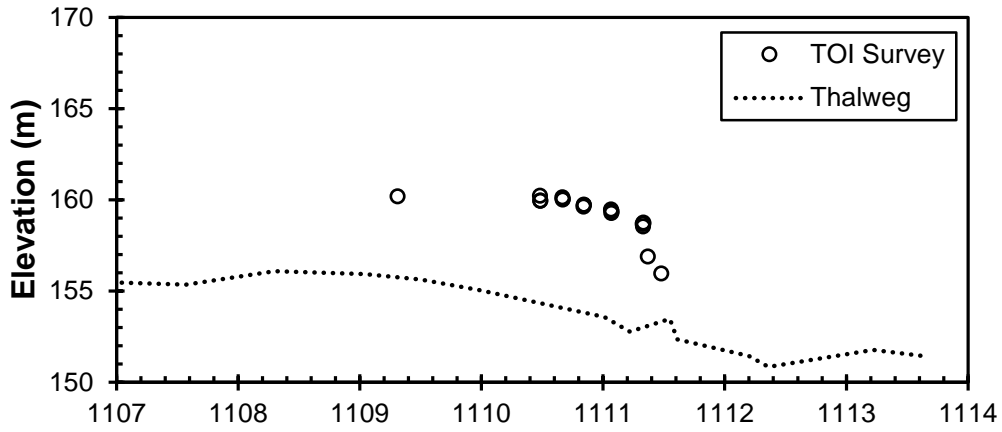
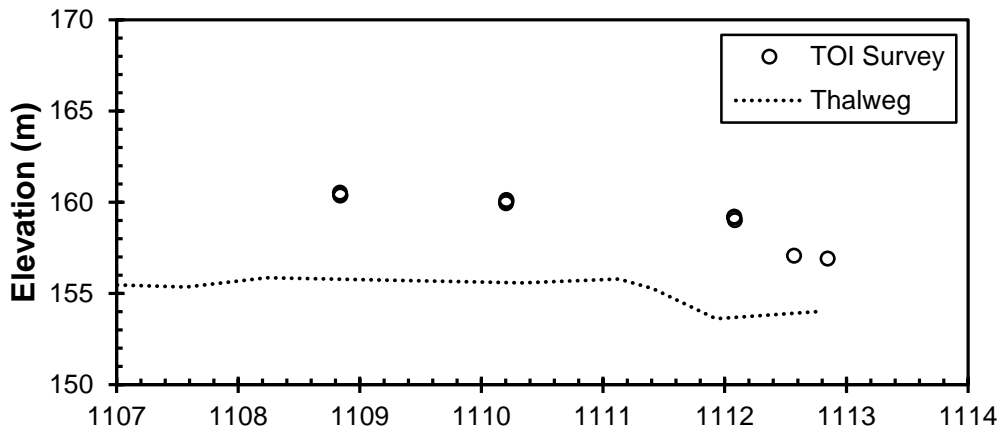


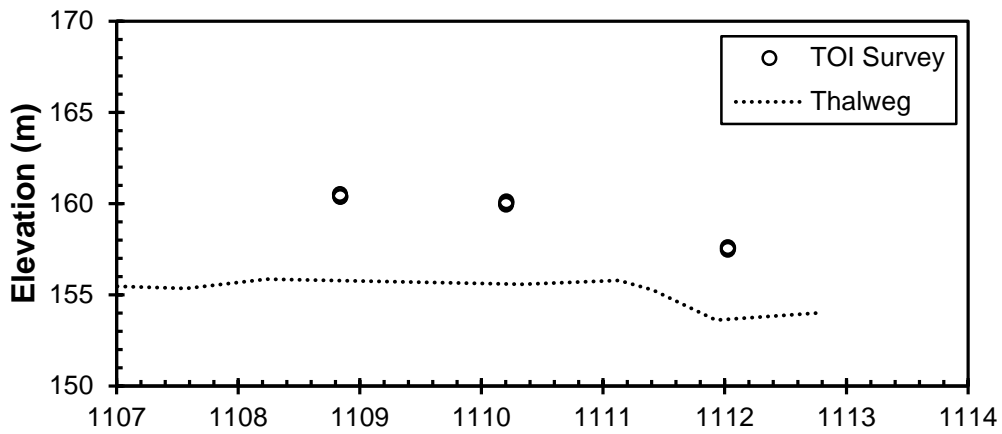
Figure 2.24 The surveyed top of ice profiles from the evening of 3-May-09 in the East Channel.



(a)

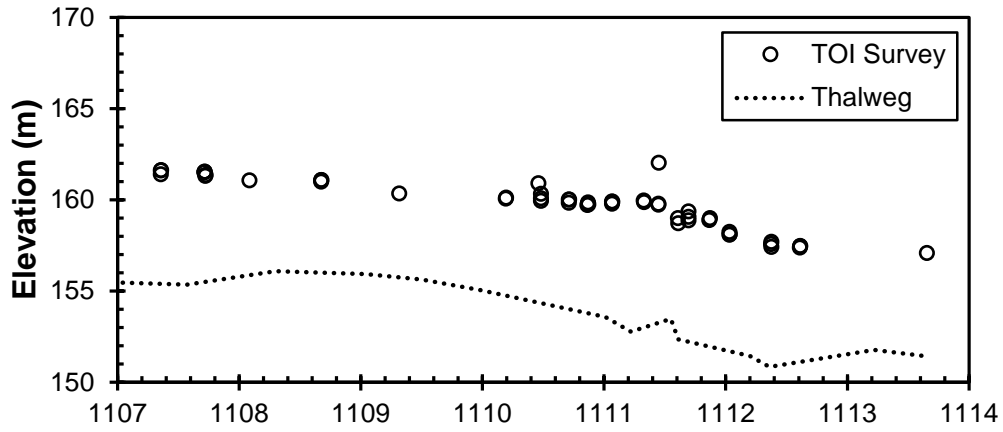


(b)

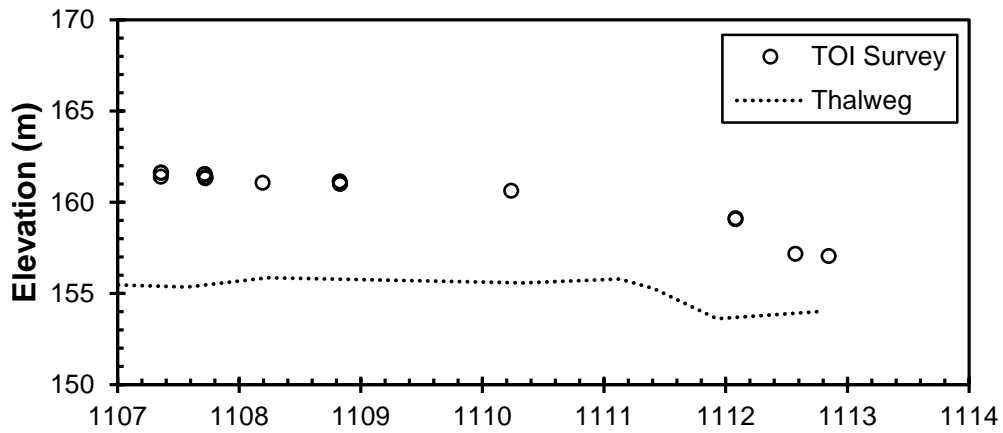


(c)

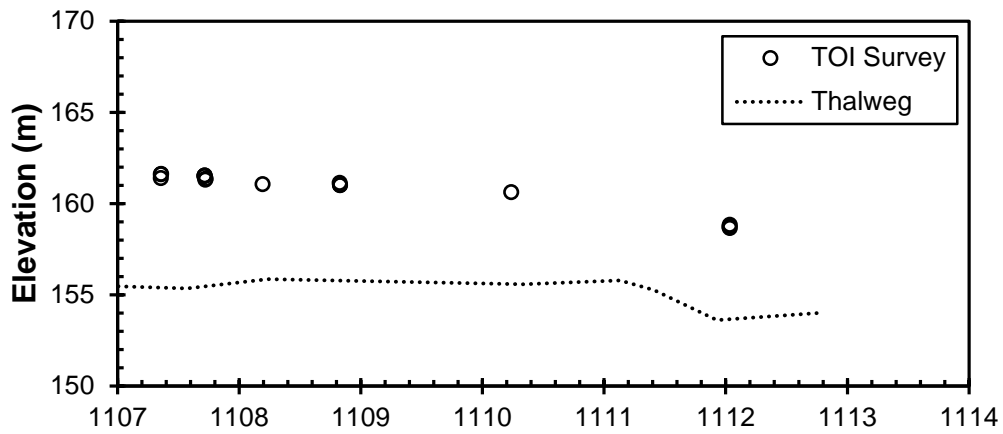
Figure 2.25 The surveyed top of ice profiles from the afternoon of 4-May-09 in the (a) East, (b) Fishing Village and (c) Rudd Channels.



(a)

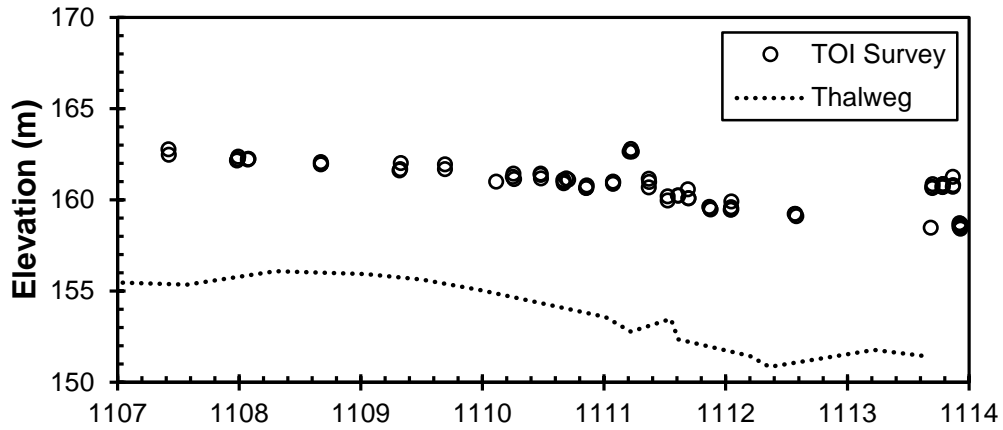


(b)

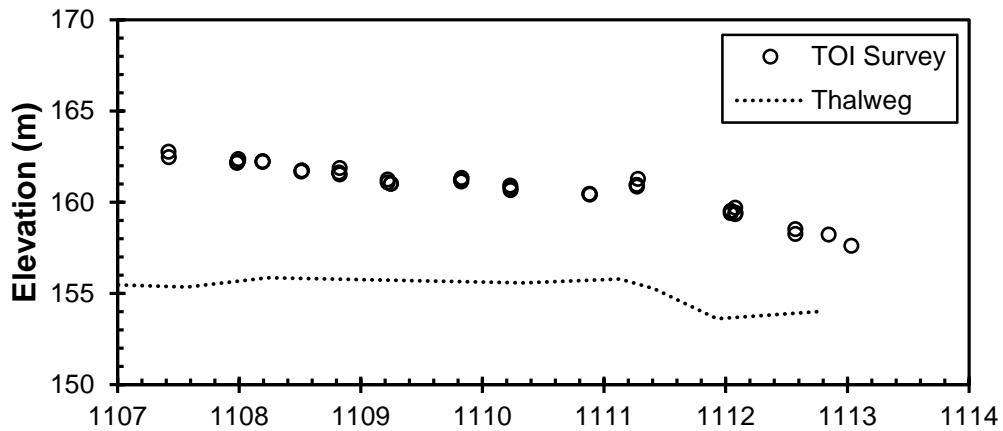


(c)

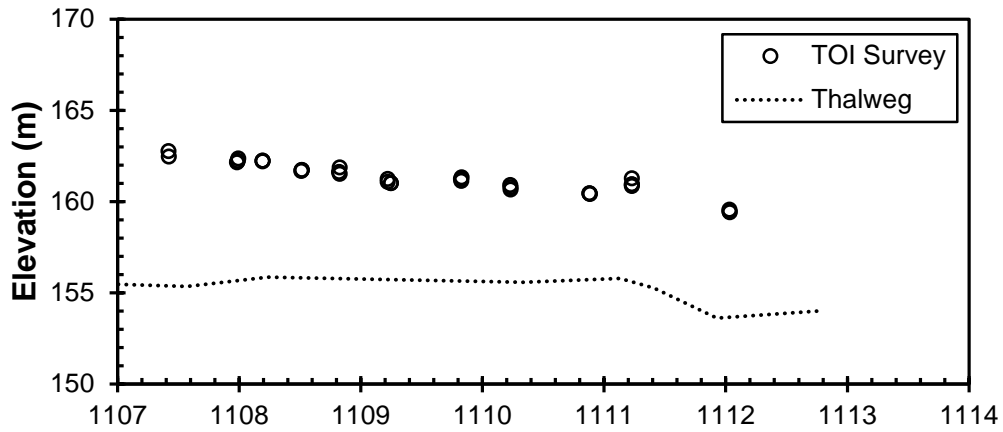
Figure 2.26 The surveyed top of ice profiles from the morning of 5-May-09 in the (a) East, (b) Fishing Village and (c) Rudd Channels.



(a)



(b)



(c)

Figure 2.27 The surveyed maximum top of ice profiles from the night of 6-May-09 in the (a) East, (b) Fishing Village and (c) Rudd Channels.

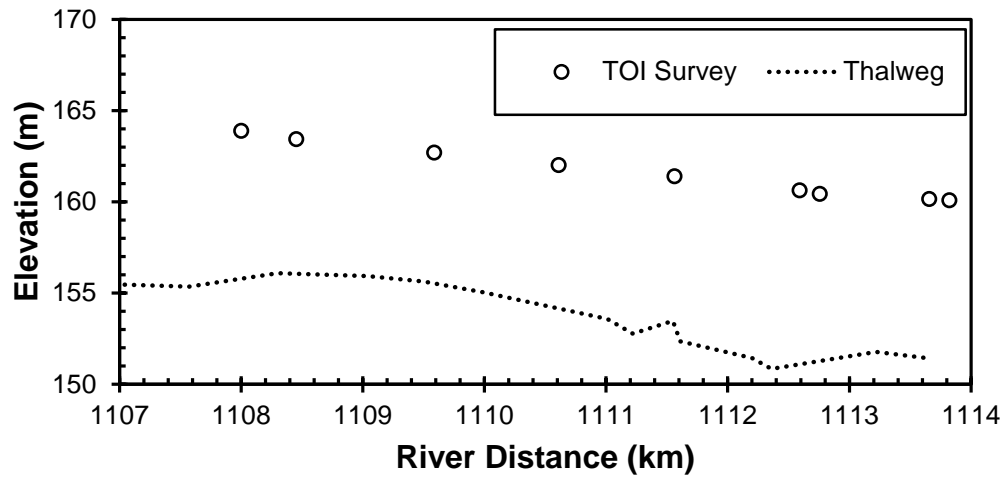


Figure 2.28 The surveyed top of ice profiles from the 1963 breakup in the East Channel.

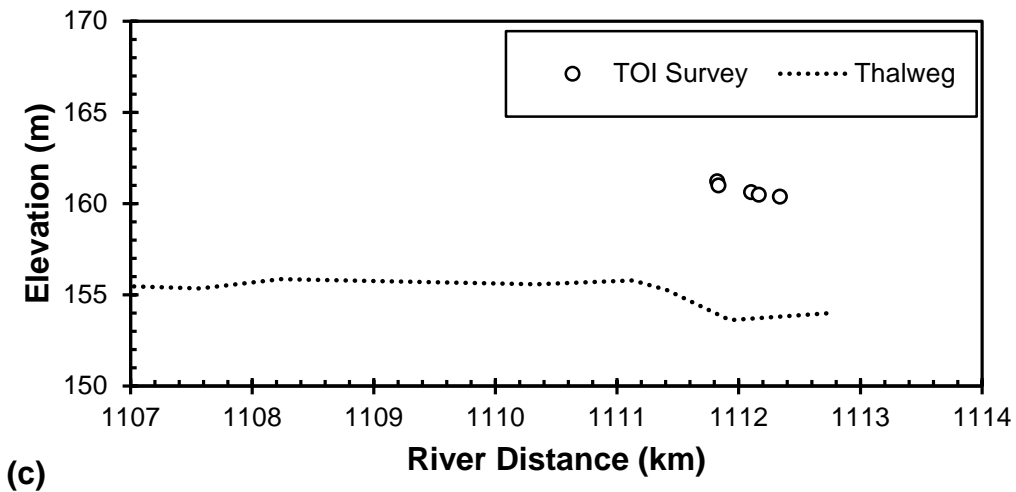
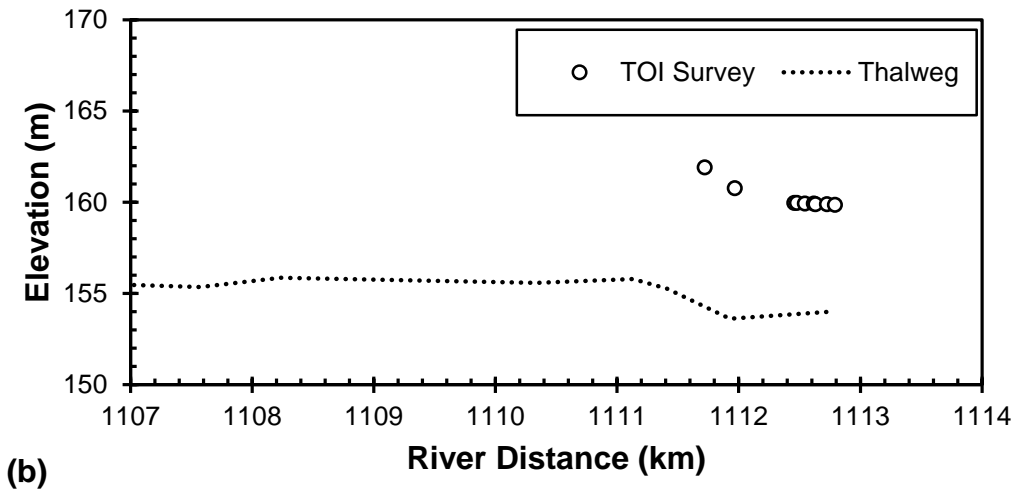
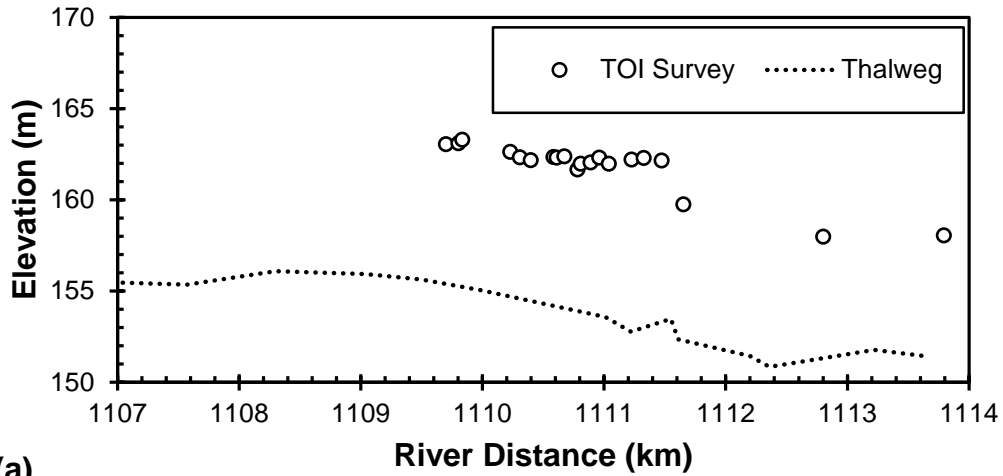
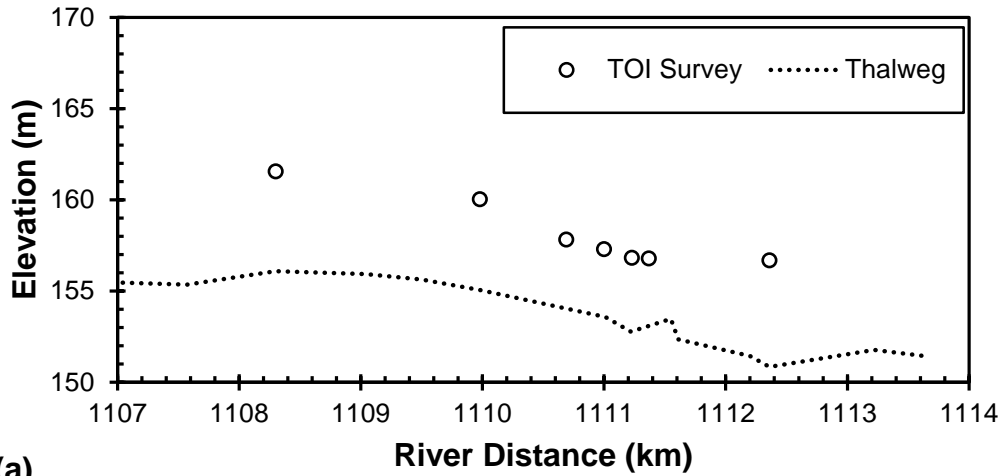
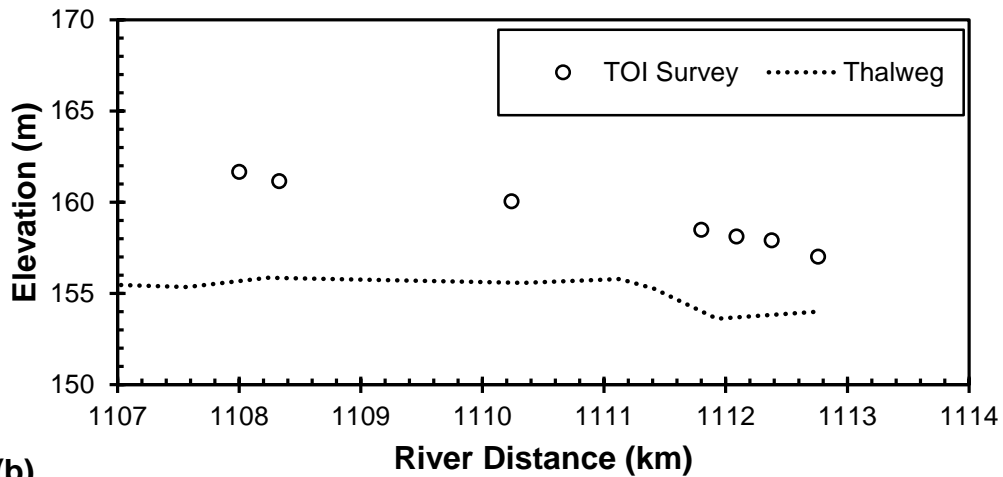


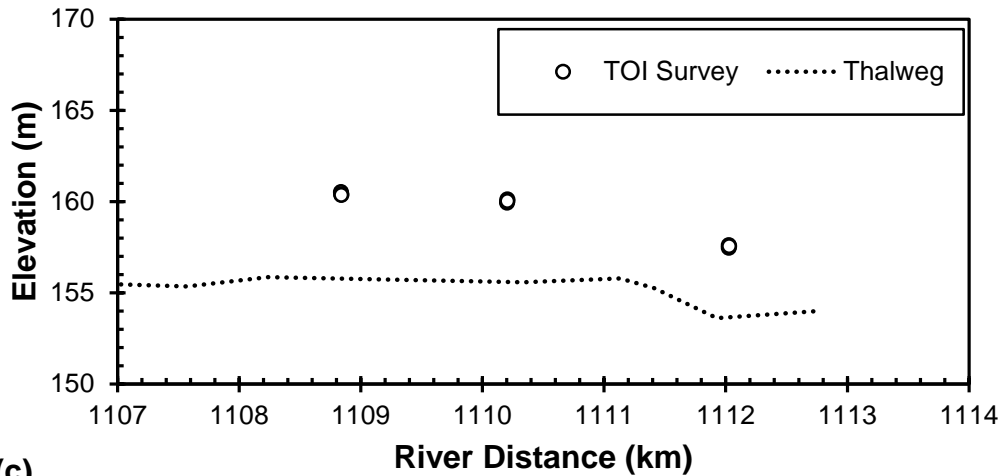
Figure 2.29 The surveyed top of ice profiles from the 1985 breakup in the (a) East, (b) Fishing Village and (c) Rudd Channels.



(a)



(b)



(c)

Figure 2.30 The surveyed top of ice profiles from the 1988 breakup in the (a) East, (b) Fishing Village and (c) Rudd Channels.

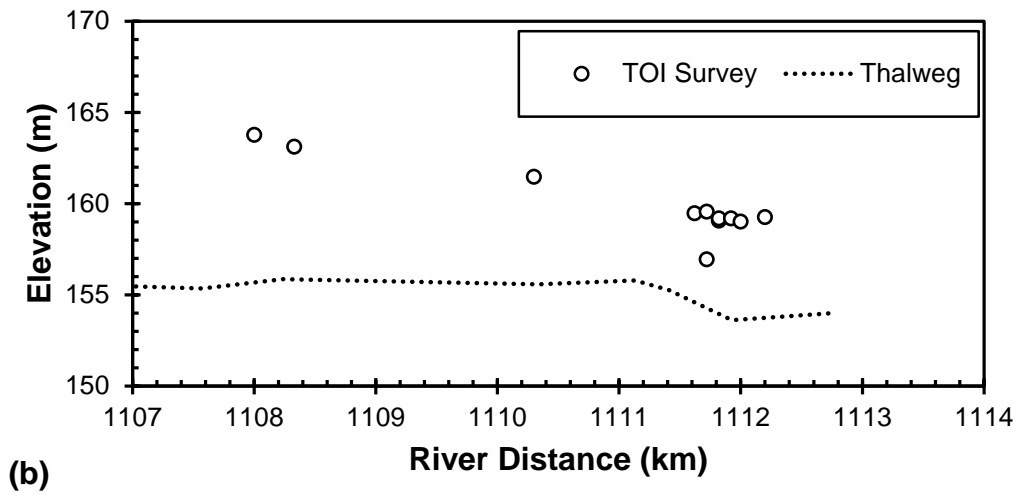
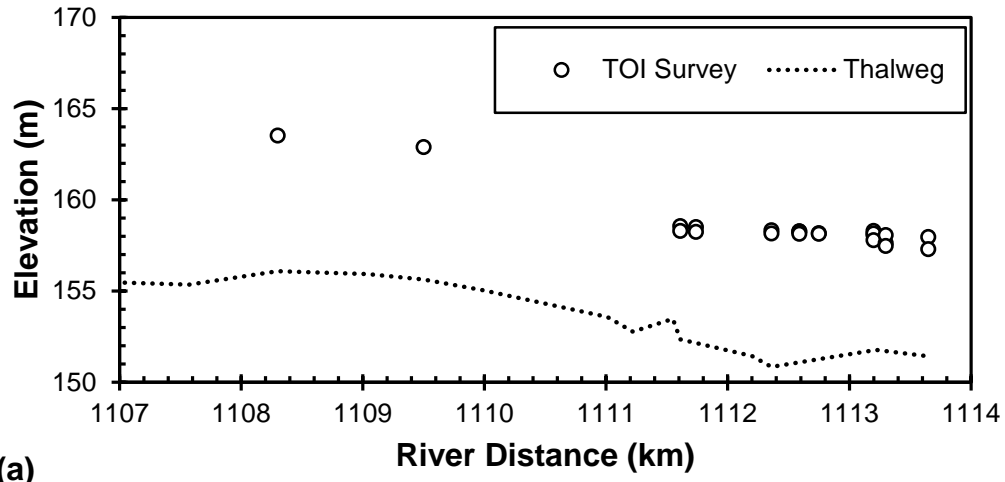


Figure 2.31 The surveyed top of ice profiles from the 1989 breakup in the (a) East and (b) Rudd Channels.

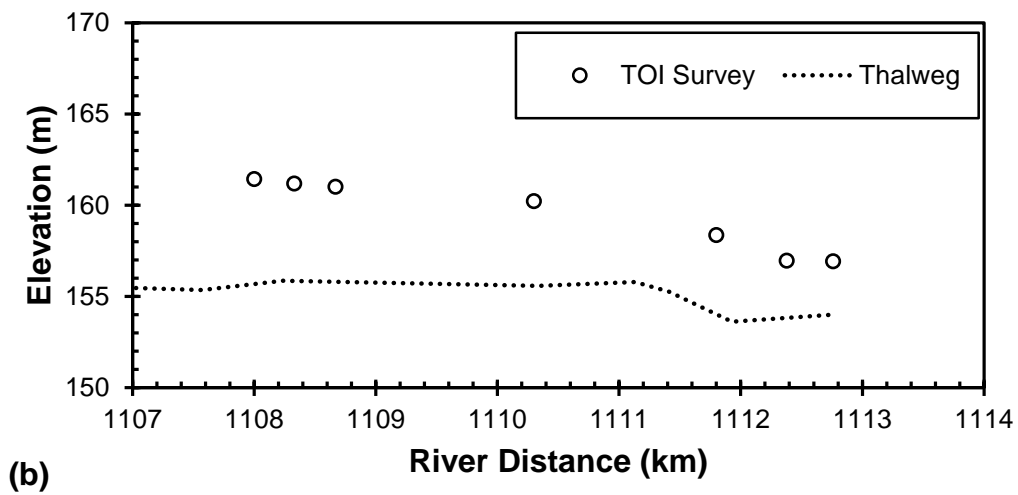
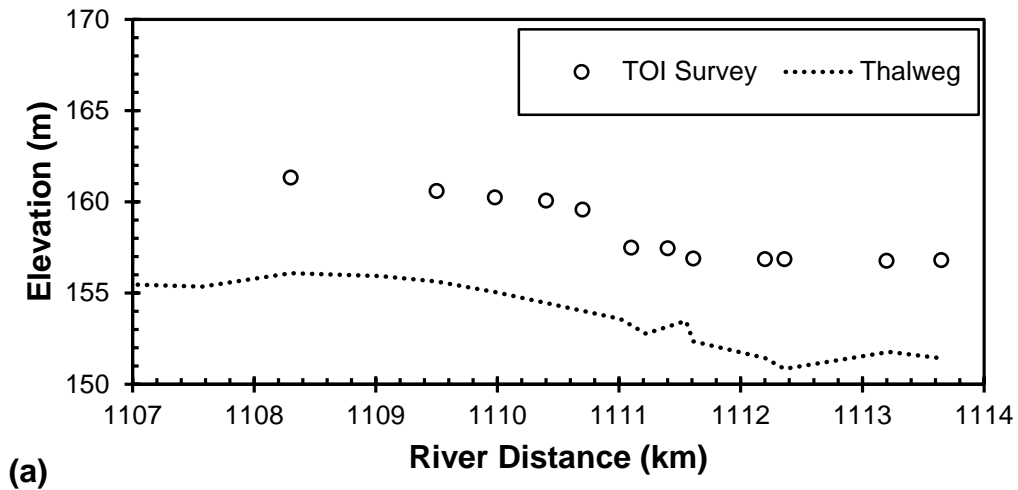


Figure 2.32 The surveyed top of ice profiles from the 1990 breakup in the (a) East and (b) Fishing Village Channels.

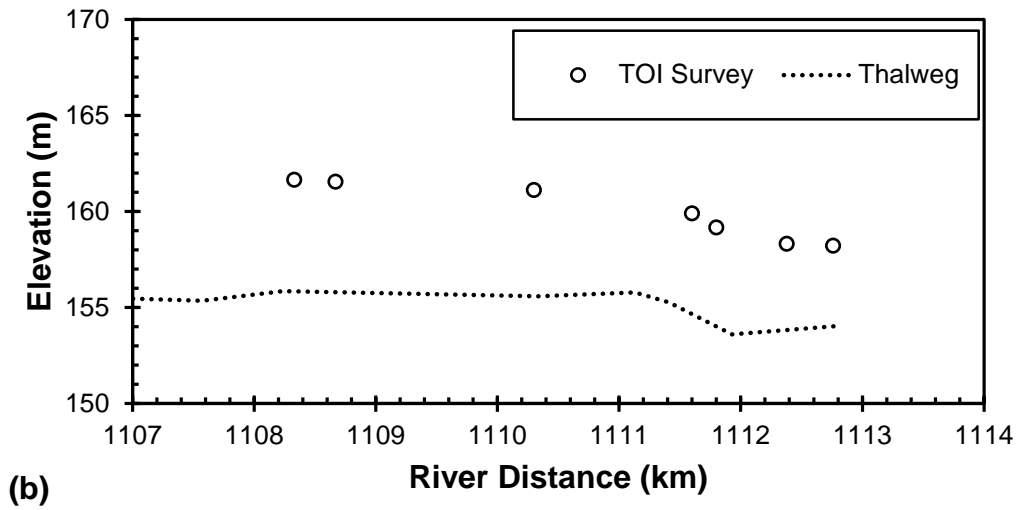
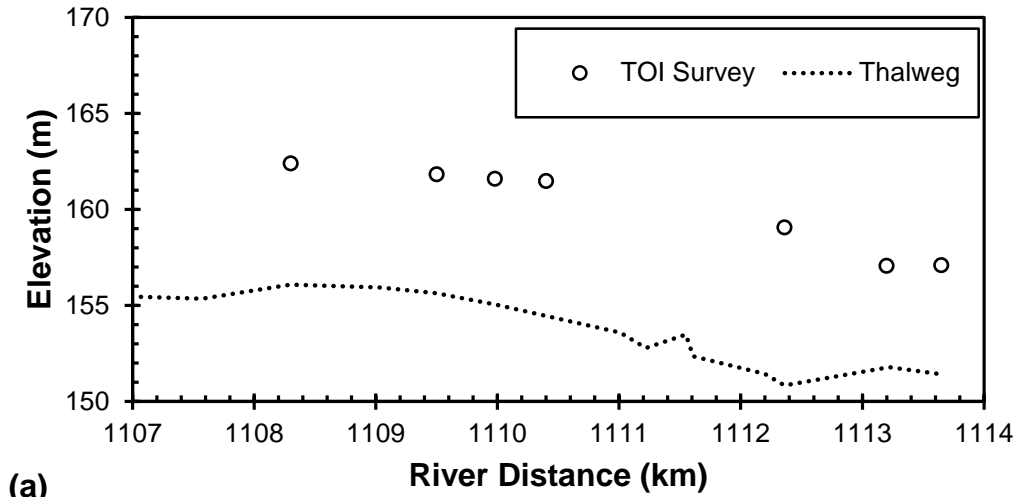


Figure 2.33 The surveyed top of ice profiles from the 1992 breakup in the (a) East and (b) Fishing Village Channels.

3.0 Model Description and Testing

The ability to predict when and where an ice jam will form during breakup, along with the resulting water elevations, would be valuable information for evacuation planning in Hay River. A numerical model can be a useful tool to better understand physical processes such as ice jam formation and ice jam hydraulics. Two models with different capabilities were selected for this study to test their suitability for predicting ice jam formation and for modeling water elevations. The first model, CRISSP2D, developed by Dr. Hung Tao Shen at Clarkson University, is capable of modeling dynamic ice conditions. The second model, River2D, developed at the University of Alberta by Dr. Peter Steffler, is capable of modeling stable ice covered conditions.

This chapter documents the basic equations and capabilities of each model and discusses preliminary testing. The hydrodynamic equations for both models are presented and the required model inputs are discussed. The ice dynamic equations in CRISSP2D are also presented. Testing was conducted on the CRISSP2D model to achieve a better understanding of the model inputs and their effects on the results. Similar testing was not done with River2D because large amounts of testing results are available in the public domain.

3.1 CRISSP 2-D

CRISSP 2D is an unsteady two-dimensional numerical river model capable of modeling thermal and dynamic ice processes in conjunction with flow hydrodynamics. The model is able to simulate ice formation and movement in

complex river geometries and flow conditions. CRISSP2D is also able to model steady state problems. This thesis tested the model capabilities under open water and freeze-up conditions and focused on modeling breakup conditions.

The CRISSP2D model is broken down into six modules that can be turned on or off depending on the key processes required. The six processes are:

hydrodynamics, ice dynamics, thermal, ice breakup, sub-surface ice transport and anchor ice. This thesis explored the hydrodynamic, ice dynamics, thermal and ice breakup modules. For a presentation of the required model inputs refer to the CRISSP2D user manual (Shen, 2005a) and for a discussion of the importance of the model inputs, refer to the CRISSP2D programmers manual (Shen, 2005b).

Default model input parameters are provided in Appendix A.

CRISSP 2D uses an Eulerian finite element model (FEM) to simulate the hydrodynamics because it is capable of modeling irregular river geometry with a flexible element mesh. The mesh in CRISSP 2D is composed of triangular elements. CRISSP2D has a limit to the number of elements and nodes allowed in the model. The size limitations can be a problem though in the cause of very large domains or complicated bathymetries requiring fine mesh discretization.

The CRISSP2D software package does not have the capability to generate a numerical mesh for modeling and requires additional software for this. Ice processes are modeled using a Lagrangian discrete parcel method (DPM) (Shen et al. 1993). The DPM is used because it is flexible and able to simulate deformable ice processes.

The time discretization of the hydrodynamics and the ice dynamics in CRISSP2D are set separately and must be less than the maximum time step specified by the Courant-Freidrichs-Lewy (CFL) condition. The CFL condition is related to the time it takes a shallow water wave to travel between nodes in the model. A time step less than the CFL specified time step helps to ensure model stability. No option is available to increase the time step as a model run converges on the solution. The hydrodynamics and ice dynamics are loosely coupled together at a set time interval called the coupling time step. Highly dynamic ice events require a coupling time step on the order of several seconds while slow processes only require a coupling time step on the order of several hundred seconds. An example of a dynamic ice event would be an ice jam release and an example of a slow ice process would be border ice growth during freeze-up.

3.1.1 Hydrodynamic Module

CRISSP 2D uses the depth-integrated two-dimensional hydrodynamic equations to model the free surface water flow. The basic continuity and momentum equations were modified to include the surface ice and seepage flow through the surface ice (Liu et al. 1998) and are:

$$\frac{\partial H}{\partial t} + \frac{\partial(q_{tx})}{\partial x} + \frac{\partial(q_{ty})}{\partial y} = \frac{\partial}{\partial t}(Nt_s)$$

$$\frac{\partial q_{tx}}{\partial t} + \frac{\partial}{\partial x} \left(\frac{q_{tx}^2}{H_t} \right) + \frac{\partial}{\partial y} \left(\frac{q_{tx} q_{ty}}{H_t} \right) = \frac{1}{\rho} (\tau_{sx} - \tau_{bx}) + \frac{1}{\rho} \left(\frac{\partial T_{txx}}{\partial x} + \frac{\partial T_{tyx}}{\partial y} \right) - g H_t \frac{\partial \eta}{\partial x}$$

$$\frac{\partial q_{ty}}{\partial t} + \frac{\partial}{\partial x} \left(\frac{q_{tx} q_{ty}}{H_t} \right) + \frac{\partial}{\partial y} \left(\frac{q_{ty}^2}{H_t} \right) = \frac{1}{\rho} (\tau_{sy} - \tau_{by}) + \frac{1}{\rho} \left(\frac{\partial T_{txy}}{\partial x} + \frac{\partial T_{tyy}}{\partial y} \right) - g H_t \frac{\partial \eta}{\partial y}$$

$$q_{tx} = q_{lx} + q_{ux}$$

$$q_{ty} = q_{ly} + q_{uy}$$

$$q_{lx} = q_{ix} + q_{sx}$$

$$q_{ly} = q_{iy} + q_{sy}$$

$$T_{txy} = T_{tyx} = \varepsilon_{xy} \left(\frac{\partial q_{tx}}{\partial y} + \frac{\partial q_{ty}}{\partial x} \right)$$

where:

H = total water depth (m)

η = water surface elevation (m)

q_{tx} = total unit discharge in x direction (m^2/s)

q_{ty} = total unit discharge in y direction (m^2/s)

N = ice concentration

t_s = submerged ice thickness (m)

H_t = water depth underneath ice water interface, adjusted from the real ice-water interface to include water flow between particles (m)

ρ = water density (kg/m^3)

τ_{sx} = shear stress in the x-direction at the ice-water interface (N/m^2)

τ_{sy} = shear stress in the y-direction at the ice-water interface (N/m^2)

τ_{bx} = shear stress in the x-direction at the water-bed interface (N/m^2)

τ_{by} = shear stress in the y-direction at the water-bed interface (N/m^2)

g = acceleration due to gravity (m^2/s)

The shear stress components at the water-bed interface are functions of the unit discharge in the x and y directions, the depth beneath the bottom of the ice, the water density, the Manning's roughness coefficient of the bed and the fraction of the depth beneath the bottom of the ice affected by the bed friction. The shear stress components between the water-ice interface is similar to the bed shear stress component but the relative velocities of the ice and the water are accounted for. A detailed explanation of how the model handles the apportionment between ice and bed affected flows can be found in Shen et al. (1990).

The continuity and momentum equations are solved using the finite element theory with the characteristic dissipative Galerkin method. This method is capable of modeling both sub and super critical flows experienced during ice jam events. A modified explicit time integration technique known as the leapfrog method is used to integrate the finite element equations with respect to time. The leapfrog method is conditionally stable and the critical time step is calculated by:

$$\Delta t_c = 1.5 \frac{\Delta L_m}{\sqrt{2gH_M}}$$

where:

Δt_c = critical time step (s)

ΔL_m = minimum triangle side length (m)

H_M = maximum water depth (m)

3.1.2 Ice Dynamics Module

The Ice Dynamic module was developed by Shen et al. (1993) and uses a Lagrangian discrete parcel method to simulate dynamic surface ice transport. The method treats the ice as a two dimensional continuum of individual parcels which carry mass, momentum and energy. The inflow rate of surface ice is input for each parcel as the ice concentration and the ice thickness. CRISSP2D has a limit to the number of parcels allowed in a model to reduce the maximum computation time. Theoretical background for Shen's method was based on research in smooth particle hydrodynamics done by Lucy (1977) and Gingold and Monaghan (1977).

The momentum equation of the surface ice, from Shen et al (1990), is written in its Lagrangian form as:

$$M_i \frac{D\vec{V}_i}{Dt} = \vec{R} + \vec{F}_a + \vec{F}_w + \vec{G}$$

where :

$$\frac{D\vec{V}_i}{Dt} = \text{acceleration of ice parcels } (m^2/s)$$

$$\vec{V}_i = \text{ice velocity } (m/s)$$

$$M_i = \text{ice mass per unit area } (kg/m^2)$$

$$\vec{R} = \text{internal ice resistance } (Pa)$$

$$\vec{F}_a = \text{wind drag force } (Pa)$$

$$\vec{F}_w = \text{water drag force } (Pa)$$

$$\vec{G} = \text{gravitational force } (Pa)$$

The wind drag force is a function of the wind speed, the air density and a calibrated wind drag coefficient. The water drag force is a function of the water velocity, the ice velocity, the water density, the Manning's roughness of the ice underside and the fraction of the flow depth affected by the ice friction. The gravitational force is due to the downslope component of the ice mass induced by the water surface slope. The internal ice resistance forces are determined using the viscoelastic-plastic constitutive relationship presented by Ji et al. (2004).

Not included in the above equation is the resistance the ice experiences when it becomes grounded against the model bed or when it contacts a model boundary

such as an island. The bed resistance is based on the weight of submerged ice and the bed to ice friction angle. Boundary friction is based on a dynamic Mohr-Coulomb yield criterion developed by Hanes and Inman (1985). It is a function of the dynamic friction angle and the normal force of the ice acting on the boundary. The normal force at a boundary in CRISSP 2-D is determined using method of images from Shen and Chen (1992). When an ice jam occurs in CRISSP2D the Manning's roughness of the ice is scaled up to a maximum roughness value. No explanation about how the ice roughness is scaled up in an ice jam is provided in Shen (2005a) or Shen (2005b). Default model parameters are provided in Appendix A.

3.1.3 Breakup Module

The breakup module enables the user to specify criteria under which to fracture an intact ice cover and instigate an ice run. The model domain is broken up into distinct regions allowing the model to instigate breakup in specified locations. Each region has an ice cover thickness and possible breakup controls depending on the desired situation. Several different breakup controls are available for each region depending on the desired results. They include instigating breakup at a specific water elevation, at a specific water elevation change rate, or a specific time. Ice in a region can also be set to breakup if breakup is instigated in an adjacent region. The breakup module is the only way to specify an intact ice cover in CRISSP2D.

3.1.4 Thermal Module

Though not the focus of this thesis, CRISSP2D is also equipped to handle the modeling of thermodynamic ice processes. The thermal modeling module allows for the generation of suspended frazil ice, border ice and frazil pans. Once an ice cover has developed, the thermal module can also thermally thicken or decay the ice cover depending on the ambient temperature.

Thermal modeling begins with the energy exchange between the atmosphere and the water surface. If meteorological data exists for the model site, a complete energy exchange model is used, including short and long wave radiations, evapo-condensation, sensible heat exchange and precipitation. In most cases though, the necessary data is not available and the model uses a linear approximation to calculate surface heat exchange. The model accomplishes the thermal modeling of the ice by separating the ice-water continuum into a suspended and surface layer and manages the energy and mass exchange between them. Suspended ice is generated as frazil when the water supercools and is transported in the suspended layer. Surface ice forms as either border ice, skim ice, or as frazil pans. For a more detailed discussion of these model components refer to the thesis by Wojtowicz, (2010). Default model parameters are provided in Appendix A.

3.2 River 2-D

River 2-D is an unsteady two-dimensional, depth averaged Eulerian finite element model capable of simulating river hydraulics under open water and stationary ice

conditions. The model uses a triangular finite element mesh to discretize the river bathymetry and to solve the following hydrodynamic equations:

$$\frac{\partial H}{\partial t} + \frac{\partial(q_{lx})}{\partial x} + \frac{\partial(q_{ly})}{\partial y} = 0$$

$$\begin{aligned} \frac{\partial q_{lx}}{\partial t} + \frac{\partial}{\partial x} \left(\frac{q_{lx}^2}{D} \right) + \frac{\partial}{\partial y} \left(\frac{q_{lx} q_{ly}}{D} \right) + g \left(\frac{\partial}{\partial x} \left(\frac{H^2}{2} \right) - t_s \frac{\partial(H)}{\partial x} \right) \\ = gD(S_{0x} - S_{fx}) + \frac{1}{\rho} \left(\frac{\partial(D\tau_{lxx})}{\partial x} + \frac{\partial(D\tau_{lxy})}{\partial y} \right) \end{aligned}$$

$$\begin{aligned} \frac{\partial q_{ly}}{\partial t} + \frac{\partial}{\partial x} \left(\frac{q_{lx} q_{ly}}{D} \right) + \frac{\partial}{\partial y} \left(\frac{q_{ly}^2}{D} \right) + g \left(\frac{\partial}{\partial y} \left(\frac{H^2}{2} \right) - t_s \frac{\partial(H)}{\partial y} \right) \\ = gD(S_{0x} - S_{fx}) + \frac{1}{\rho} \left(\frac{\partial(D\tau_{lyx})}{\partial x} + \frac{\partial(D\tau_{lyy})}{\partial y} \right) \end{aligned}$$

where:

H = total water depth (m)

q_{lx} = unit discharge in x direction beneath the ice (m^2/s)

q_{ly} = unit discharge in y direction beneath the ice (m^2/s)

D = flow depth beneath the ice (m)

t_s = submerged ice thickness (m)

g = acceleration due to gravity (m^2/s)

S_{0x} = bed slope in the x direction (m/m)

S_{0y} = bed slope in the y direction (m/m)

S_{fx} = friction slope in the x direction (m/m)

S_{fy} = friction slope in the y direction (m/m)

ρ = water density (kg/m^3)

τ_{lxx} = xx component of turbulent stress tensor ()

τ_{lxy} = xy component of turbulent stress tensor ()

τ_{lyy} = yy component of turbulent stress tensor ()

The friction slope under ice covered conditions is the result of both the bed and the ice friction. River 2-D uses effective roughness height (k) when determining the friction slope. The effective roughness height under ice covered conditions is a composite of the bed and ice roughness heights calculated using the Sabaneev equation (Ashton, 1986). Steffler and Blackburn (2002) provide a detailed explanation of the friction slope development.

River 2-D is an unsteady flow model capable solving both transient and steady state analyses. The unsteady flow engine solves for steady state conditions by iterating from an initial condition until a steady state solution is reached. River2D solves the continuity and momentum equations using the finite element method based on the Streamline Upwind Petrov-Galerkin weighted residual formulation. The model is stable under subcritical, supercritical and transcritical flow situations. A solution at each time step is obtained implicitly using the iterative Newton-Raphson method. The Newton-Raphson method is solved using an iterative solver called the Generalized Minimal Residual method (Saad and Schultz, 1986). The time step is optimized through the model duration based on the Courant-Lewy-Freidrichs (CFL) condition to maintain stability and decrease the convergence time.

The modeling of an ice jam with River2D presents several challenges. Ice jams can significantly reduce the flow area in both the channel and the overbank area. The flow area in the channel is reduced by the ice jam toe and the overbank flow area is reduced when ice sheets are floated over the top of bank. If the ice jam toe is grounded the flow area is reduced to zero and flow is through the pores of the ice jam. River2D does not support porous ice flow and encounters stability issues when the flow depth approaches zero.

3.3 Geometry and Computational Mesh

The development of the geometry and computational meshes is a key component of a two dimensional hydrodynamic model. River2D was used to develop the

geometry and the computational meshes for both models because of its convenient graphical user interface. CRISSP2D does not come with a graphical user interface to develop either mesh.

The geometry mesh defines the lateral extends of the model domain and creates a surface that approximates the actual channel bed. Three types of boundaries are used: discharge, elevation, and no-flow. Generally, when the flow is subcritical the upstream boundary is a discharge boundary across which the inflow discharge is specified. At the downstream end of the model an elevation boundary is used. Two types of no-flow boundaries are used in both models: internal and external. External no-flow boundaries connect the discharge and elevation boundaries and do not allow water to flow across them. Internal no-flow boundaries generally go around islands where the flow will not be modeled. No-flow boundaries generally have an elevation above the maximum modeled water elevation. In situations where this is not the case, a no flow boundary behaves like a solid frictionless vertical wall. Practically there is no limit to the number of distinct sections of boundary type but CRISSP2D sets limits on the order of one thousand.

Bed and bank elevation points within the model boundary are combined together in the geometry mesh in a Triangulated Irregular Network (TIN). A TIN connects the bed and bank nodes into triangular elements. The elevation is interpolated along each element edge to create a continuous surface. Breaklines are added between nodes and prevent elements from interpolating incorrectly. Examples of locations where breaklines are often used include the top and bottom of the bank, the water's edge, and the deepest point of the channel (thalweg).

The governing equations of both models are solved along the edges of each element using the finite element method. The geometry mesh produces a poor solution because there is a very large variation in triangular element shape and size. Ideally all of the element shapes would be equilateral triangles. To improve the solution, a computational mesh is developed based on the geometry mesh. The elements in the computational mesh are much closer to equilateral triangles and element sizes vary gradually instead of suddenly. Smaller elements in the computational mesh result in a more accurate representation of the geometry mesh and a more accurate solution but require a longer computation time. Steffler and Blackburn (2002) recommend ten elements across a horizontal flow feature for accurate results. Smaller elements are used when flow direction or velocity change suddenly.

3.4 CRISSP2D Model Testing

Preliminary model testing was done with CRISSP2D to get a better understanding of its inputs. This testing was conducted because very little documentation of model inputs was provided with the model. Similar testing was not done with River2D because extensive testing and documentation is available in the public domain. The objective of the tests was to explore the ice dynamic processes of the model and to determine how selected input parameters affected the results. The hydrodynamic and ice dynamic modules were used for the model testing. Testing results did not focus on the hydrodynamics of CRISSP2D because the equations were very similar to River2D.

Two simple domains were developed for the model testing. The first domain was a simple trapezoidal channel and the second was a converging trapezoidal channel. The input parameters that were assessed with the simple trapezoidal channel were the coupling time step between the ice dynamics and the hydrodynamics and the initial ice parcel size. These two parameters were important because they have a large effect on modeling time. Also tested with the simple trapezoidal channel were the ice boom function and the ice parcel stopping velocity. Both were tested to assess their ability to stop ice parcels and form an ice jam. The converging trapezoidal channel was used to study how ice parcels interact in the model with changing channel geometry and to evaluate the effects of the coupling time step and the internal angle of friction on ice parcel consolidation. Attempts were also made to stop the ice in the constriction to form an ice jam.

3.4.1 Simple Trapezoidal Channel Model

The domain of the simple trapezoid channel was designed to illustrate the basic ice processes of the CRISSP2D model and to test the variation in computation time. The simple trapezoidal channel model domain was 1000 m long and had a 0.0001 m/m slope. The numerical mesh for the model was generated using the River2D interface and imported into CRISSP2D. The average node spacing of the numerical mesh was 10 m to try to have between eight and ten elements across the top width of the channel. The number of nodes and elements in the simple trapezoidal channel model were 1564 and 2863 respectively. The Manning's roughness was 0.025.

Figure 3.1 shows the model domain cross-section. A uniform flow depth of 2.5 m was selected for the model runs. This equates to a discharge of $96 \text{ m}^3/\text{s}$ and a water surface top width of 90 m. The dimensions were selected to be similar to the Hay River East Channel and to have a mean channel velocity between 0.5 and 1.0 m/s. Ice parcels were injected at the upstream boundary of the model domain across a width of 40 m, above the horizontal portion of the bed cross section. Ice was injected across less than half of the top width to limit the interaction between the ice and the bed. This helped to ensure that changes in ice thickness and concentration were the result of ice parcel interaction. The hydrodynamic and ice dynamic time steps used for the simple trapezoidal channel model runs were 0.5 s. The initial ice parcel thickness was 0.20 m and the internal friction angle was set at 45° . The ice thickness was selected to keep the expected consolidated ice thickness below one meter. This reduced the chance of a high water surface slopes developing through a thick ice pack and affecting the model stability. Three model inputs were varied to study the effect on the results. The inputs were the coupling time step between the ice dynamics and the hydrodynamics, the initial ice parcel size and the initial ice concentration. Varying the initial ice concentration was found to have no obvious effect on the ice mechanics of the model. Therefore, only results from the 50% ice concentration tests are discussed below. Each model test was run for 7 model hours and the computation time was recorded. The processor speed of the computers used for the modeling varied but the computation times illustrate the general trend. Table 3.1 presents the details of the completed test program and summarizes the computation time results.

Table 3.1 Summary of the analyzed simple trapezoidal channel tests.

| Case # | Initial Ice Parcel Size (m) | Coupling Time Step (s) | Number of Ice Parcels after 7 hr | Computation Time (hrs) |
|---------------|------------------------------------|-------------------------------|---|-------------------------------|
| 1 | 10 | 0.5 | 435 | 5.4 |
| 2 | 10 | 1 | 425 | 4.1 |
| 3 | 10 | 2 | 378 | 0.9 |
| 4 | 10 | 5 | 374 | 0.8 |
| 5 | 10 | 10 | 346 | 0.9 |
| 6 | 10 | 25 | 330 | 0.6 |
| 7 | 10 | 50 | 331 | 0.5 |
| 8 | 10 | 100 | 332 | 0.5 |
| 9 | 10 | 200 | 333 | 0.6 |
| 10 | 2.5 | 5 | 5320 | 18.9 |
| 11 | 5 | 5 | 1372 | 3.2 |
| 12 | 15 | 5 | 165 | 0.9 |
| 13 | 20 | 5 | 98 | 0.8 |
| 14 | 25 | 5 | 65 | 0.7 |

The first set of tests conducted with the simple trapezoidal channel looked at the how the coupling time step between the hydrodynamics and ice dynamics affected the model results and the computation time. The outputs that were examined were the surface ice concentration and the ice discharge. Ice discharge is the flux of ice volume across a section and is specified as a model input indirectly via the surface ice concentration and surface ice thickness. The results are presented as ratios of the coupling time step relative to the hydrodynamic and ice dynamic time steps. Ice discharge was measured at 750 m downstream of the input boundary. This measurement distance was selected in an attempt to maximize the time for ice dynamics to occur while staying away from any potential effects at the downstream boundary. The surface ice concentration was sampled at 4800s

model time. This ensured that the leading ice parcels in most model tests had reached the downstream boundary.

Several relationships were observed from the coupling time tests. Figure 3.2 shows the ice discharge averaged over time for each of the tests. The trend is that as the coupling time step increases, the ice discharge decreases. A plateau occurs at a ratio of approximately 1:50. Comparing the maximum coupling time ratio of 1:400 to the 1:1 ratio, the ice discharge at the maximum coupling time is 19% less than the minimum. Table 3.1 shows a plateau at the same ratio for the number of parcels after 7 model hours. The plateau in the number of parcels is believed to be the cause of the ice discharge plateau. Figure 3.3 shows the ice concentration for each test at 4800s model time. It illustrates that there is more spatial variation in concentration with smaller coupling times. Figure 3.4 reinforces this observation, showing how the mean absolute deviation from the mean ice discharge over time changes with coupling time. There appears to be a plateau in the variation until around approximately 1:50 ratio, after which the mean absolute deviation declines. Table 3.1 presents the relationship between the computation time and the coupling time. Over a 400% increase in computation time is seen when reducing the coupling time step from 2 s to 0.5 s. The difference between a coupling time step of 200 s and 2 s is only a 50% increase.

The second test set looked at the effect of the initial ice parcel size on the ice dynamics and the computation time. The ice parcel size results are presented as ratios of the average mesh node spacing to the initial ice parcel size. The average mesh node spacing used in the model was 10 m. The output parameters that were

considered were the ice discharge and the surface ice concentration, similar to the analysis done on the ice coupling time tests.

Several relationships were documented from the ice parcel size tests. Figure 3.5 shows the ice discharge averaged over time for each test. The trend is that the average ice discharge increases with increasing ice parcel size. Figure 3.6 shows the absolute mean deviation of the ice discharge over time. The trend is that more variation in the ice discharge is seen with smaller ice pans. Figure 3.7 shows the ice concentration at model time five hours and it supports this trend. The initial ice parcel size has a large effect on the computation time. This is due to the rapid increase in number of ice parcels in the model as the ice parcel size is decreased. A plateau in the computation time is seen at a ratio of 1:1. Decreasing the initial ice parcel size from 10 m to 2.5 m increases the number of ice parcels by over 1300 % and increase the computation time by more than 2000 %. The difference in the computation time between an initial ice parcel size of 25 m and 10 m is only 30%.

The final set of tests used the ice boom function and the ice parcel stopping velocity to try to instigate an ice jam. The model inputs matched those of Case 1 in Table 3.1. No guidance was provided in Shen (2005a) or Shen (2005b) for selecting the ice boom parameters or for setting the ice parcel stopping velocity. Several ice boom tests were conducted, starting with the default ice boom parameters in Shen (2005a). Additional ice boom tests were conducted, varying the critical submergence load and the submerged depth of the boom.

Unfortunately, the ice boom did not stop ice parcels under any test conditions

attempted. In the next series of tests the ice parcel stopping velocity was varied from 0.0001 m/s to 0.1 m/s. No effect was seen in the model runs when this velocity was set close to zero. For the model runs with the ice parcel stopping velocity close to 0.1 m/s, the model developed a consolidated ice cover over 10 m thick at isolated locations along the water's and then crashed.

3.4.2 Simple Trapezoidal Channel with a Constriction

The second simple test domain was setup with a constriction to illustrate the effect of changing geometry on the ice processes in the CRISSP2D model. A good understanding of the interaction between the channel shape and ice processes is important because it plays a major role in ice jam formation. The simple trapezoidal channel with a constriction had the same length, slope and bed roughness as the simple (constant width) trapezoidal channel. The initial top width under uniform flow conditions was 90m and the top width converged to 55.1m. This convergence occurs gradually between 250 m and 750 m of channel length. The node spacing of the computational mesh was 5 m. The bottom elevation after the convergence was set so that the water surface remained at the same elevation under uniform flow conditions as with the un-converged cross section.

Ice parcels were introduced across the majority of top width at a concentration of 90% and a thickness of 0.20m. The reason that ice was not injected across the entire top width is to limit the amount of interaction between the bank and ice parcels upstream of the constriction. The total surface ice concentration was

approximately 78%. The hydrodynamic and ice dynamic time steps were set to 0.25 s. Table 3.2 summarizes the model tests that were completed.

Table 3.2 Summary of the simple trapezoidal channel with a constriction model tests.

| Case # | Coupling Time (s) | Internal Friction Angle (°) |
|---------------|--------------------------|------------------------------------|
| 1 | 60 | 45 |
| 2 | 30 | 45 |
| 3 | 5 | 45 |
| 4 | 5 | 40 |
| 5 | 5 | 50 |

The first model parameter that was varied was the coupling time step. The results are presented as ratios relative to the hydrodynamic and ice dynamic time step.

All other model inputs were the same as the previous model tests. The model test goal was to see how the coupling time step affects the ice parcel consolidation.

The ice concentration and ice thickness results were compared after 2400 s model time. Ice concentration and ice thickness results are shown in Figure 3.8. It shows that the ice consolidated further into the constriction with the smaller coupling time steps. The maximum ice thickness also increased, though there is very little difference between the 5 s and 30 s coupling times. The ice concentration reached 100% in Figure 3.8 but did not come to a stop and form an ice jam.

The second parameter that was varied was the internal friction angle of the ice.

The results for ice concentration and ice thickness are displayed in Figure 3.9.

The figures show that the higher the internal angle of friction, the less consolidation that occurs. This results in the consolidated ice pushing furthest

along the channel for the smallest angle. The smallest angle also develops a higher maximum thickness at the head of the consolidation. The ice thickness results in Figure 3.9 shows quite well how the interaction with the model bed along the water's edge causes additional consolidation, as described in the model equations.

3.4.3 Discussion of Results

The results from the CRISSP2D model testing provide important insights into the effects that the model inputs have on the results. The major concern with CRISSP2D was the balance between model accuracy and computational time. Testing on the simple trapezoidal channel showed that both the coupling time and the initial ice parcel size can have a large effect on the computational time. The simple trapezoidal channel testing also showed that both inputs affect the ice discharge and the distribution of ice in the model.

Selecting appropriate inputs for CRISSP2D model of the Hay River is very important because the model domain was an order of magnitude larger than the simple model tests. Shen (2005a) provides some guidance for selecting the coupling time step. It suggests a coupling time step of a few seconds for dynamic processes such as an ice jam release. For thermodynamic ice processes a coupling time step on the order of one thousand seconds is recommended. The simple model testing suggested that a ratio between the hydrodynamic and coupling time step of 1:50 would result in minimal reduction in data accuracy while minimizing the computation time. No guidance for selecting the initial ice parcel size is

provided in Shen (2005a) or in Shen (2005b). The simple trapezoidal channel testing suggests that 1:1 ratio between the average element size and the initial ice parcel size provides a compromise between accuracy and computational time.

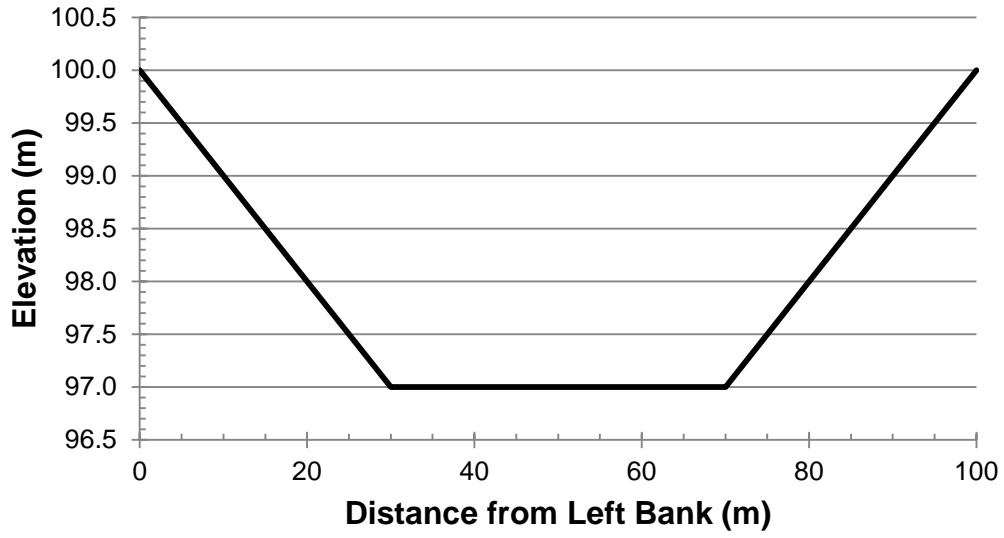


Figure 3.1 Channel cross section of the simple trapezoid channel model.

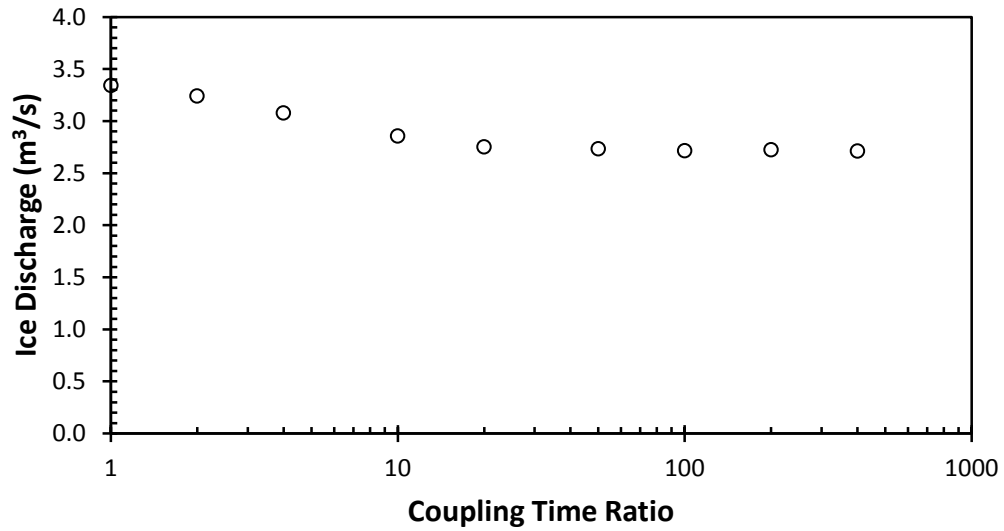


Figure 3.2 Variation of mean ice discharge with increasing coupling time ratios.

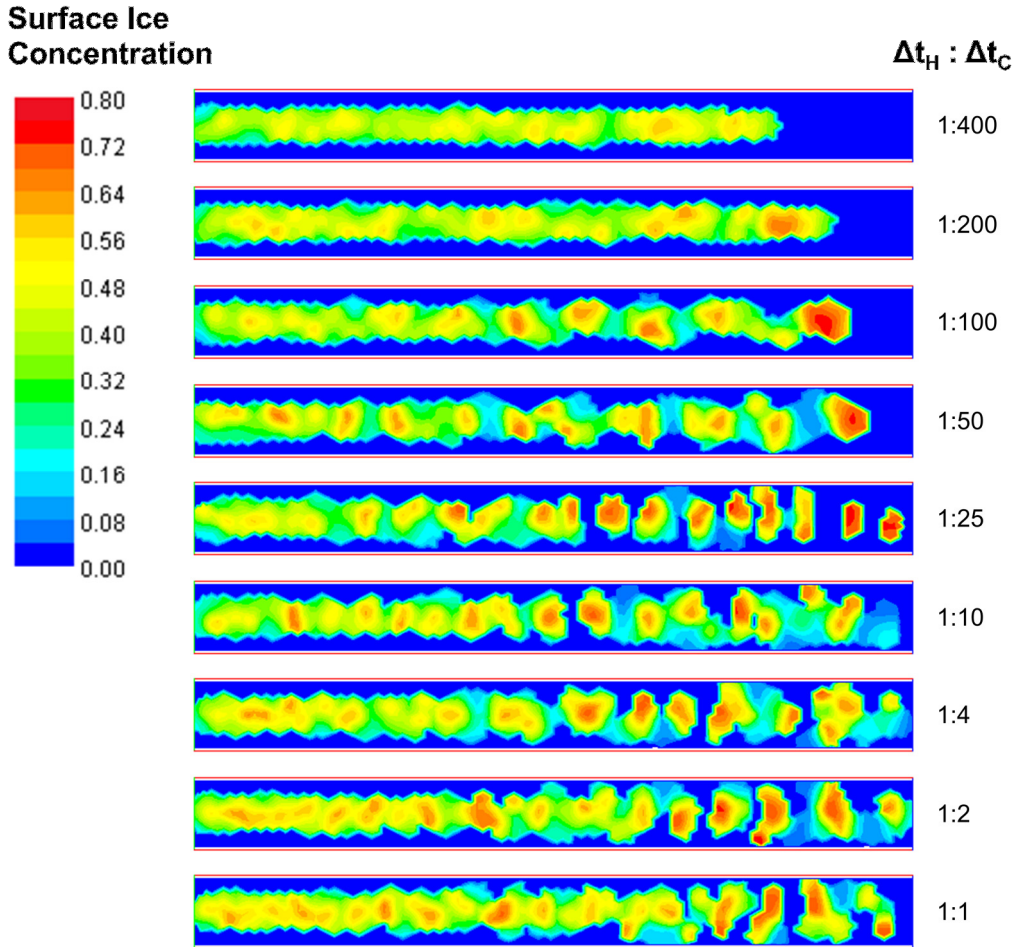


Figure 3.3 Surface ice concentration results with varying coupling time ratios at model time $t = 4800s$.

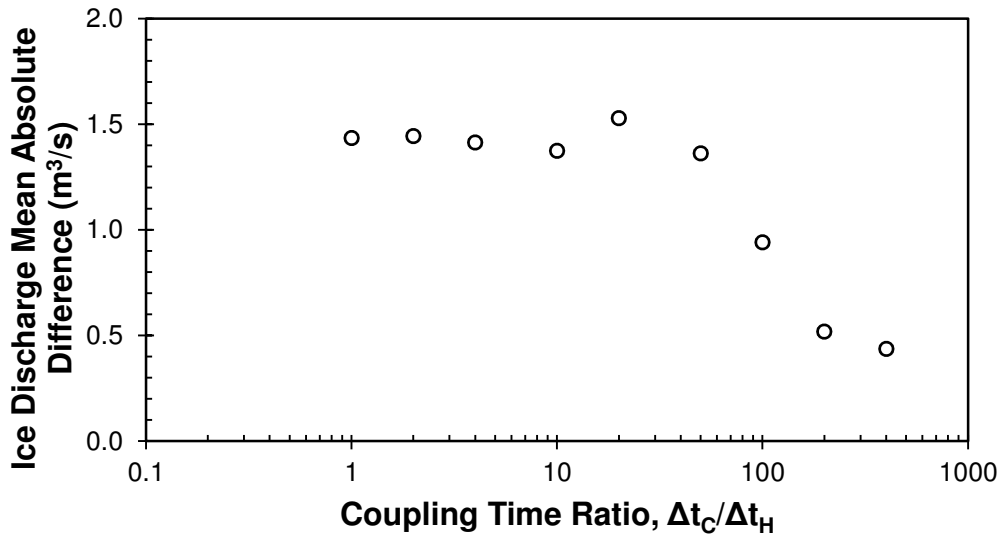


Figure 3.4 Variation of mean absolute mean difference of the ice discharge from the mean with the coupling time ratio.

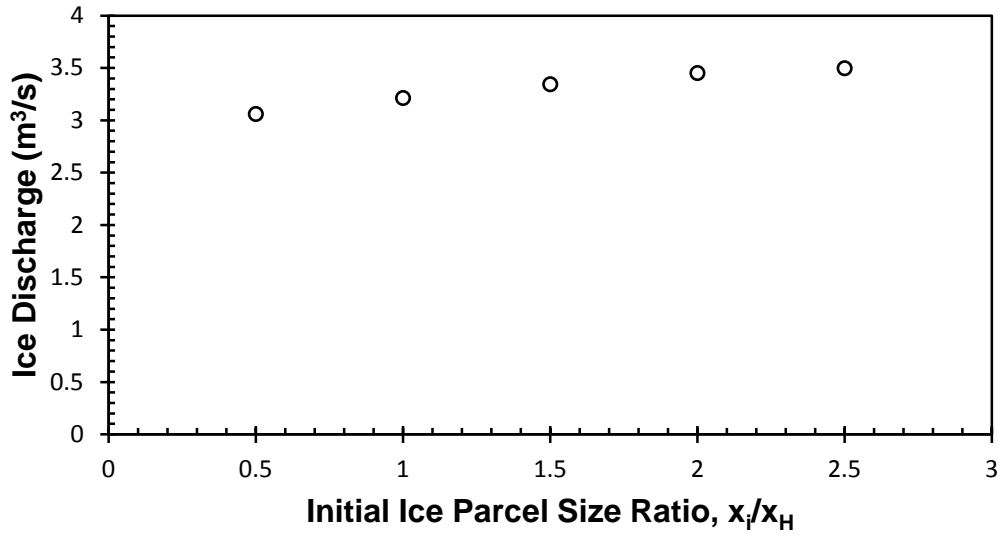


Figure 3.5 Variation of average ice discharge with the initial ice parcel size ratio.

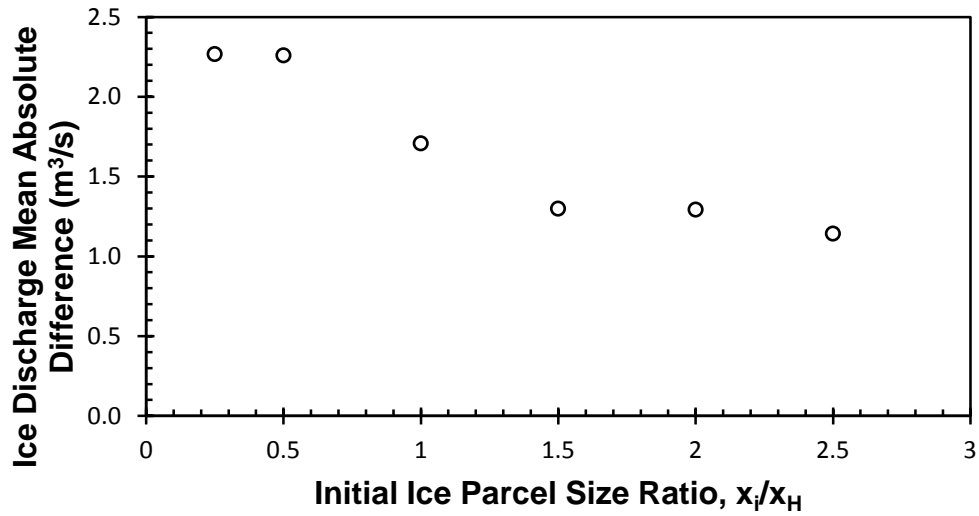


Figure 3.6 Variation of mean absolute mean difference of the ice discharge from the mean with the initial ice parcel size ratio.

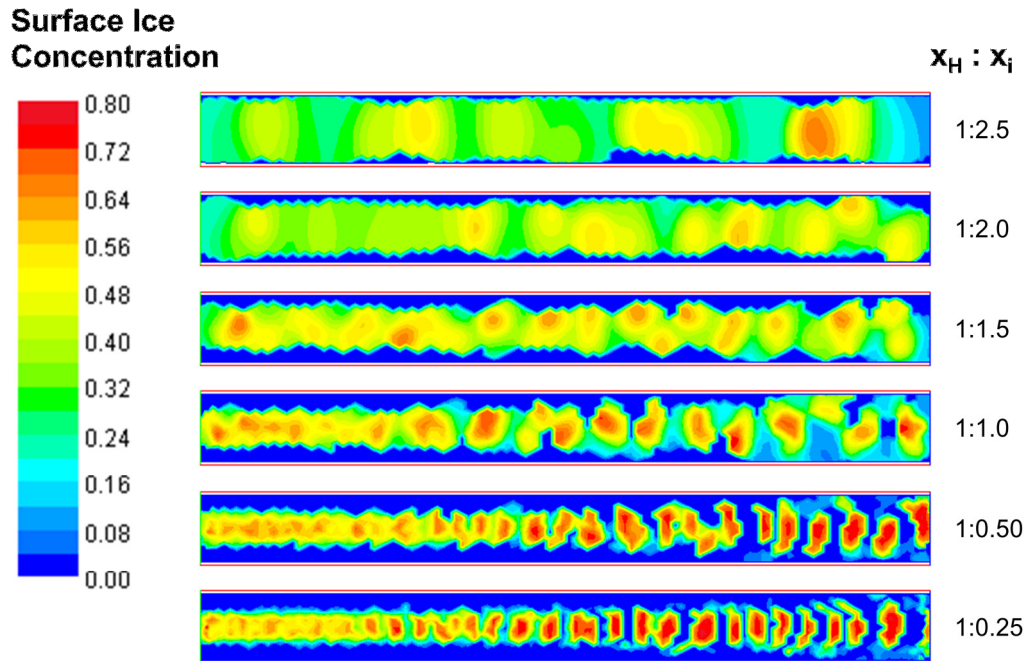


Figure 3.7 Variation of surface ice concentration with the initial ice parcel size ratio at model time $t = 5$ hrs.

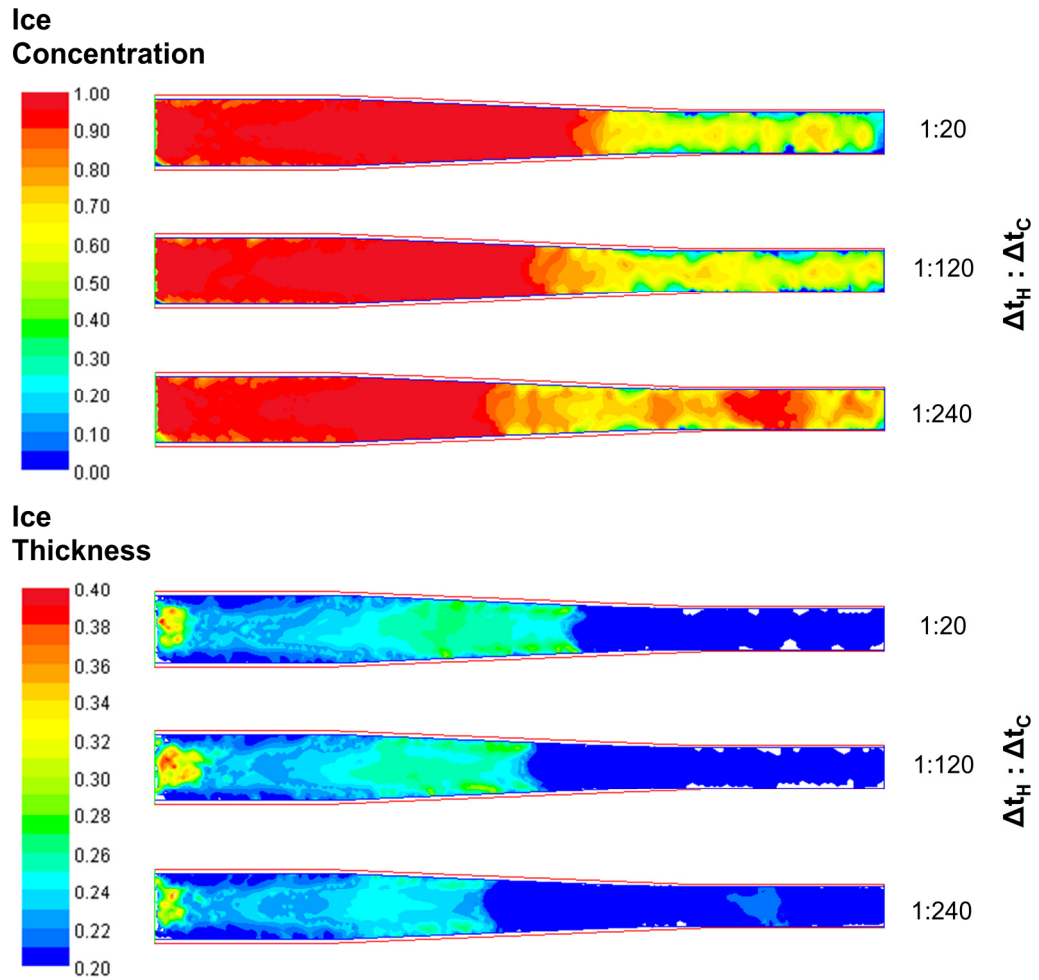


Figure 3.8 Variation of ice thickness and ice concentration with coupling time ratio.

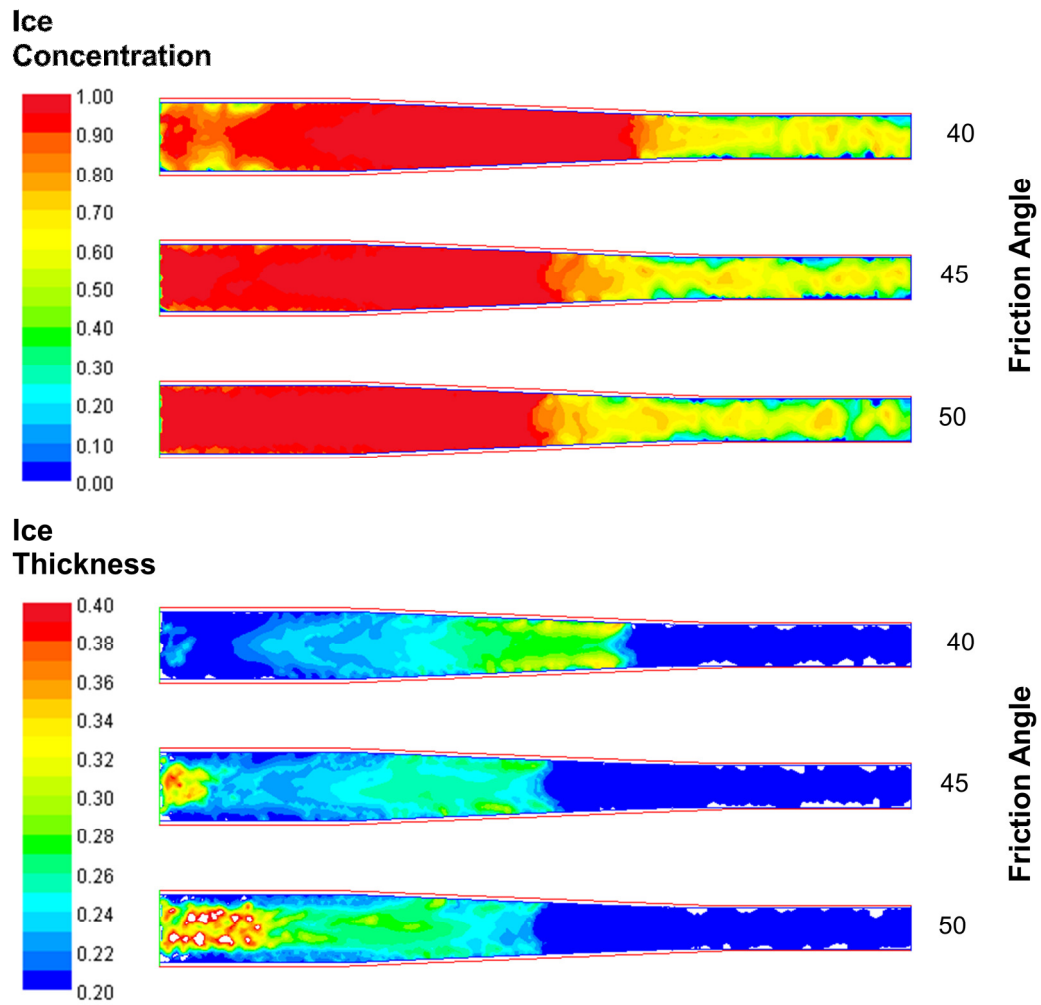


Figure 3.9: Variation of ice thickness and ice concentration with internal friction angle.

4.0 Models' Application to Hay River, NWT⁴

The town of Hay River is threatened by ice jams every spring. To assist town officials with coordinating evacuation efforts, two dimensional models runs of ice jams in the delta were developed in CRISSP2D and River2D. Each model run was developed using data obtained from the field programs. One dimensional models have been used by previous researchers on the Hay River but are unable to accurately model the flow and ice split between the East and West Channels of the delta. Two dimensional models are therefore ideal for the situation.

The modeling effort was broken up into four stages based on the ice conditions of the river. Open water modeling was completed with CRISSP2D and River2D first to calibrate the bed roughness for future model runs. The open water results also provided data to create an open water rating curve for the East West Channel split. The second stage of testing occurred under simple (intact) ice covered conditions. It was necessary to calibrate the intact ice roughness in CRISSP2D for the freeze-up and breakup model runs. Freeze-up modeling was done with CRISSP2D to analyze the sequence of ice formation in the fall and to test the model's ability to match field observations. The final stage of testing was done with both models to see how well each was able to match observed ice jam profiles. River2D was used to model more ice jam profiles than CRISSP2D because River2D has a shorter computation time. Numerous relationships from

⁴ A version of this chapter describing CRISSP2D model testing has been published as a conference paper entitled "2-D Modeling of Ice Processes on the Hay River NWT" by Michael Brayall and Faye Hicks for the 15th Workshop on River Ice in St. John's Newfoundland and Labrador, June 15-17, 2009.

the model data are discussed and to provide insight into the breakup process at Hay River.

4.1 Geometry and Computational Mesh

River2D was used to develop the geometry and the computational meshes based on bed and bank elevation data from the extensive summer field work program. The final bed mesh is often shown as an elevation contour map of the bed and banks and was shown in Figure 2.1. One discharge boundary is in the model domain at the bottom of the figure just upstream of the East-West Channel split. The model has three elevation boundaries: two in the West Channel and one in the East Channel. Two internal boundaries were used around Islands A and B in the East Channel. This was done because the vegetation was too dense on both islands for surveying. This was an acceptable approximation because the islands have only been inundated with ice once in documented events (during the 1963 event). A no-flow boundary was used across the channel between Island C and Island D and Vale Island. This was an acceptable simplification because no flow passes through the two channels and only a small volume of ice accumulates in each channel when ice jam toe forms downstream of Island C.

The computational mesh for the River2D and CRISSP2D models is shown in Figure 4.1. To overcome the node and element limitations of CRISSP2D, care was taken to maximize node spacing and element size while meeting the recommendation by Steffler and Blackburn (2002) to have at least 10 elements across each channel. The domain was divided into regions based on the open

water top width observed during the 2007 summer survey. The node spacing was adjusted in each general region. Figure 4.2 illustrates a variety of node spacing and element sizes at the East-West Channel split. Comparing region 1 to region 2, the elements used in the West Channel were smaller than the elements in the East Channel because it is narrower. Comparing region 1 to region 3, smaller elements were used at the split than in the East Channel to better model the change in flow direction. In the West Channel downstream of the West Channel Bridge, less complex flow patterns were observed. This allowed for the use of slightly elongated triangles, which is seen when comparing region 4 to region 2. Finally, large triangles were used in regions above the expected water elevation, shown in region 5. The total number of nodes and elements used in the model were 7169 and 13057, respectively.

4.2 Open Water Modeling

Open water modeling was important to the study of the CRISSP 2D and River2D models to test and compare the hydrodynamic capabilities of each model. Three goals were accomplished with the open water modeling. The first was the calibration of the bed roughness for future model runs. Both models had to be calibrated separately as CRISSP2D uses Manning's n as a measure of the bed roughness while River2D uses the roughness height, k . A well calibrated model is able to match water surface profiles and velocity profiles obtained from the field. The second goal was the development of a rating curve at the East-West Channel split. The final goal was to establish a relationship between discharge and the

East-West Channel flow split. Only River 2D was used to complete the final two goals as it operates much faster than CRISSP 2D.

Previous modeling of the Hay River provided guidance for the expected range of bed roughness height. Stanley (1988) determined a roughness height of 0.18 m at a discharge of 270 m³/s using HEC-2. Hicks et al. (1992) found that the roughness height on the Hay River could vary between 0.05m to 0.55m. No guidance for selected Manning's *n* values was available on the Hay River for CRISSP2D.

The modeling was conducted under the flow conditions experienced during the August 2005 survey (Phase 1). The important data inputs were the discharge at the upstream boundary and the water elevation at the downstream boundary. The discharge was obtained from the Water Survey of Canada gauge at Hay River. The downstream boundary condition, Great Slave Lake water level and the river discharge (upstream boundary condition) were gathered from the Water Survey of Canada (WSC) gauge data. The hydraulic time step used for the CRISSP2D to maintain model stability was 0.3 s. The remaining model input parameters were the defaults presented in Appendix A. Only the hydrodynamic module was used for the open water testing. The bed roughness calibration was difficult for two reasons. First, the vertical error was larger than ideal due to the use of a total station in the 2005 survey, as discussed in section 2.1. The second problem was that the discharge decreased from 258 m³/s to 160 m³/s over the seven days of surveying.

Model runs were conducted while varying the bed roughness until the modeled water surface profile matched the surveyed water elevations. Figure 4.3 (a) and (b) display the modeled water surface profiles for the East and West Channels respectively at $160 \text{ m}^3/\text{s}$ from both CRISSP2D and River2D and compares them to the surveyed water levels. Figure 4.4 (a) and (b) displays the modeled water surface profile in the East and West Channels at $258 \text{ m}^3/\text{s}$. The Manning's roughness used in CRISSP 2D was 0.025 and the roughness height used in River 2D was 0.05 m. Due to the high vertical error in the water surface profile data (discussed previously), a sensitivity analysis was conducted on the roughness height with River 2D. A similar analysis was not conducted with CRISSP 2D and Manning's n roughness due to the extensive computational time required. Figure 4.5 (a) and (b) displays the water surface profile down the East and West Channels respectively for three tested roughness heights. Comparing the selected roughness height to previous research, it falls in the expected range of values as presented by Hicks et al (1992).

To further validate the model calibration a model was developed to compare to the ADCP velocity profiles from July 2007. Figure 4.6 shows the comparison on the measured and modeled velocities just upstream and downstream of the East-West Channel split. Generally, the modeled velocity profile shape is similar to the measured data from the field. The common difference is that the modeled velocity is higher than the measured velocity in the center of the channel and lower along the banks. The modeled maximum velocity is within 10 and 25 percent of the measured maximum.

Development of an open water rating curve at the East-West Channel split was the second goal of open water modeling. This was done by Gerard and Stanley (1988) using HEC-2, but not with a two dimensional flow model. Several runoff events were selected to develop the rating curve from the WSC record ranging from $160 \text{ m}^3/\text{s}$ to $1350 \text{ m}^3/\text{s}$. Three roughness heights were tested due to differences between the calibrated bed roughness and the bed roughness suggested in previous research. Figure 4.7 shows the computed rating curves and compares them to Gerard and Stanley's work. The shape of the HEC-2 rating curve and the River2D curves are quite different. The slope of the HEC-2 curve is steeper below $300 \text{ m}^3/\text{s}$, but similar above this discharge. A second difference is that above $300 \text{ m}^3/\text{s}$, the water elevation of the HEC-2 rating curve is 0.6 m higher than the River2D rating curve, when comparing the same roughness height. Three reasons were expected to account for the differences between the rating curves. The first expected reason is that survey accuracy has increased tremendously since Gerard and Stanley's work. Figure 4.8 compares the cross section just upstream of the East-West Channel split from Gerard and Stanley (1988) and Meliefste and Hicks (2006). The two cross sections are very similar and prove that survey error is not the reason for the difference between the ratings curves. The second reason is that Gerard and Stanley developed the rating curve using potentially erroneous discharge data (Jasek, 1993). The third reason for the error then is that a two dimensional model such as River2D more accurately models the flow split between the East and West Channels.

The final goal of open water modeling was to determine the variation in flow split between the East and West Channel as a function of discharge. The data was extracted from the River2D models used to develop the open water rating curve and a similar sensitivity analysis was also conducted. Figure 4.9 shows the relationship between flow split and discharge and its sensitivity to model bed roughness. One validation point was available from ADCP measurements in 2007 and it agrees with the modeled flow split extremely well.

4.3 Ice Cover Modeling

Modeling under ice covered conditions was done with CRISSP 2D to determine a Manning's roughness for intact ice (n_i). Three CRISSP2D modules were used to calibrate the ice roughness. The breakup module was used to generate an intact ice cover but not used to instigate an ice run. The hydrodynamic and ice dynamic modules modeled the interaction between the stationary ice and the water flow. The required data for model input were the inflow discharge, the downstream water elevation and the ice thickness. The bed roughness of 0.025 was used, based on the open water calibration. The top of ice profile from 28-Apr-08 was selected for the modeling. The ice thickness distribution in the delta was obtained from a survey conducted by the town of Hay River in early April, 2008. The downstream water elevation was obtained from the Great Slave Lake WSC gauge. A discharge measurement was conducted by WSC on 14-Apr-08. The discharge was $10.8 \text{ m}^3/\text{s}$. In order to estimate the discharge on 28-Apr-08, the change in water level at the WSC gauge at Hay River was determined. On 16-Apr the stage

was 2.06m and on 26-Apr it was 2.24m. This is an elevation difference of 0.18 m.

The model was run for several discharges and compared to the WSC measurement of $10.8 \text{ m}^3/\text{s}$ to estimate the change in discharge between the dates. Two ice roughnesses were used to test the sensitivity of the model results. Table 4.1 presents the resulting upstream boundary water elevations for each model configuration. The difference between the $10 \text{ m}^3/\text{s}$ models and the $20 \text{ m}^3/\text{s}$ and $30 \text{ m}^3/\text{s}$ models for both roughness values were compared. Table 4.1 shows that the water elevation difference between $10 \text{ m}^3/\text{s}$ and $20 \text{ m}^3/\text{s}$ for both model roughnesses is greater than the 0.18 m water elevation increase observed at the WSC gauge. This indicates that the discharge at the time of the survey should be between $10 \text{ m}^3/\text{s}$ and $20 \text{ m}^3/\text{s}$. Figure 4.10 shows the top of ice profile for $20 \text{ m}^3/\text{s}$ for an ice roughness of 0.020. The model results match the surveyed profile.

Table 4.1 Intact ice cover results for a range of inflow discharges and ice roughness values.

| Discharge (m ³ /s) | n _i | Upstream Boundary Water Elevation (m) | Water Elevation Difference (m) ⁵ |
|-------------------------------|----------------|---------------------------------------|---|
| 10 | 0.015 | 157.14 | - |
| 20 | 0.015 | 157.50 | 0.36 |
| 30 | 0.015 | 157.70 | 0.56 |
| 10 | 0.020 | 157.22 | - |
| 20 | 0.020 | 157.53 | 0.33 |
| 30 | 0.020 | 157.73 | 0.53 |

4.4 Freeze-up Modeling

Freeze-up modeling was done with CRISSP2D to test its ability to model freeze-up processes in the Hay River delta. Freeze-up testing was done before breakup testing for two reasons. The first reason was because the ice dynamics during freeze-up are less complex than during breakup. The second reason is because freeze-up observations from 2008 showed similar ice movement patterns to those that have been observed during breakup. Therefore, freeze-up modeling provided insight into the distribution of ice runs entering the delta during breakup. Three CRISSP2D modules were used for the freeze-up modeling. The thermal module generated border and frazil ice in the model. The ice dynamic module introduced ice pans from upstream. The hydrodynamic and ice dynamic modules modeled the interaction between the pans, the stationary ice and the flow.

CRISSP2D model input data was specified based on freeze-up observations from 28-Oct-08. Table 4.2 presents the important model inputs. Typically

⁵ The difference in the modeled water elevation when compared to the model results with a discharge of 10 m³/s and the same ice roughness.

measurements would be made to calibrate the energy exchange between the air and the water. This was not done because the focus of the freeze-up testing was to model the ice pan movements. Therefore default values were used for the remaining inputs and can be found in Appendix A. The model was run for one hour before ice was injected along the right bank upstream of the East-West Channel split. This ice inflow distribution was chosen to be similar to what was observed (Figure 2.7). Each parcel had an initial ice concentration of 80% and an ice thickness of 0.20m⁶. The model was run until the ice cover concentration in the delta reached approximately 100%. This took around 4.5 hours model time to occur. One problem encountered during modeling was that injected ice parcels were pushing through the border ice growth across the channel width and exiting out the downstream boundary. This problem was overcome by increasing the ice internal friction angle from 45° to 75°. An internal friction angle of 75° is much higher than internal friction angles from the literature but it was necessary to achieve accurate modeling results.

⁶ The University of Alberta research group measured ice pan thicknesses of 20 to 50 cm on the North Saskatchewan River in 2009 and 2010. 20 cm was chosen for the Hay River since it is substantially smaller and shallower than the North Saskatchewan.

Table 4.2 CRISSP2D model input values for freeze-up modeling.

| Input File | Input Parameter | Abbreviation | Value | Unit |
|----------------------|--|---------------------|--------------|-------------------|
| Boundary Flux | upstream discharge | qbt | 140 | m ³ /s |
| Boundary Elevation | downstream water elevation | hb | 156.834 | m |
| Water Temperature | inflow water temperature | twbc | 0 | °C |
| Weather | ambient air temperature | tair | -10 | °C |
| Time Control | hydrodynamic simulation time step based on the CFL condition | deltath | 0.35 | s |
| | ice dynamic simulation time step | deltati | 0.35 | s |
| | coupling time step between the hydrodynamics and the ice dynamics | tintvl | 60 | s |
| Geometry Information | bed Manning's roughness coefficient | cnn(i) | 0.025 | |
| Ice Flux information | maximum concentration of ice parcels | anmax | 0.99 | |
| | initial concentration of each parcel | an0 | 0.8 | |
| | initial ice parcel edge length | hpi0 | 20 | m |
| | initial surface ice thickness of each parcel | thi0 | 0.2 | m |
| | Manning's roughness coefficient of single ice layer | cni | 0.02 | |
| Physical Parameters | probability of deposition of frazil particles reaching the surface layer for open water | theta0 | 0.8 | |
| | probability of deposition of frazil particles reaching the surface layer under ice cover | theta1 | 0.8 | |
| | coefficient of re-entrainment of surface ice into suspension per unit area | beta1 | 0.2 | |
| | maximum concentration of frazil ice parcel from suspended layer to surface layer | anmaxfra | 0.99 | |
| | minimum water depth | htmin | 0.2 | m |

The model results were analyzed at several different output times and compared to 2008 freeze-up observations. Figure 4.11 shows the model results after ten minutes. Thermal ice developed in the downstream end of both channels where the flow velocity was low. The regions of 100% ice concentration in Figure 4.11 at the downstream end of the model have an ice thickness just above zero. An ice thickness just above zero has little physical significance but is necessary for initiating thermal ice growth. Comparing Figure 4.11 to Figure 2.5, the model does an adequate job of modeling the extents of thermal ice growth in the East Channel. Results in the West Channel are less promising. Thermal ice growth was observed only in the Fishing Village Channel shown in Figure 2.6, but the model developed thermal ice in both the Rudd and Fishing Village Channel. Figure 4.11 also shows thermal ice formation into the main stem of the West Channel, up to km 1109.

Ice parcels were injected at the upstream boundary after one hour of modeling. Figure 4.12 displays the results after 1.5 hours of modeling and shows the ice parcels going down the East Channel. The ice parcels moved down the East Channel first, stopping and consolidating against the thermal ice growth. The stopping front moved upstream to the East-West Channel split and parcels began going down the West Channel. This is similar to what was observed in the field, shown in Figure 2.7. Figure 4.13 shows the final model output with a 100% ice concentration.

The final top of ice profile from the freeze-up model run was compared to the profile measured on 26-Apr-09. The comparison is shown in Figure 4.14. The

maximum error in the modeled profile is 0.8 m at the East-West Channel split. Field observations from 2008 showed hydraulic thickening occurring down the East Channel. This is illustrated in Figure 2.7. The large error suggests that the model was unable to hydraulically thicken the ice pack against the thermal ice in the East Channel. This was not possible because the high internal friction angle limited the ice consolidation.

4.5 Breakup Modeling

Breakup modeling was done with both the CRISSP2D and River2D models to test their ability to match observed top of ice profiles from past breakup events. The ability of the CRISSP2D model to create jams in the correct locations was also tested.

4.5.1 CRISSP 2-D

The objective of the CRISSP2D model testing was to see if it was capable of forming an ice jam with only boundary conditions as inputs and to see how well the modeled ice jam profiles compared to surveyed profiles. A total of four models runs were conducted, based on an ice jam profile from 2008 and three ice jam profiles from 2009. Table 4.3 presents the common CRISSP2D model inputs in each model run. Appendix A contains the remaining default model inputs.

Table 4.3 CRISSP2D model input values for breakup modeling.

| Input File | Input Parameter | Abbreviation | Value | Unit |
|----------------------|---|---------------------|--------------|-------------|
| Time Control | hydrodynamic simulation time step based on the CFL condition | deltath | 0.2 | s |
| | ice dynamic simulation time step | deltati | 0.2 | s |
| | coupling time step between the hydrodynamics and the ice dynamics | tintvl | 60 | s |
| Geometry Information | bed Manning's roughness coefficient | cnn(i) | 0.025 | |
| Ice Flux information | maximum concentration of ice parcels | anmax | 0.99 | |
| | initial concentration of each parcel | an0 | 0.8 | |
| | initial ice parcel edge length | hpi0 | 20 | m |
| | initial surface ice thickness of each parcel | thi0 | 1.0 | m |
| | Manning's roughness coefficient of single ice layer | cni | 0.02 | |

The CRISSP2D user manual suggests that the model is able to form an ice jam without specifying the ice jam toe location. Therefore, the goal of the first model simulation was to see whether CRISSP2D could form an ice jam in the typical location at river km 1111.0 in the East Channel. The model was based on data collected on 5-May-08. The boundary conditions are provided in Table 2.2 and the initial intact ice thicknesses were obtained from the late winter survey done by the Town of Hay River. The intact ice was released into an ice run using the breakup module. Additional ice was injected at the upstream boundary, mimicking an incoming ice run. The model was run until the accumulated ice thickness reached a point of equilibrium. Figure 4.15 presents ice thickness and concentration after the model had stabilized. Notice the increase in ice thickness around river kilometer 1111 in the East Channel. These results match what has been observed in the field quite well. However, no ice parcels came to a stop in the model to form an ice jam. As a result, it was decided that CRISSP 2-D could not form an ice jam without forcing the toe location with the default model inputs.

Three methods for instigating an ice jam toe were tested. The first method was to use an ice boom at river km 1111.0. Section 3.3.1 presented the preliminary ice boom tests. Several tests were conducted to see if the ice boom would be able to instigate an ice jam in the Hay River model, but all were unsuccessful. The second method tested was to use the ice parcel stopping velocity. Using the ice parcel stopping velocity caused the model to crash, similar to the results in Section 3.3.1. The final method tested to force an ice jam toe was to leave a portion of the ice cover intact using the breakup module. The hypothesis was that

the model would accumulate incoming ice floes against the upstream edge of the intact ice and form an ice jam.

Four ice jam model runs were setup based on data collected during the 2008 and 2009 breakup monitoring programs. The selected top of ice profiles for the model runs are shown in Table 4.4. The upstream and downstream boundary conditions for each model are provided in Table 2.2. The East, Fishing Village and Rudd Channels were each divided into an upstream reach and a downstream reach. The ice cover in the upstream reach of both channels was specified to release into an ice run using the breakup module. The ice in the downstream reach was specified to remain intact. Table 4.4 documents the model input boundary conditions and the location of the transition from an ice run to intact ice in the East and Fishing Village Channels. Exact stopping locations were not provided in the Rudd Channel because survey profiles were not dense enough to establish the exact jam toe location. The jam toe location was assumed to be 50 m upstream of the model downstream boundary.

In each model test, the ice run specified in the upstream reach of each channel consolidated against the upstream edge of the intact ice. Ice parcels were injected at the upstream boundary to simulate an incoming ice run. In initial testing the upstream ice run was continuous. Problems were encountered because the incoming ice run would reach a surface ice concentration of 100% in the whole model domain and consolidate into a thick ice cover at the upstream end of the reach. This large ice accumulation at the upstream boundary did not match field observations and also caused the model to crash as the flow area under the ice

reduced to zero. To overcome this problem, a series of incoming ice runs, each 30 minutes in duration and followed by 30 minutes zero ice inflow, were introduced. This allowed the ice run to consolidate into the existing ice pack. Incoming ice runs were continued until the surface ice concentration in the model domain was 100% and no changes in ice thickness were observed during the 0.5 hours of open water flow.

Table 4.4 Summary of CRISSP2D ice input conditions and model run results.

| # | Date | Location of intact ice-ice run transition (km) | | Max Difference between modeled and surveyed top of ice profile(m) | | Max Ice Thickness (m) | | Profile Figure # |
|----|----------|--|-------------------------|---|--------------|-----------------------|--------------|------------------|
| | | East Channel | Fishing Village Channel | East Channel | West Channel | East Channel | West Channel | |
| 6 | 5-May-08 | 1111.1 | - | -2.2 | - | 2.5 | - | Figure 4.16 |
| 8 | 3-May-09 | 1111.0 | 1110.0 | -2 | -1.4 | 2 | 1.1 | Figure 4.17 |
| 9 | 4-May-09 | 1111.4 | 1112.4 | -1.8 | -1.8 | 2.5 | 1.6 | Figure 4.18 |
| 10 | 5-May-09 | 1111.9 | 1112.2 | -1.9 | -1.6 | 2.8 | 1.8 | Figure 4.19 |

The final top of ice profiles of each model run were compared to top of ice surveys. Common to Figure 4.16 through Figure 4.19 is that the modeled top of ice profiles were consistently below the surveyed top of ice profiles. Table 4.4 presents the maximum differences between the survey and each model run for both the East and the West Channels. Also shown in Table 4.4 is the maximum consolidated ice thickness in the model for each event. The reason that the modeled profiles are below the surveyed profiles is that the water level does not rapidly increase through the ice jam toe. This is believed to be the result of two contributing factors. The first is that the model is unable to recreate a realistic ice jam toe thickness. The second reason is that the default maximum ice roughness in the ice jam may not be high enough.

Several input parameters were varied to see if the modeled water level could better match the surveyed profiles. The 5-May-09 event was selected for the model tests for two reasons: first, the top of ice survey spanned the length of the model in both East and West Channels; and second, the ice jam toes in both the East and Fishing Village Channels were well documented with aerial photographs. The first test was to increase the maximum Manning's ice roughness coefficient for ice jams from the default value of 0.06 to 0.10. Figure 4.20 shows that the model results with the default value of 0.06 and the tested value of 0.10 are almost identical. The second test was to decrease the initial ice parcel size from 20 m to 10 m. Figure 4.21 compares the computed profiles for the two modeled initial ice parcel sizes to the survey data; the results are nearly identical. The third test was to decrease the coupling time between the

hydrodynamics and the ice dynamics from 60 s to 30 s. As Figure 4.22 shows, again the model results are nearly identical. The final test done in an effort to improve the match between the surveyed and the modeled top of ice levels was to decrease the internal friction angle of the ice parcels from 45° to 40° . Figure 4.23 compares the model results to the surveyed top of ice profiles. Small improvement in the top of ice elevation occurs when the internal friction angle was decreased. However, the model was still unable to reproduce the distinct ice jam toe shape that was surveyed.

4.5.2 River 2-D

4.5.2.1 Model Setup and Results

The objective of the River2D breakup modeling was to determine whether it could effectively match observed top of ice profiles. Eleven profiles were selected for River 2-D modeling. Each model run required upstream and downstream boundary conditions and an ice input file. The upstream and downstream boundary conditions for each model run were presented in Table 2.2. The ice input file contains the ice thickness and roughness throughout the reach. Both the ice thickness and the ice roughness are unknown and cannot be calibrated independently. There are numerous combinations of ice thickness and ice roughness that could match the observed top of ice profiles. For the model runs, the ice roughness was set based on past research and the ice thickness was adjusted to match the observed top of ice profiles. A model run was not developed for the largest ice jam flood on record, 1963, for two reasons. First, the West Channel Bridge had not been completed yet and there was still a dyke across

the channel width. Time was not available to develop a new model geometry. Second, no discharge measurement was available for the upstream boundary condition of the model.

A unique ice input file was generated for each model run based on field observations. The first step was to estimate the position of the ice jam toe based on the most downstream location of ice movement in the East, Fishing Village and Rudd Channels. In some of the top of ice profiles, the survey captured points upstream and downstream of the most downstream ice movement. In several years, no profile data was collected in the vicinity of the most downstream ice movement, so the location had to be approximated from written records and aerial photographs. Each channel was divided up into three ice thickness regions. Moving in the upstream direction, they were: the intact ice region, the ice jam toe region, and the ice accumulation region. The intact ice region had an ice roughness height of 0.1 m. River2D has difficulty modeling a proper ice jam toe (section 3.2) so a region of high uniform thickness was employed in ice jam toe region. The length of this region was two channel widths long. This was selected based on the average length of the region in each surveyed ice jam where the top of ice slope was at its maximum. The location and length of the ice jam toe region for each model run is shown in Table 4.5. Stanley (1988) used an ice jam roughness height of 1.1 m to model past Hay River ice jams. A roughness height of 1.0 m was used for the River2D model runs. The ice accumulation region upstream of ice jam toe region was modeled as a uniform thickness with the same ice roughness as the ice jam toe region.

Two special ice jam configurations were required to match the top of ice survey of several of the model runs. In several of the top of ice profiles, the ice jam toe region pushed beyond river km 1111.0 in the East Channel and stopped before the mouth of the channel. In order to match the surveyed top of ice profile, a secondary ice jam toe region was required in the vicinity of river km 1111.0. The ice thickness in the secondary ice jam toe region is shown in brackets in Table 4.5. In several of the top of ice profiles, the ice jam toe region was at the mouth of the East or West Channels and beyond the downstream boundary of the model. For this situation, no thickness of the ice jam toe region is provided in Table 4.5. As well, no intact ice region exists so no thickness is provided. These events were modeled with only an ice accumulation region and a secondary ice jam toe region, when required.

Each River 2D model run was started under open water conditions and the ice cover thickness was added in increased in discrete steps until the top of ice profile matched the surveyed profile. An ice cover was added incrementally to ensure that the ice did not become grounded and cause the model to become unstable (Section 3.2). The initial conditions for each increase in ice thickness were from the previous ice thickness steady state solution. The model was then run until a new steady state solution was achieved. Care was taken to increase the ice thickness only in regions where the ice sheet was not close to becoming grounded. For example, the ice thickness in the ice jam toe region would be thicker over the channel thalweg than along the water's edge.

Table 4.5 Summary of River2D model run ice inputs and the corresponding top of ice profile figure numbers.

| # | Intact Ice Region | | Ice Jam Toe Region | | | | | | | | | Ice Accumulation Region | | Profile Figure # |
|----|-------------------|------|--------------------------|---------|---------|--------------------|------|------|-------------------|------|------|-------------------------|------|------------------|
| | | | Downstream Location (km) | | | Region Length (km) | | | Ice Thickness (m) | | | | | |
| | Thickness (m) | | East | West | | East | West | | East | West | | Thickness (m) | | |
| | East | West | | FVC | Rudd | | FVC | Rudd | | FVC | Rudd | East | West | |
| 1 | 0.7 | 0.7 | 1112.23 | 1112.00 | 1111.85 | 0.48 | 0.38 | 0.13 | 5 | 4.5 | 4.5 | 4.0 | 2.0 | Figure 4.24 |
| 2 | 0.5 | 1.0 | 1110.68 | 1112.50 | 1111.85 | 0.60 | 0.38 | 0.13 | 2.4 | 1.8 | 1.8 | 2.0 | 1.2 | Figure 4.25 |
| 3 | 1.0 | 1.0 | 1111.50 | 1111.28 | 1111.28 | 0.60 | 0.14 | 0.14 | 5 | 3.0 | 3.0 | 3.5 | 3.0 | Figure 4.26 |
| 4 | 0.5 | 0.5 | 1111.10 | 1112.18 | 1111.87 | 0.60 | 0.29 | 0.12 | 3.5 | 2.0 | 2.3 | 1.8 | 1.8 | Figure 4.27 |
| 5 | 0.5 | 1.0 | 1112.70 | 1111.88 | 1111.87 | 0.35 | 0.32 | 0.12 | 3.0 (5.0) | 2.5 | 2.5 | 2.5 | 2.0 | Figure 4.28 |
| 6 | 1.0 | - | 1111.05 | - | - | 0.60 | - | - | 4.0 | - | - | 3.0 | 3.0 | Figure 4.29 |
| 7 | - | - | - | - | - | - | - | - | (5.0) | - | - | 2.5 | 3.0 | Figure 4.30 |
| 8 | 1.0 | 1.0 | 1111.00 | 1110.00 | 1110.00 | 0.60 | 0.20 | 0.20 | 3.5 | 3.0 | 3 | 1.5 | 1.5 | Figure 4.31 |
| 9 | 1.0 | 1.0 | 1111.36 | 1112.43 | 1111.94 | 0.60 | 0.38 | 0.13 | 3.8 | 3.5 | 2.5 | 1.9 | 1.9 | Figure 4.32 |
| 10 | 1.0 | 1.0 | 1111.94 | 1112.21 | 1111.97 | 0.60 | 0.32 | 0.11 | 4.0 (4.5) | 3.3 | 2.7 | 1.5 | 1.5 | Figure 4.33 |
| 11 | - | 1.0 | - | 1112.46 | - | - | 0.30 | - | (4.5) | 2.5 | - | 2.0 | 2.0 | Figure 4.34 |

4.5.2.2 Analysis

The River2D ice jam model runs were useful for comparing to past modeling work and for establishing new relationships. The results were compared to previous modeling research in Stanley (1988). A big advantage of the River2D modeling over past work is its ability to model the East-West Channel flow split. The relationship between the discharge and the location of the ice jam toe was also analyzed. Finally, the volume of ice in each modeled ice jam was compared to the total volume of ice in the Hay River.

River2D modeling enabled the comparison of water elevations at two locations to one dimensional modeling completed by past researchers. Stanley (1988) presented a rating curve at the West Channel split (river km 1111.0) for a fully developed ice jam at the West Channel mouth. Figure 4.35 compares the model results to the rating curve in Stanley (1988). The rating curve is generally lower than the River2D model results and the maximum difference is 2m. Caution should be used when making this comparison because Stanley assumed a fully developed jam at the West Channel mouth. This is not the case with several of the River2D model water elevations.

The River2D model results were compared to a second rating curve at the West Channel bridge (river km 1108.5). It was presented in Gerard and Stanley (1988) for a fully developed jam. Jasek (1993) analyzed the discharge and identified an error in discharge measurements used to develop Gerard and Stanley's rating curve. Figure 4.36 presents Gerard and Stanley's (1988) rating curve and Jasek's

(1993) updated discharge data and compares it to the River2D model results. The rating curve agrees very well with the River2D modeled water elevations.

Breakup in 2008 and 2009 were special to the record on the Hay River because the ice jams in the East Channel pushed down to the mouth of the channel. Historically this ice jam configuration has resulted in the most severe flooding for houses and businesses along the East Channel (i.e. in 1963). Stanley (1988) developed a rating curve for an ice jam at the mouth of the East Channel⁷. Figure 4.37 shows their rating curve and includes the water levels measured from 1963, 2008 and 2009. The discharge down the East Channel in 2008 and 2009 was determined from these River 2-D modeling results. Figure 4.37 illustrates very good agreement between Stanley's rating curve and the top of ice measurements from 2008 and 2009.

The River2D breakup modeling provided a relationship between the total discharge and the East-West Channel discharge split. Figure 4.38 shows modeled relationship between the total discharge and the East Channel discharge as a percentage of the total under open water and ice covered conditions. The trend between the East Channel discharge percentage and the total discharge under ice covered conditions is quite poor in contrast to the open water relationship. The discharge split ranges between 63% and 74%, if the lowest discharge point is neglected. Figure 4.39 illustrates the relationship between the total discharge and

⁷ There is still some confusion whether the discharge data Stanley used to develop his rating curve is correct or not.

the East Channel discharge. The correlation is much stronger between the discharge magnitudes than the discharge percentage. Figure 4.39 allows for a relatively accurate prediction of the discharge split if the total discharge is known.

Two correlations were investigated concerning the ice movement and the discharge. The first was an assessment of the maximum downstream extent of ice movement in both the East and West Channels related to the total discharge. The results for the East Channel are shown in Figure 4.40. The higher the total discharge, the further downstream ice movement is seen in the East Channel. The graph shows that a discharge greater than approximately $600 \text{ m}^3/\text{s}$ is necessary for the ice jam to develop downstream of the typical location at river km 1111.

Unfortunately the correlation is not strong, so no predictions can be made ($R^2 = 0.50$). A similar graph for the Fishing Village Channel jams is shown in Figure 4.41. In the West Channel the downstream extent of ice movement in Fishing Village Channel appears to be independent of discharge. A similar plot was not done for the Rudd Channel because survey the survey detail of Rudd Channel ice jams is poor.

The final analysis that was done compared the estimated ice volume before breakup in the Hay River and the ice volume in the final surveyed top of ice profile from each year. The ice volume in the river was estimated using the final ice thickness measurement from each year in the delta and calculating the river surface area from the Alberta Northwest Territories Border. The ice volume was extracted from each model run. The ice volume was increased if the ice jam toe was beyond the downstream model boundary. Aerial photos were used to

estimate the volume of ice that escaped into Great Slave Lake. Unfortunately, little information about the lateral extent of ice spreading on Great Slave Lake is available from breakups before the 2008 monitoring program, so corrections could not be reliably applied to these years. Figure 4.42 shows the results. The data is enveloped by the 50% melt line and indicates that over 50% of the ice from the border has either become stranded on land or melted by the time it reaches the Hay River delta. An example of stranded ice from the 2009 breakup is shown in Figure 4.43.

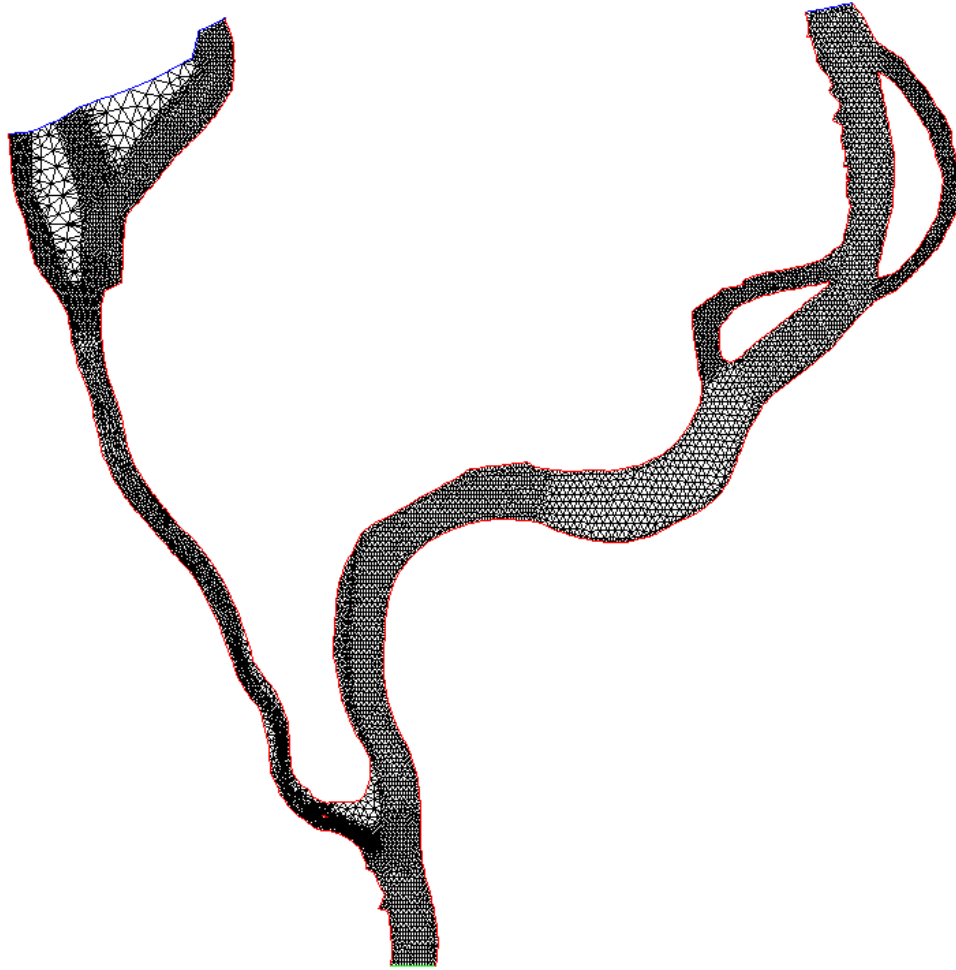


Figure 4.1: The computational mesh for the River2D and CRISSP2D models of the Hay River.

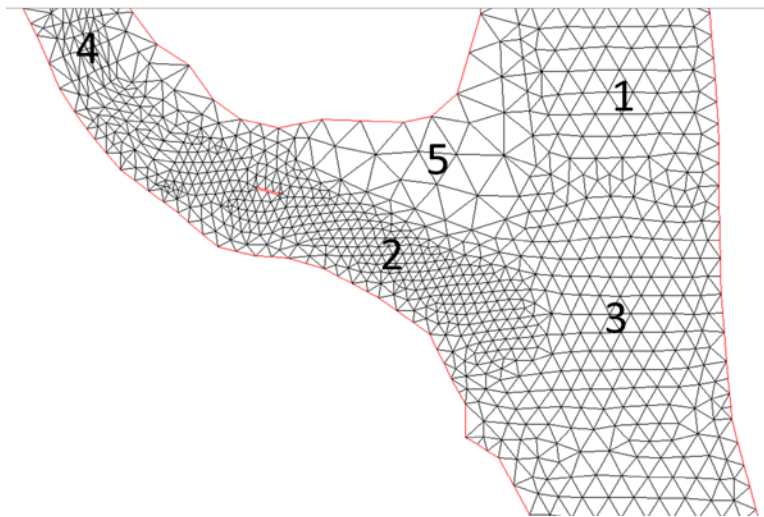


Figure 4.2: The computational mesh at the East-West Channel split illustrating techniques used to minimize the number of elements and nodes in the model.

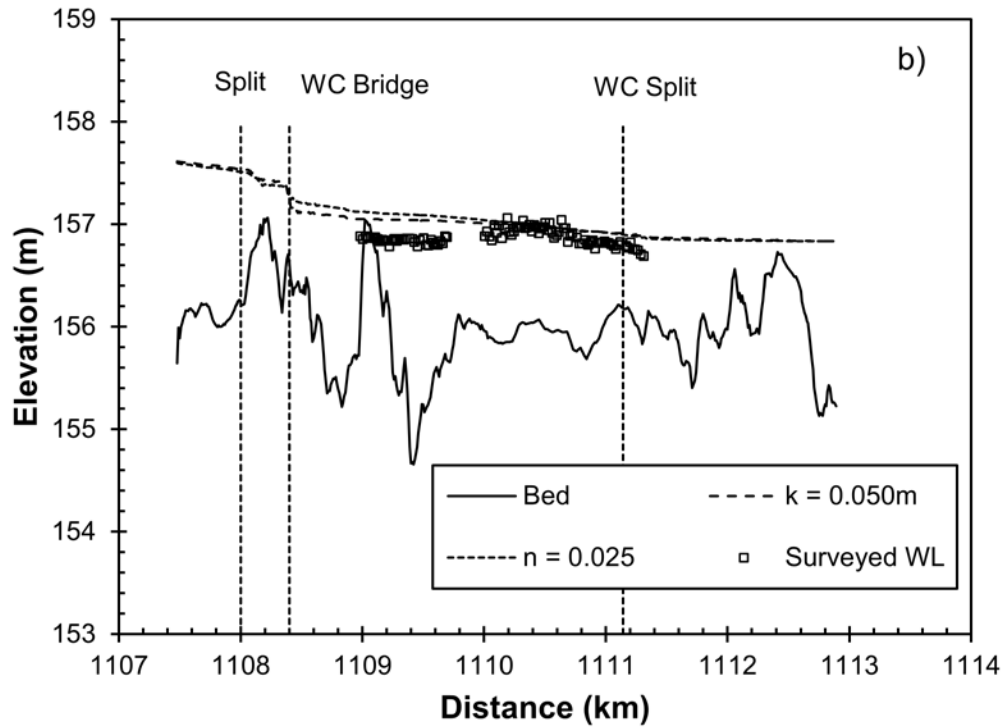
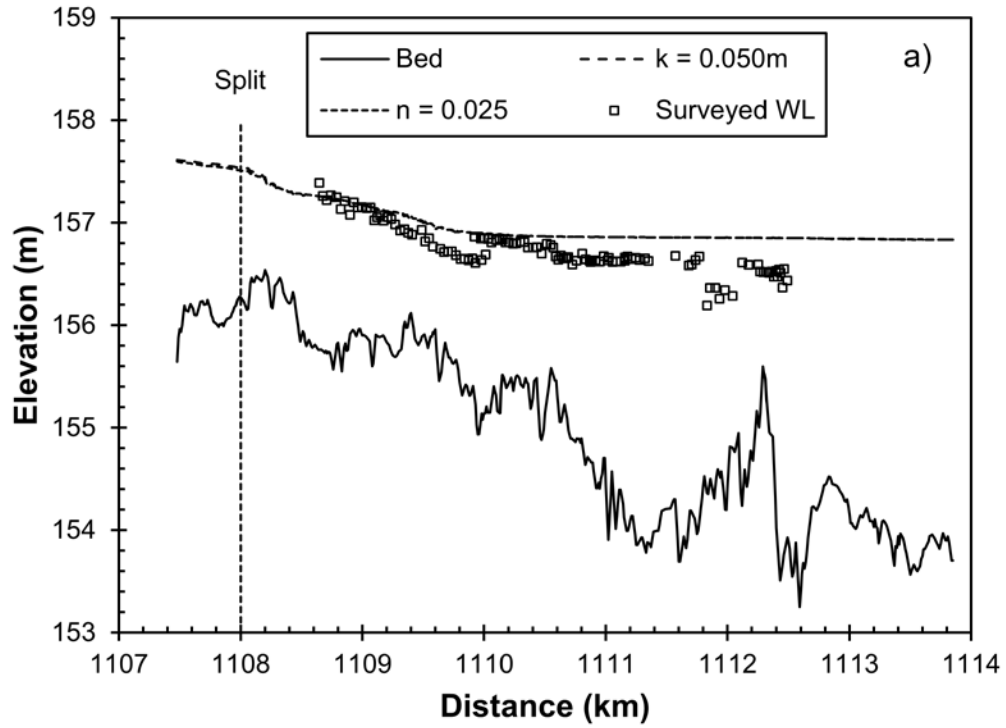


Figure 4.3 Comparison of modeled water surface profiles with surveyed water levels for the a) East and (b) West Channels at a discharge of $160 \text{ m}^3/\text{s}$.

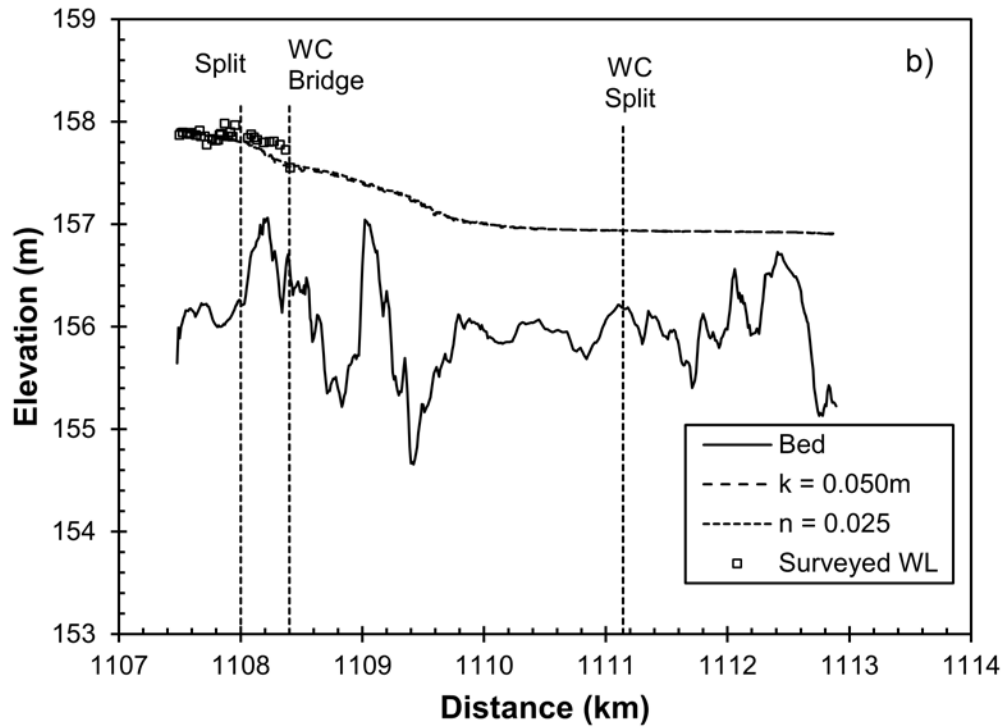
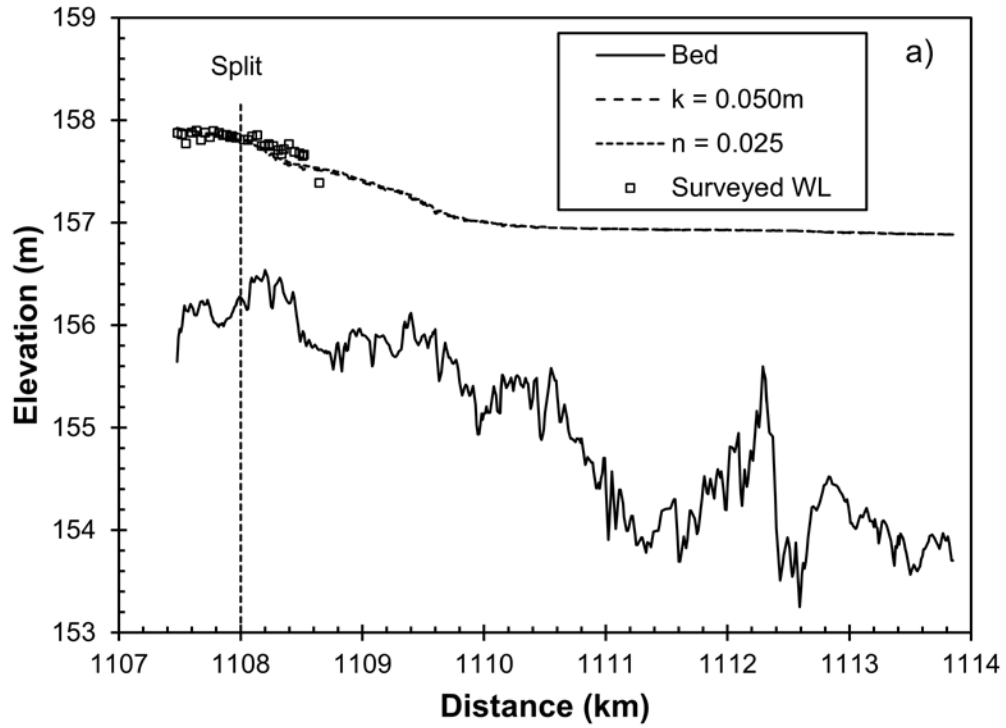


Figure 4.4 Comparison of modeled water surface profiles with surveyed water levels for the a) East and (b) West Channels at a discharge of 258 m³/s.

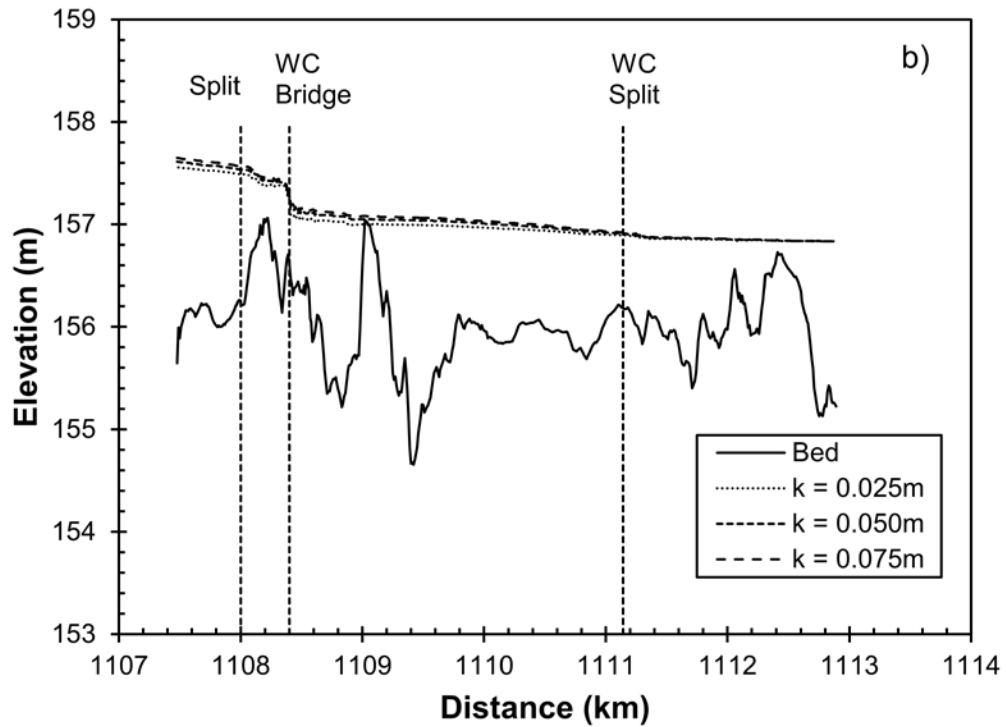
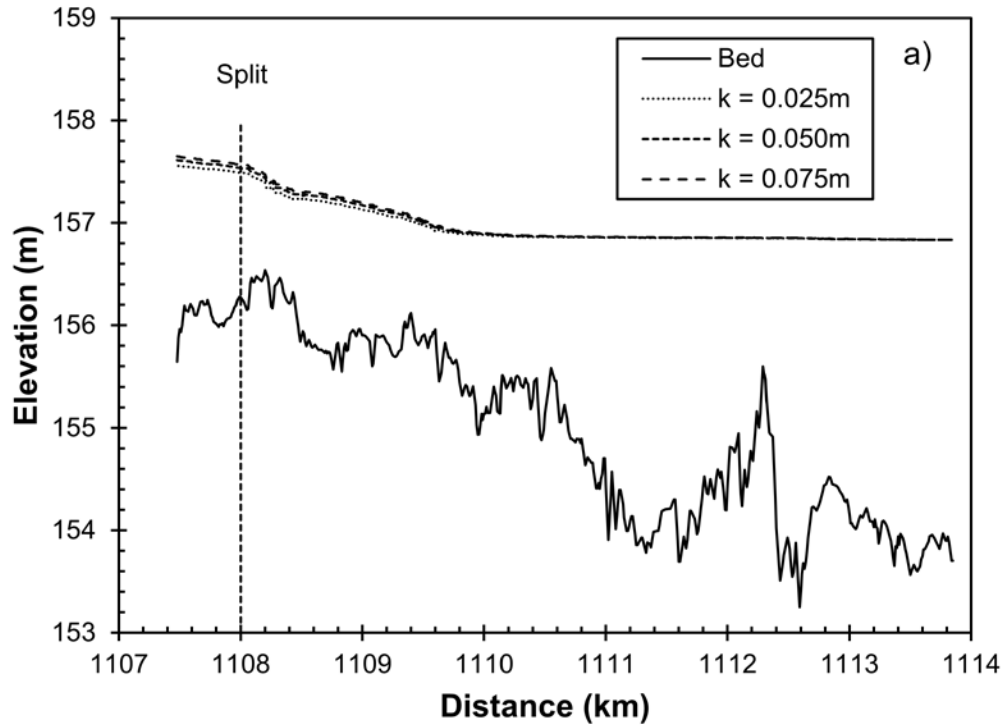


Figure 4.5 Sensitivity analysis of bed roughness with River 2-D down the a) East and (b) West Channels.

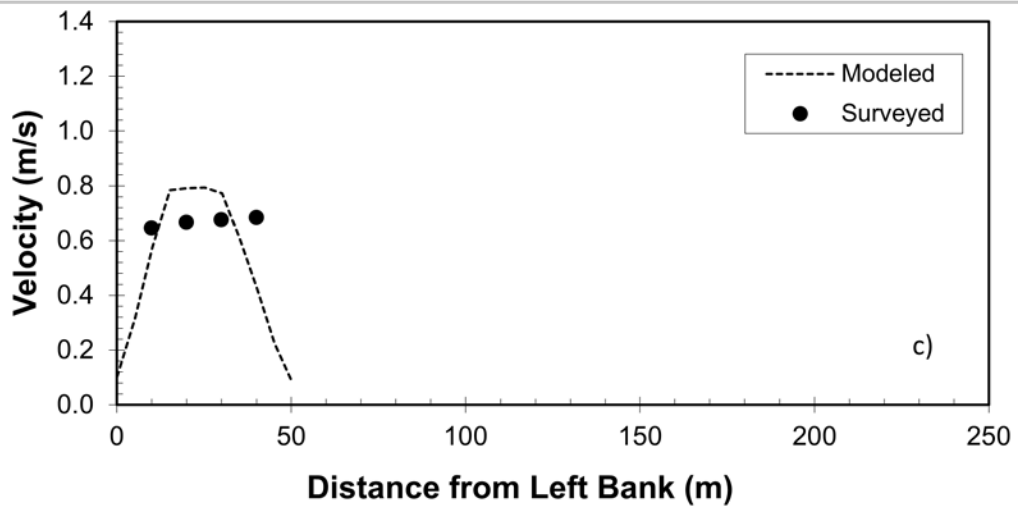
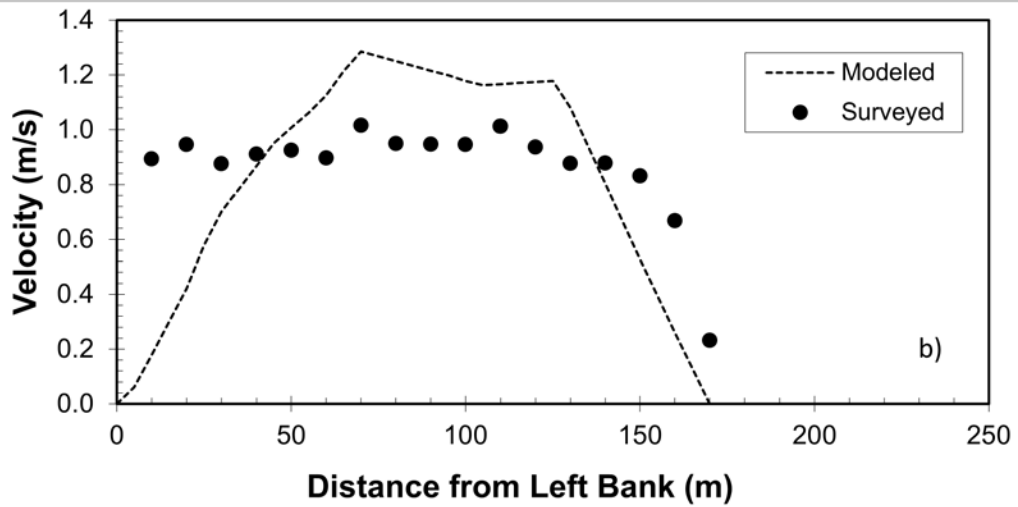
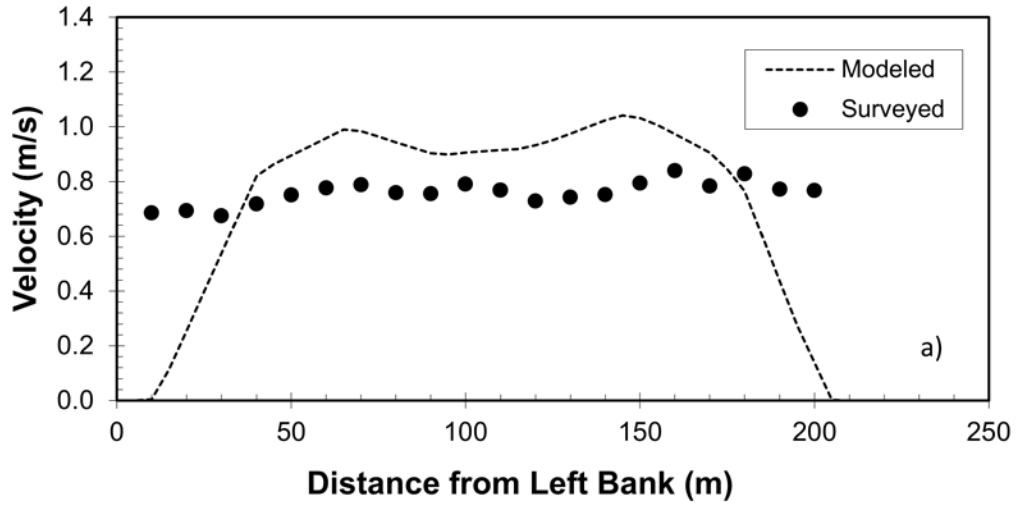


Figure 4.6 Comparison of velocity profiles measured in the field and River 2-D model results a) upstream of the split and just downstream of the split in the (b) East and (c) West Channels.

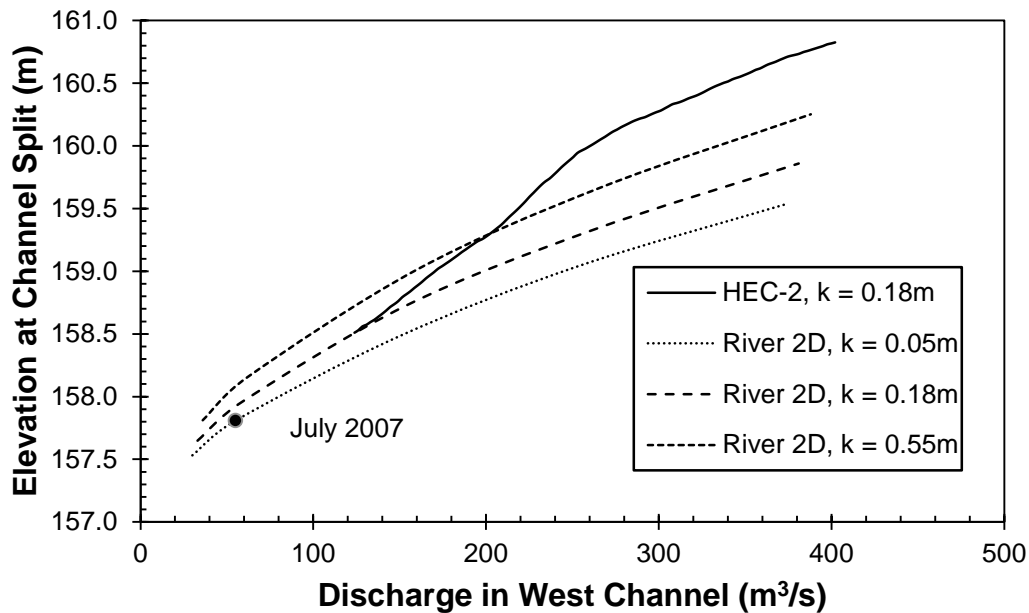


Figure 4.7 Comparison of the open water rating curve developed by Gerard and Stanley (1988) with HEC-2 and the open water rating curves developed with River 2-D at three different bed roughness heights.

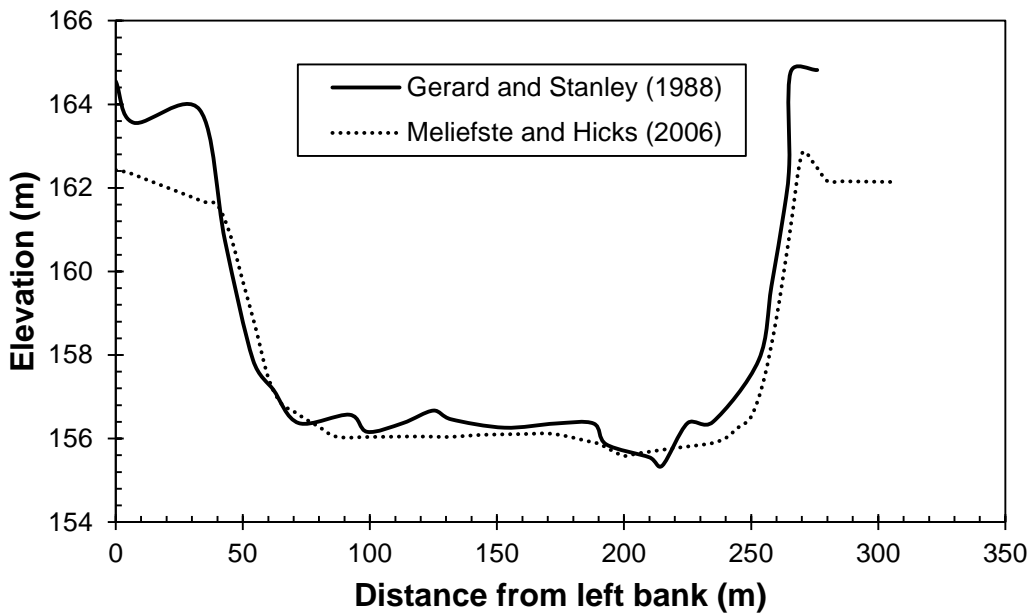


Figure 4.8 Comparison of channel cross section just upstream of the East-West Channel split from Gerard and Stanley (1988) and Meliefste and Hicks (2006).

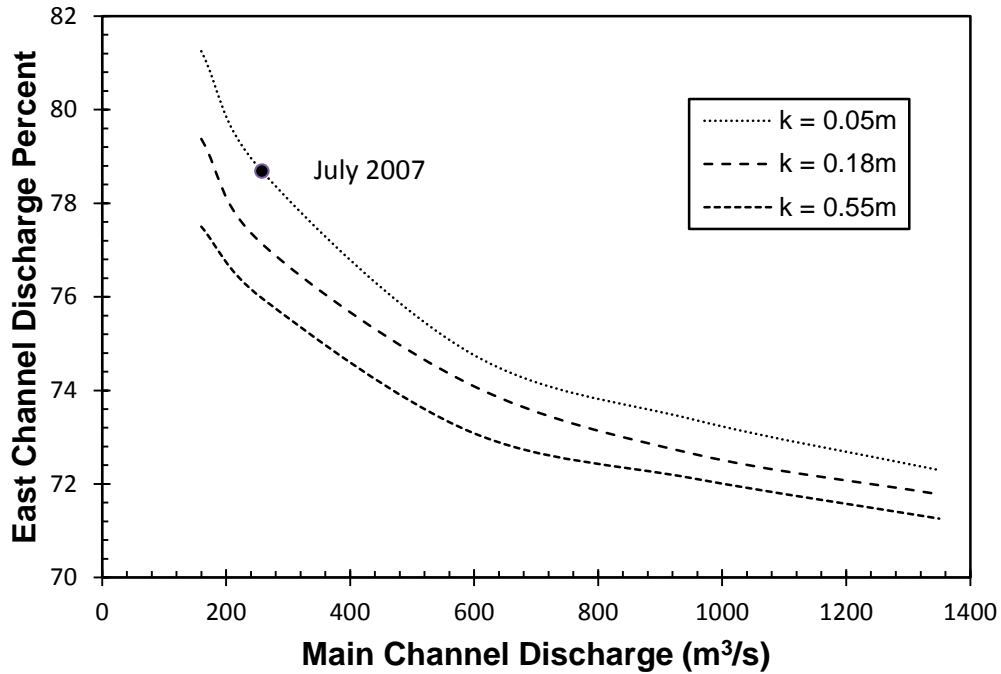


Figure 4.9 East-West Channel flow split relationship established using River 2-D at three different bed roughness heights and compared to 2007 discharge measurements.

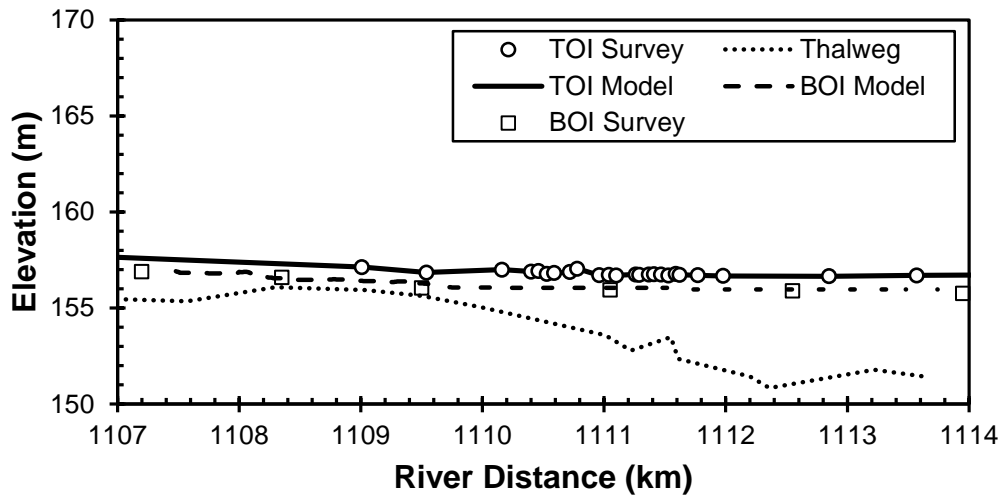


Figure 4.10 Comparison of ice survey on 28-Apr-08 and CRISSP 2-D model results.

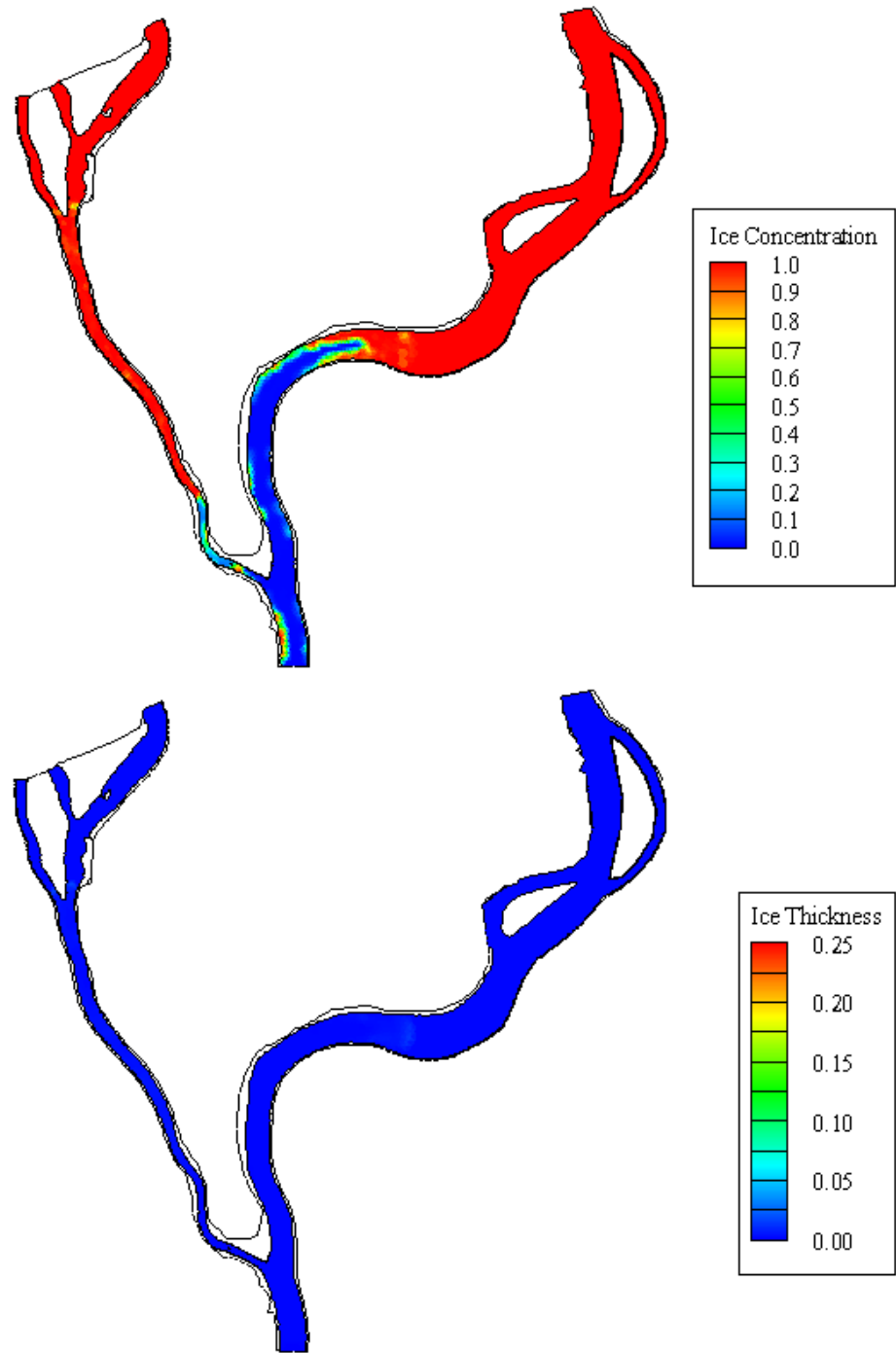


Figure 4.11 Freeze-up modeling results with CRISSP2D Model after 10 minutes model time.

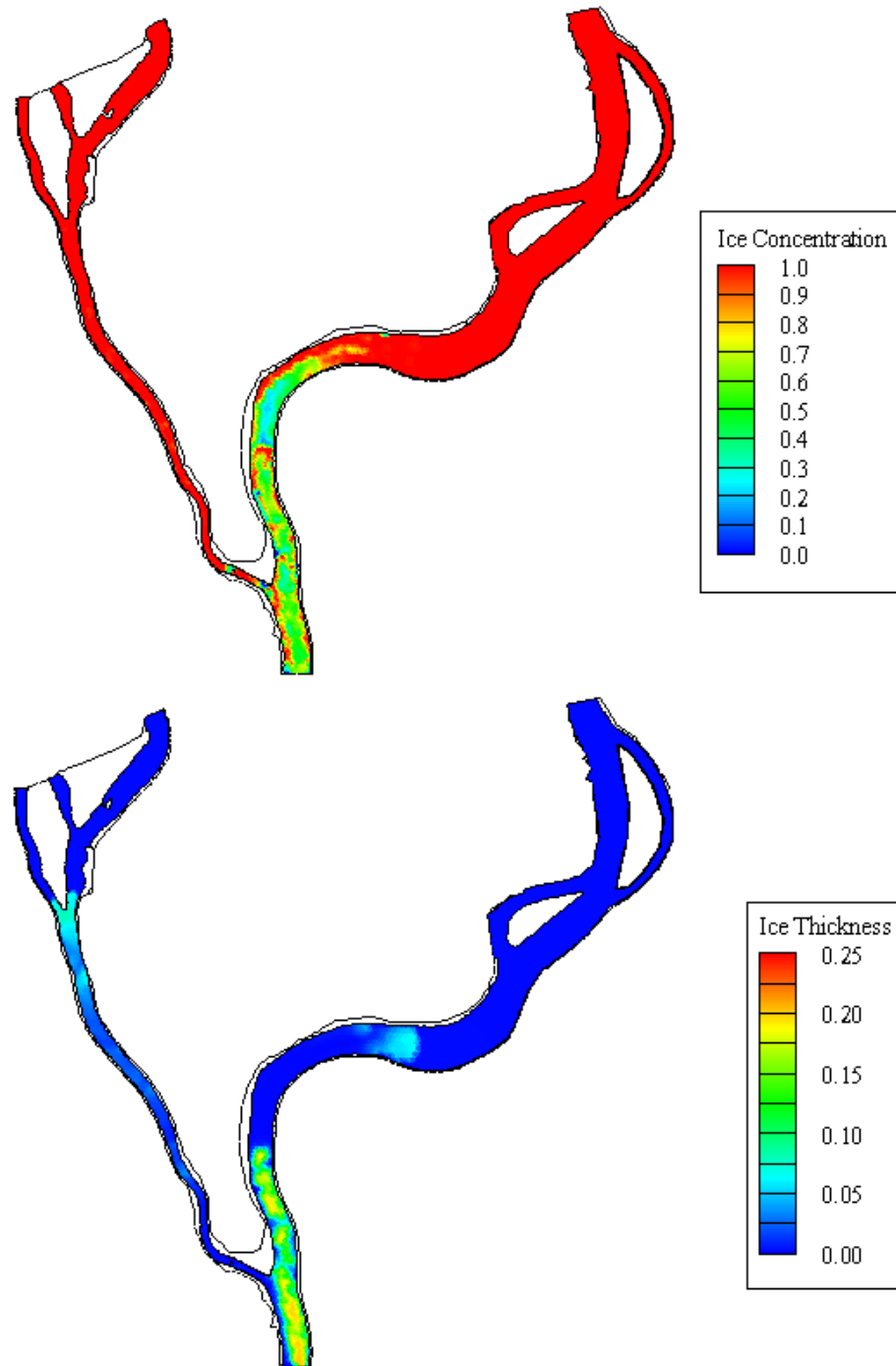


Figure 4.12 CRISSP2D Freeze-up model results after 90 minutes of model time. Ice parcels were injected after 60 minutes of modeling and shown going down the East Channel.

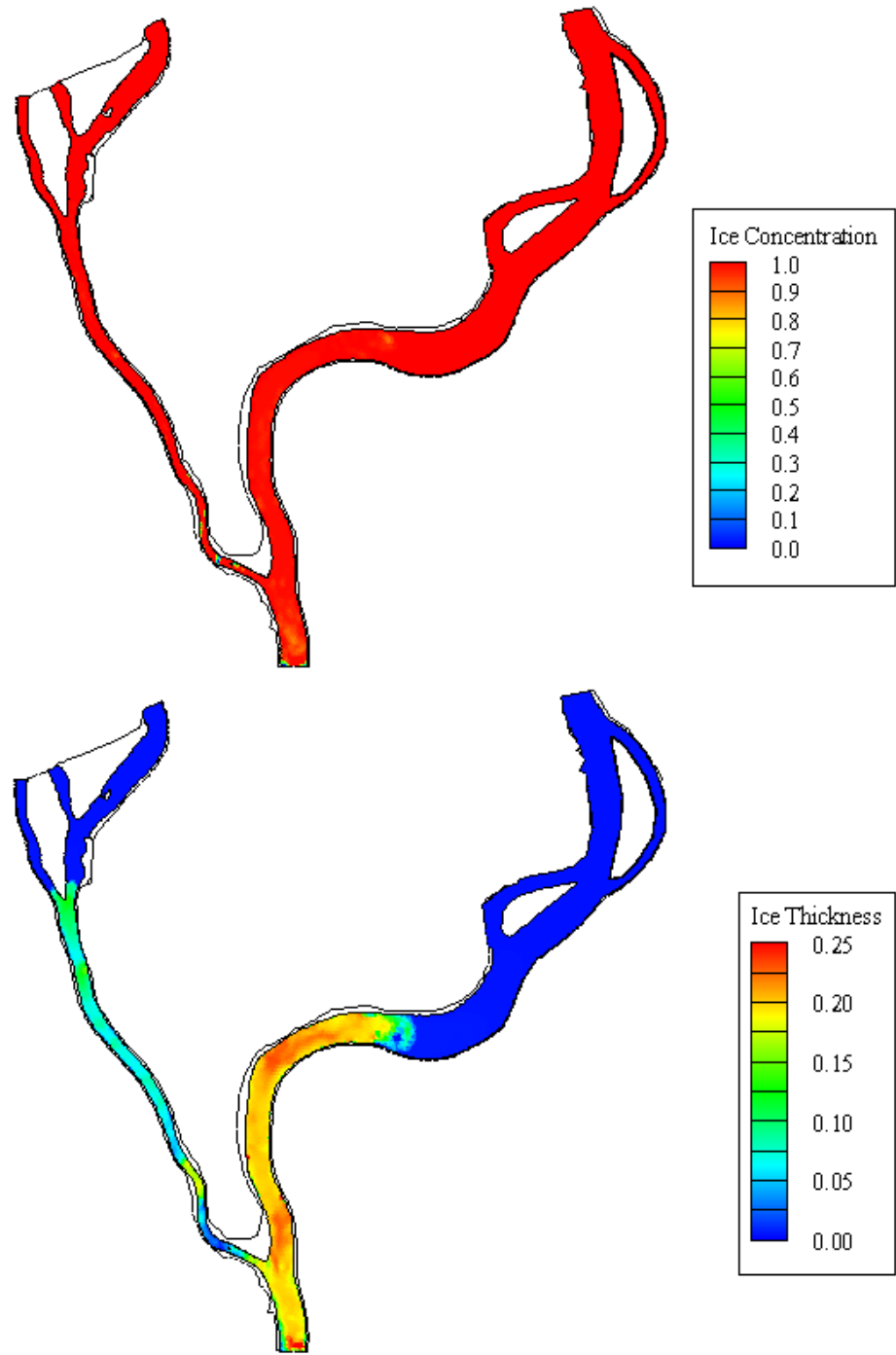


Figure 4.13 CRISP2D freeze-up modeling results after 270 minutes of model time.

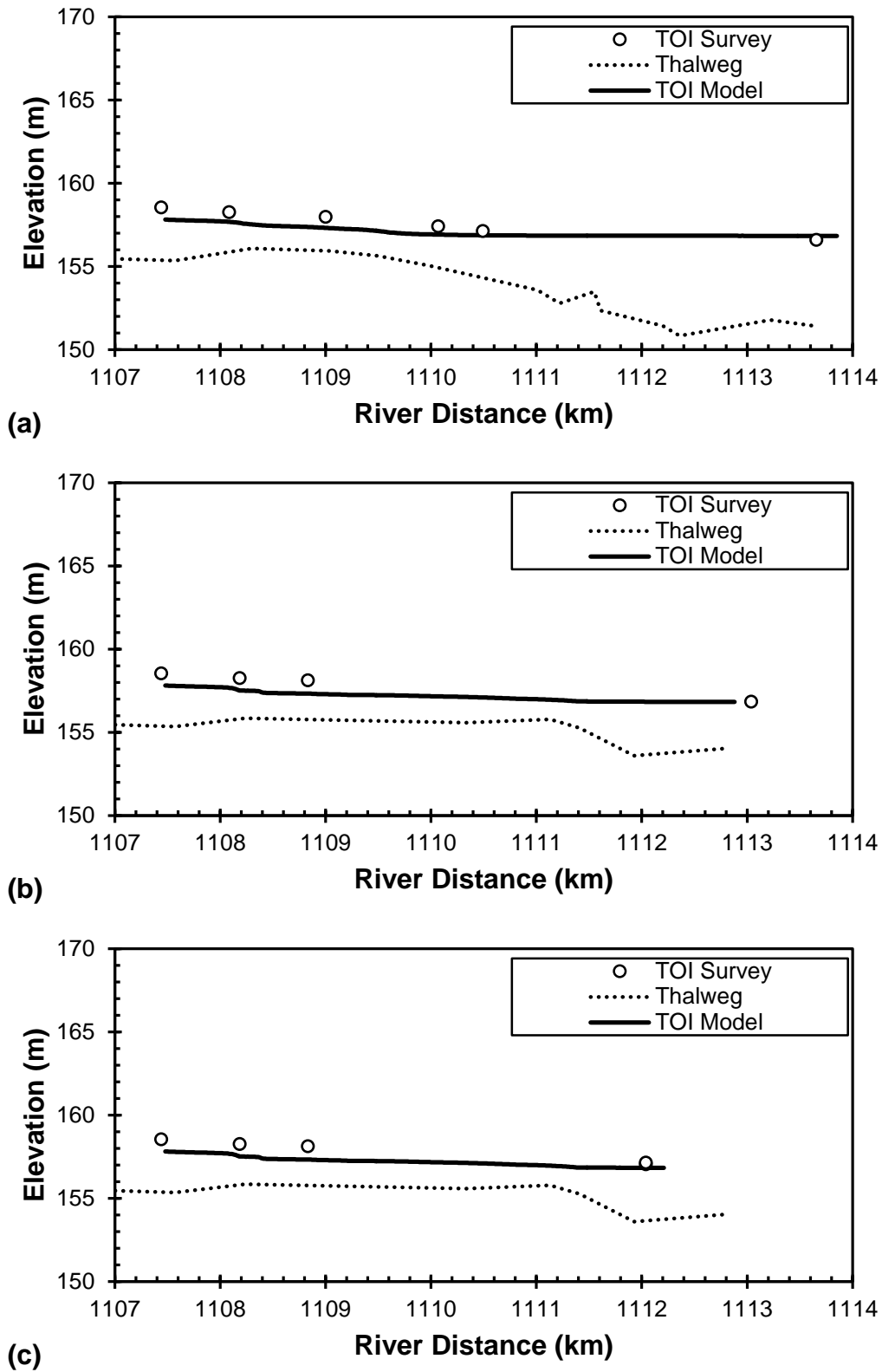


Figure 4.14: A comparison of the surveyed top of ice profiles from 26-Apr-08 and the CRISSP2D freeze-up model profile results in the (a) East, (b) Fishing Village and (c) Rudd Channels.

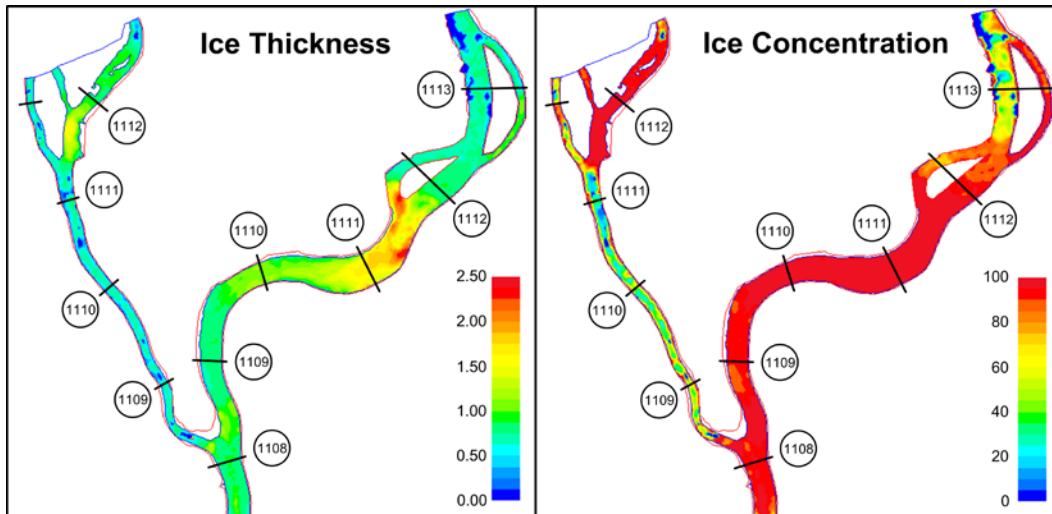


Figure 4.15 CRISSP2D 5-May-08 ice thickness and ice concentration model results without a force ice jam toe location.

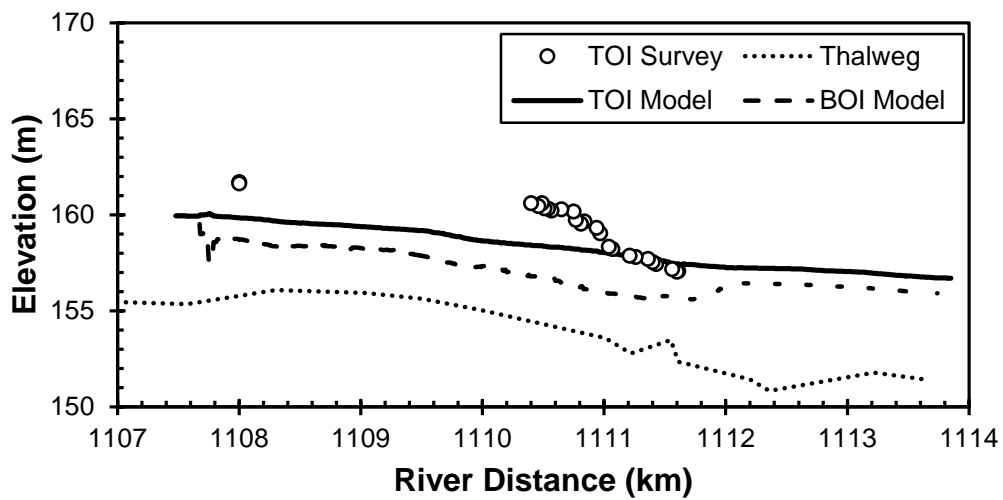
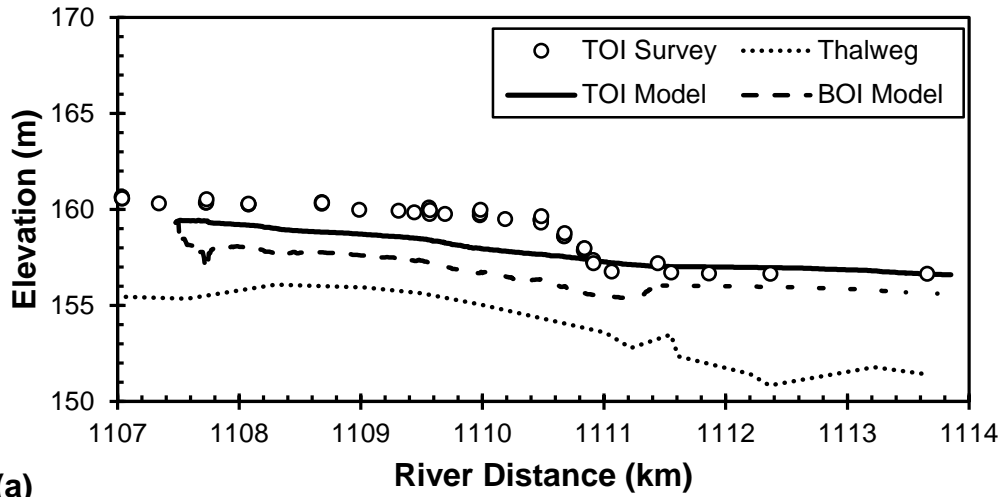
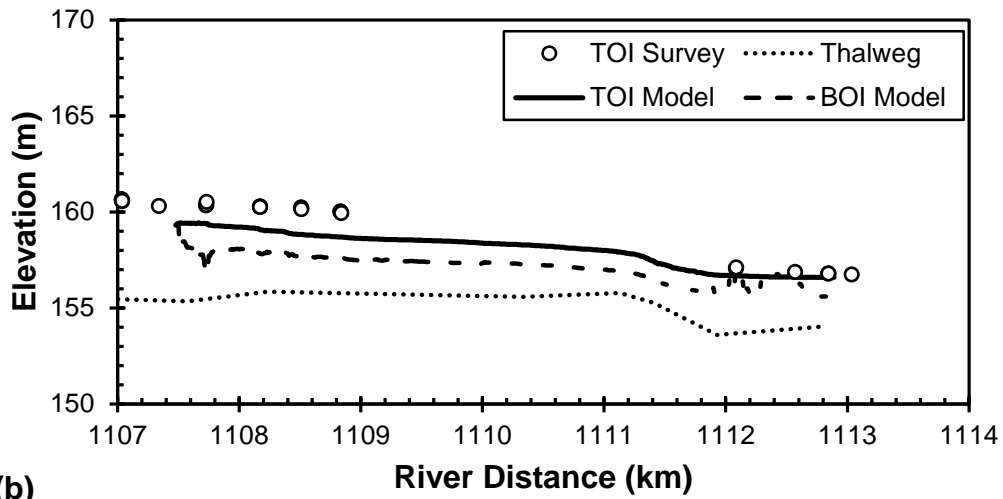


Figure 4.16 Comparison of top of ice survey from an ice jam in the East Channel on 5-May-08 and CRISSP 2-D model results.

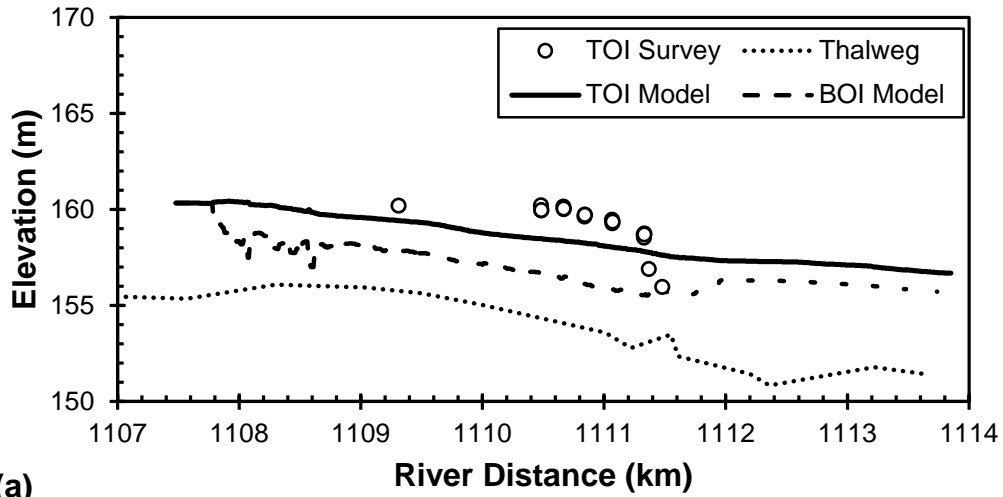


(a)

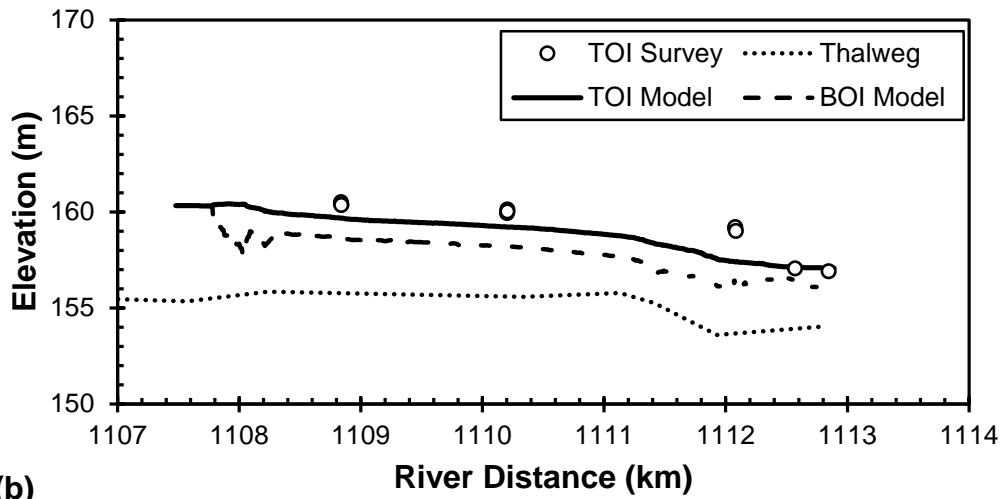


(b)

Figure 4.17 Comparison of top of ice survey from an ice jam in the East Channel on 3-May-09 and CRISSP 2-D model results.

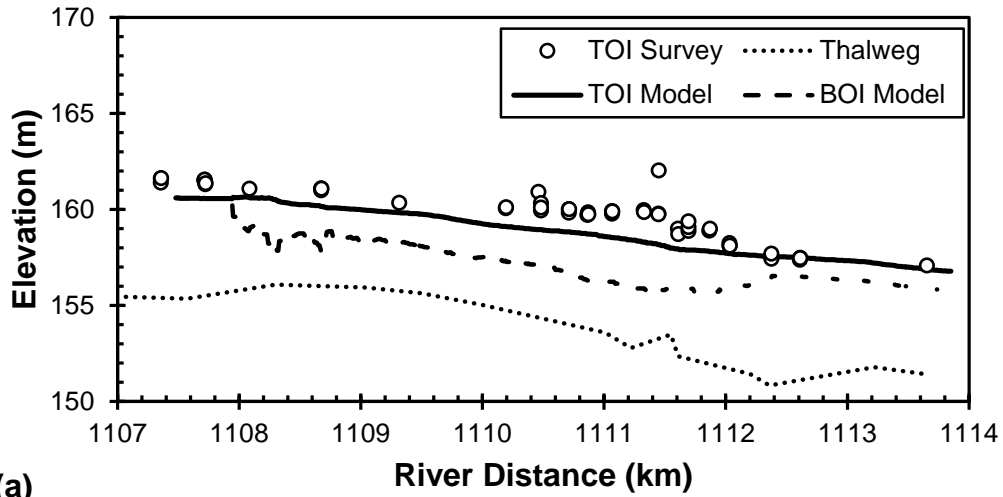


(a)

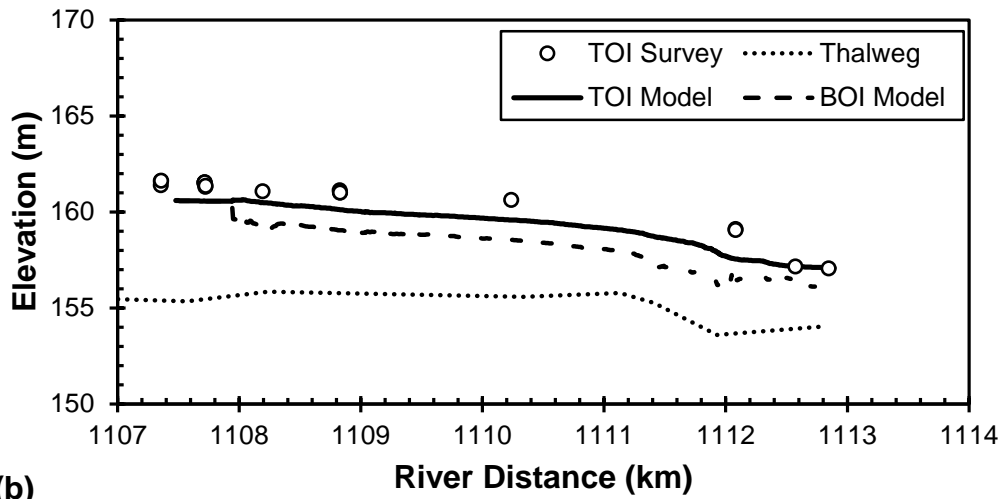


(b)

Figure 4.18 Comparison of top of ice survey from an ice jam in the East Channel on 4-May-09 and CRISSP 2-D model results.

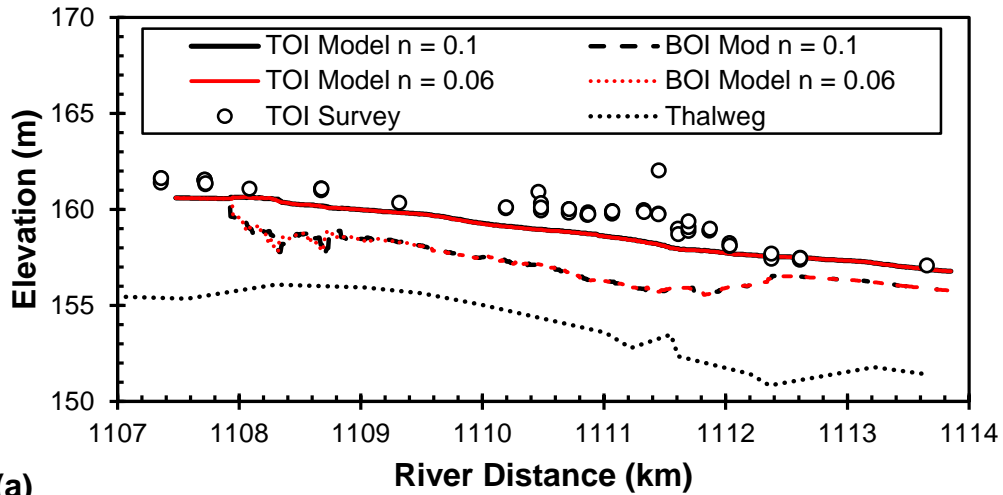


(a)

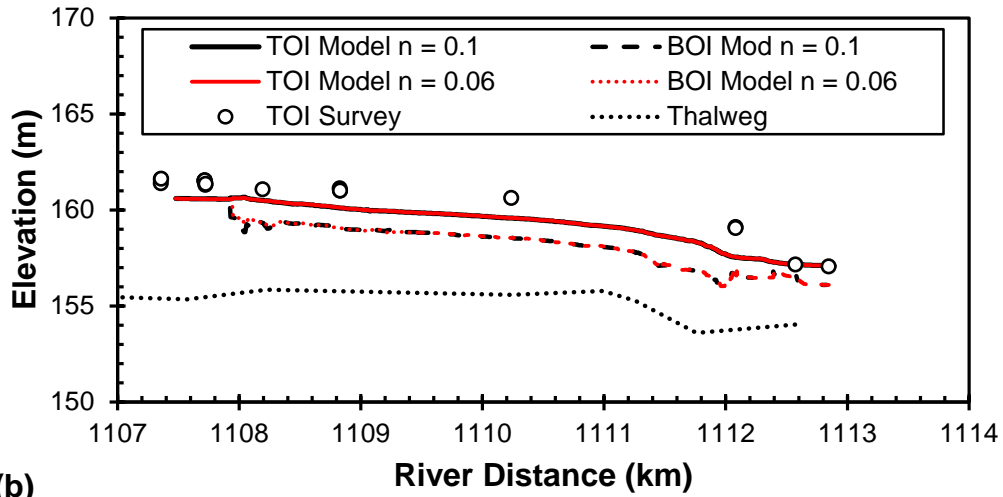


(b)

Figure 4.19 Comparison of top of ice survey from an ice jam in the East Channel on 5-May-09 and CRISSP 2-D model results.



(a)



(b)

Figure 4.20 A comparison of the modeled ice profiles from 5-May-09 for two maximum Manning's n ice roughnesses in the (a) East and (b) Fishing Village Channels.

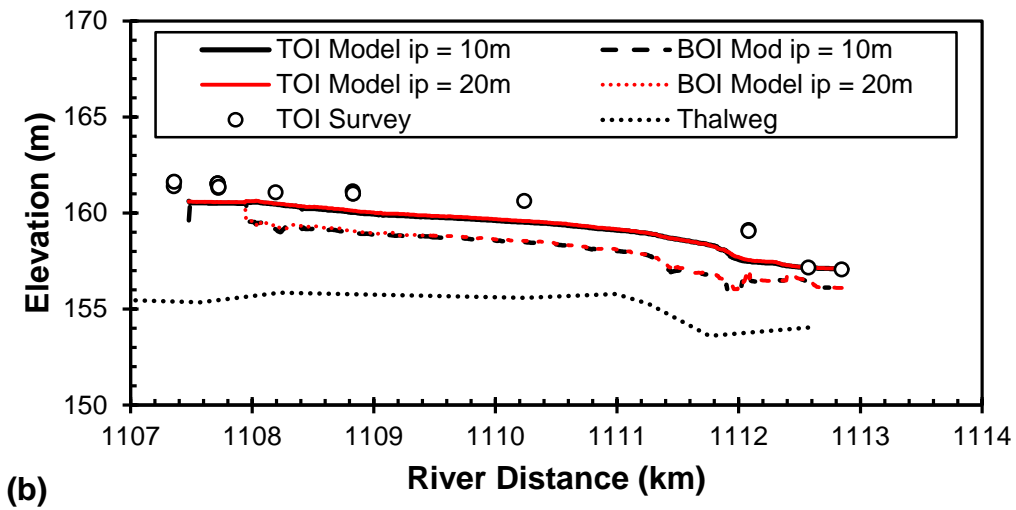
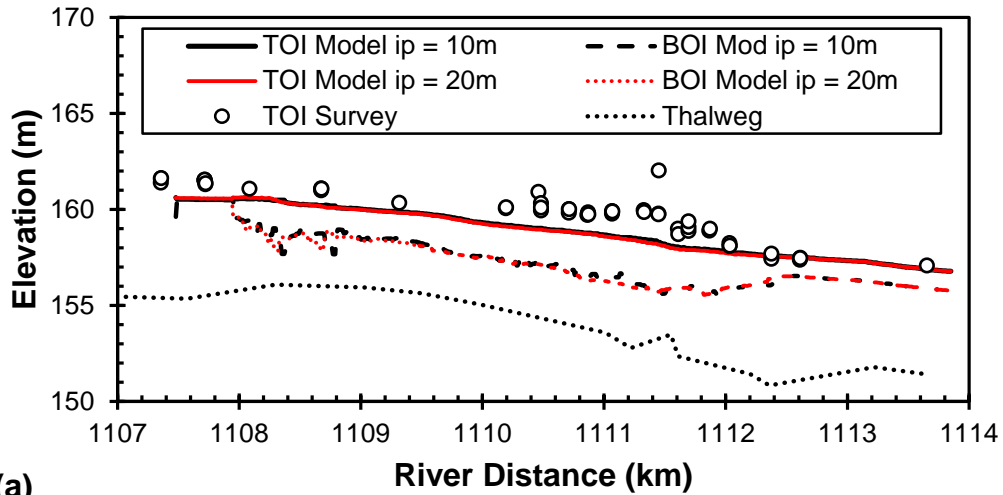


Figure 4.21 A comparison of the modeled ice profiles from 5-May-09 for two initial ice parcel sizes in the (a) East and (b) Fishing Village Channels.

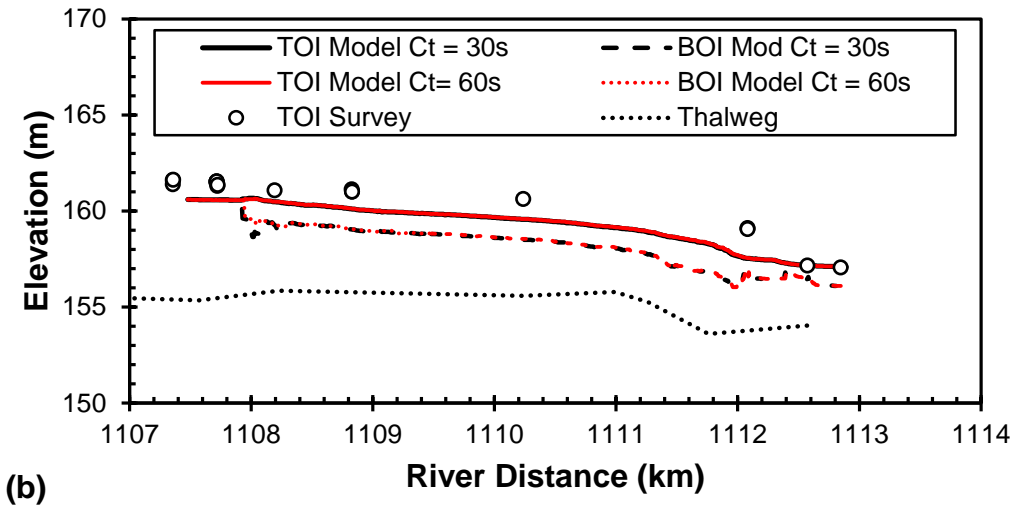
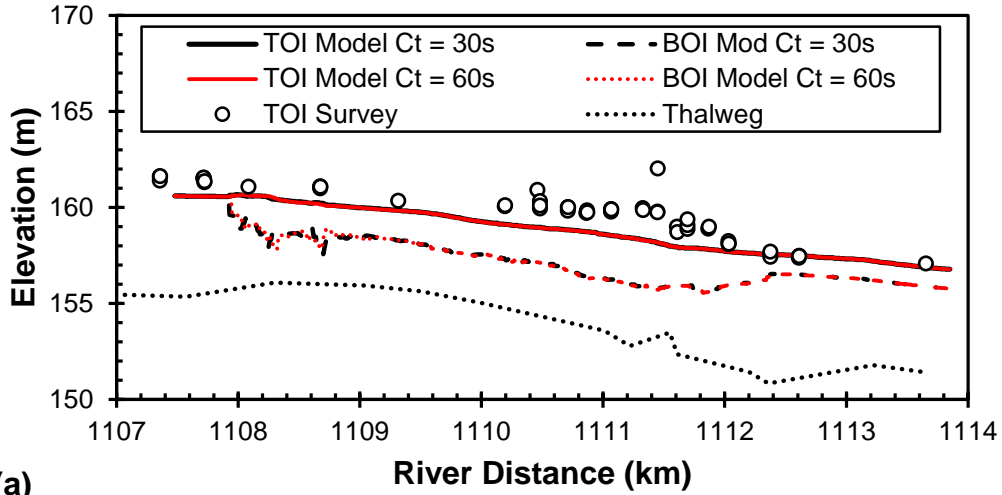


Figure 4.22 A comparison of the modeled ice profiles from 5-May-09 for two model coupling times in the (a) East and (b) Fishing Village Channels.

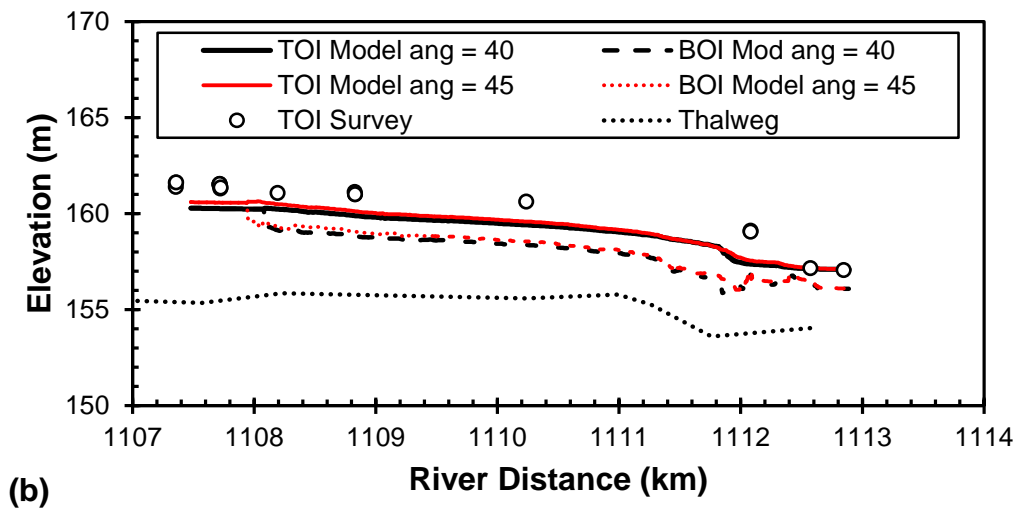
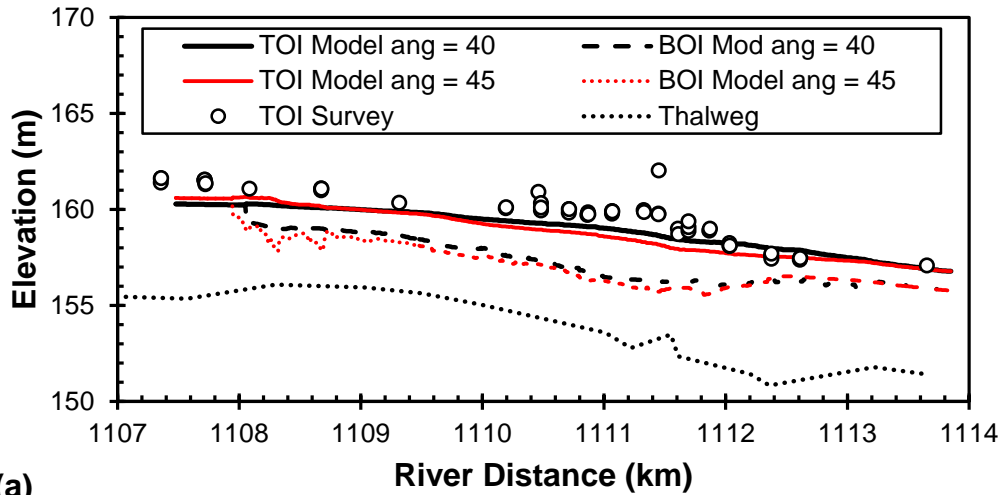


Figure 4.23 A comparison of the modeled ice profiles from 5-May-09 for two internal angles of friction in the (a) East and (b) Fishing Village Channels.

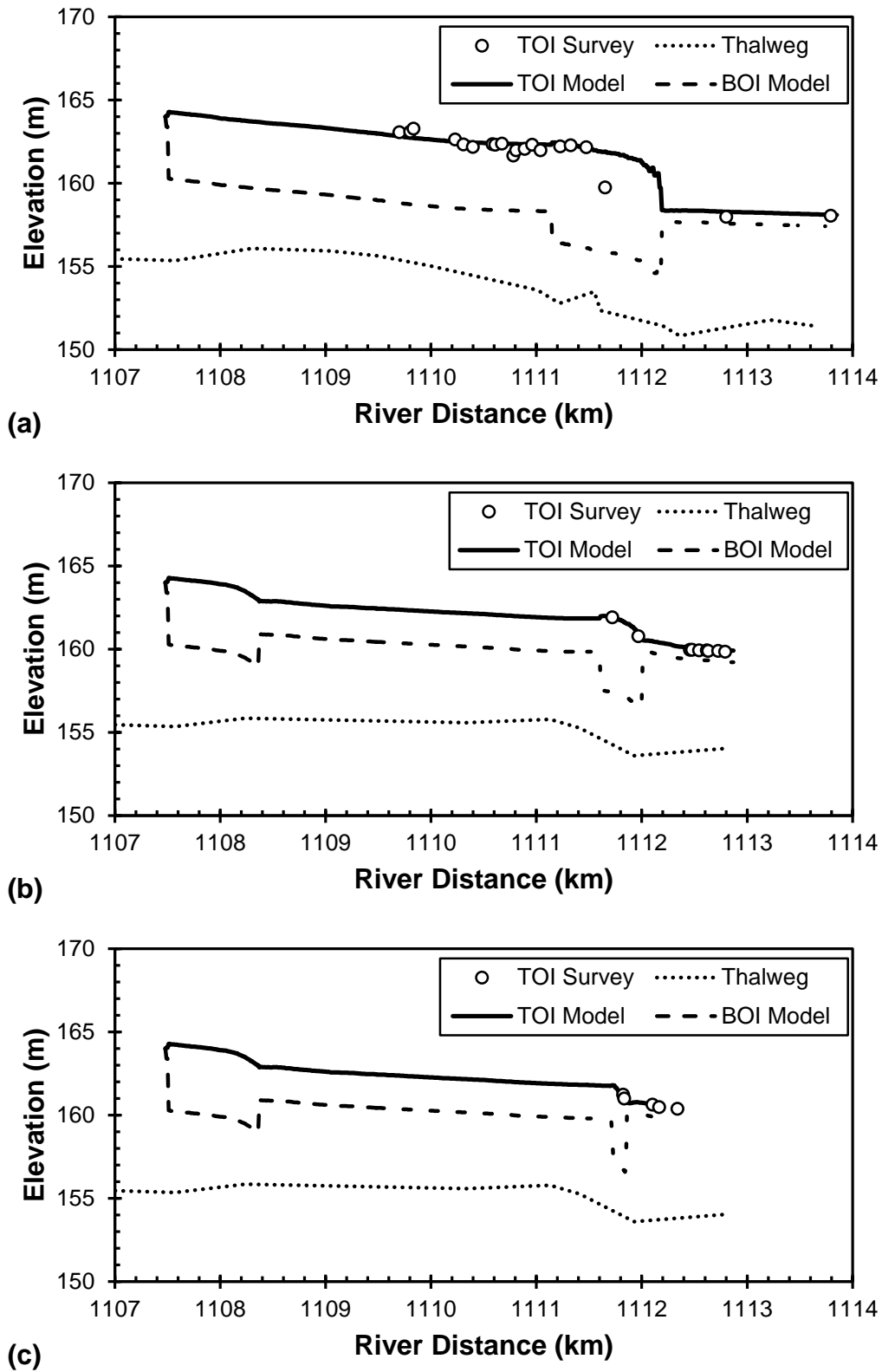


Figure 4.24 A comparison of the surveyed top of ice profiles from 1985 and the River 2-D model ice jam profile results in the (a) East, (b) Fishing Village and (c) Rudd Channels.

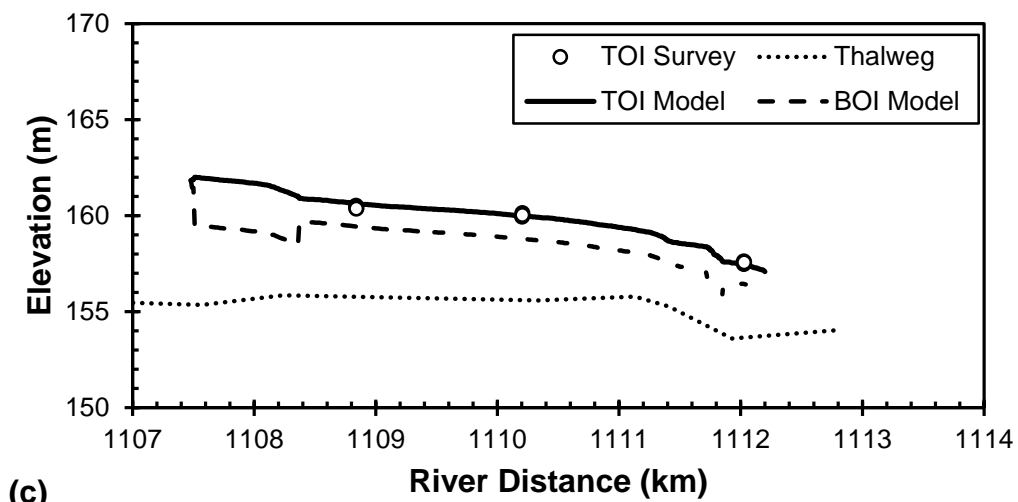
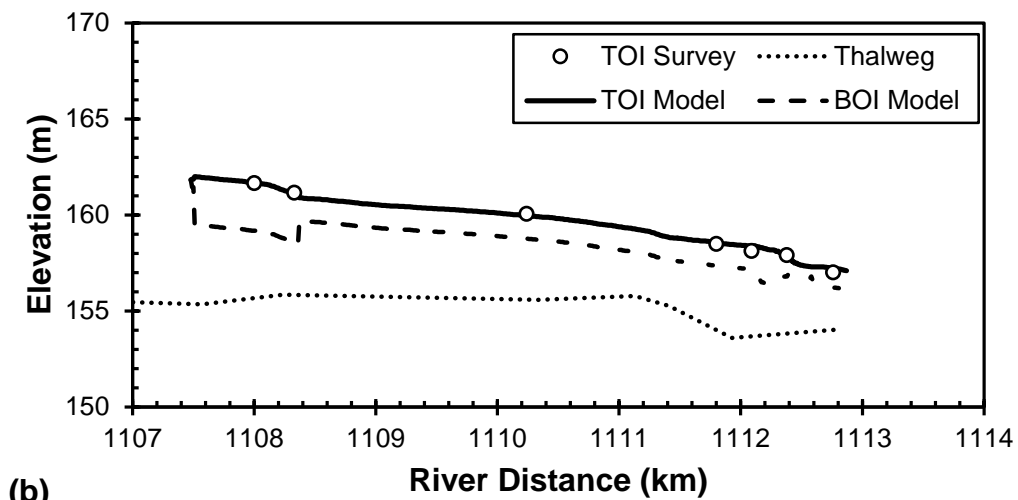
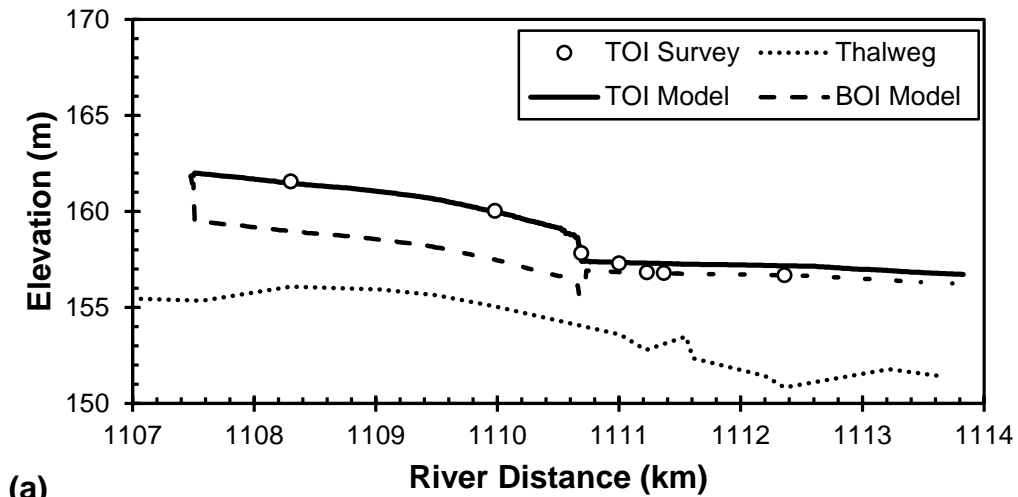
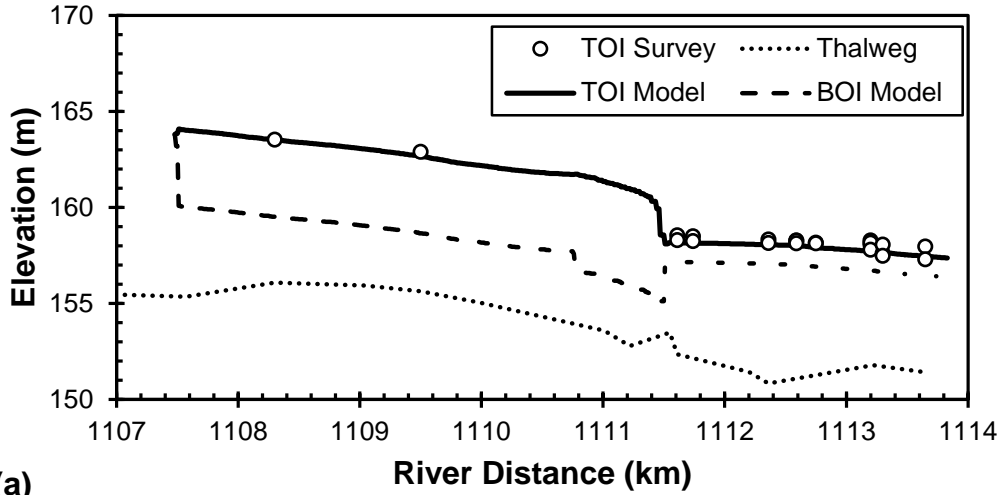
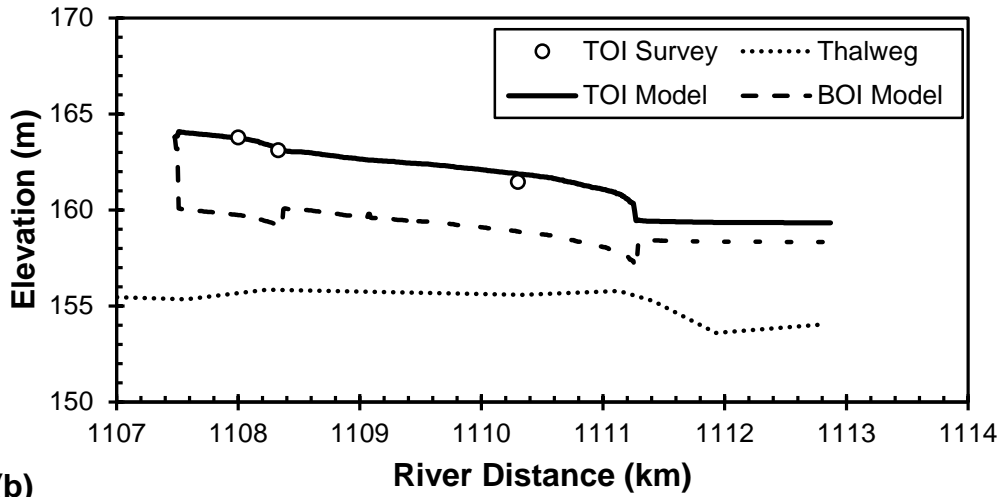


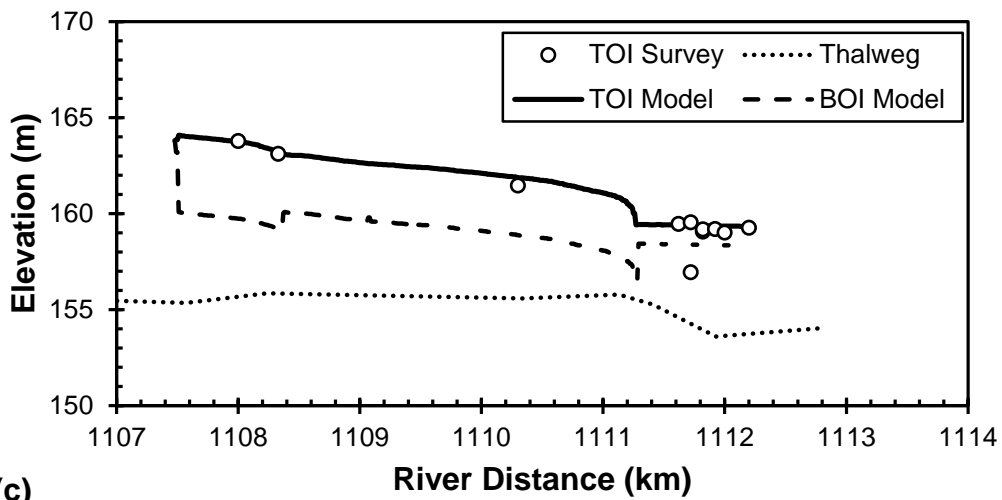
Figure 4.25 A comparison of the surveyed top of ice profiles from 1988 and the River 2-D model ice jam profile results in the (a) East, (b) Fishing Village and (c) Rudd Channels.



(a)

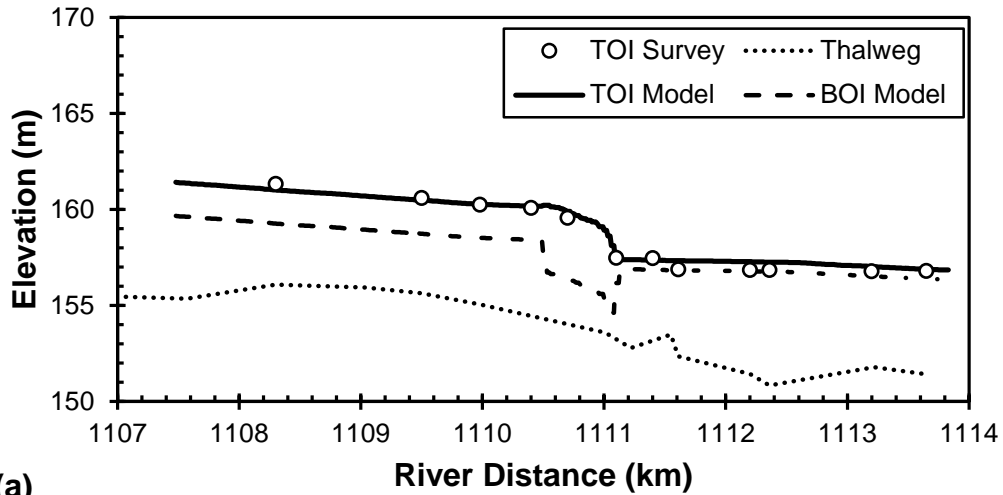


(b)

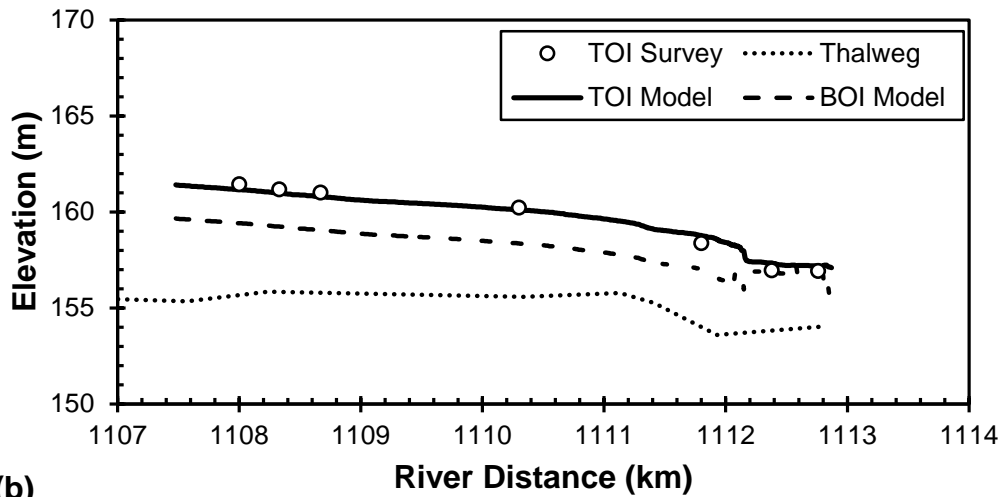


(c)

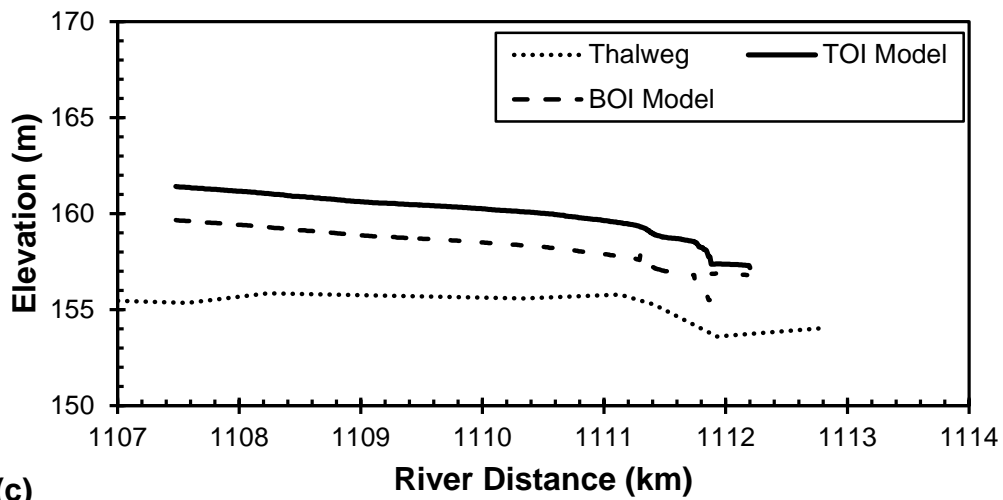
Figure 4.26 A comparison of the surveyed top of ice profiles from 1989 and the River 2-D model ice jam profile results in the (a) East, (b) Fishing Village and (c) Rudd Channels.



(a)

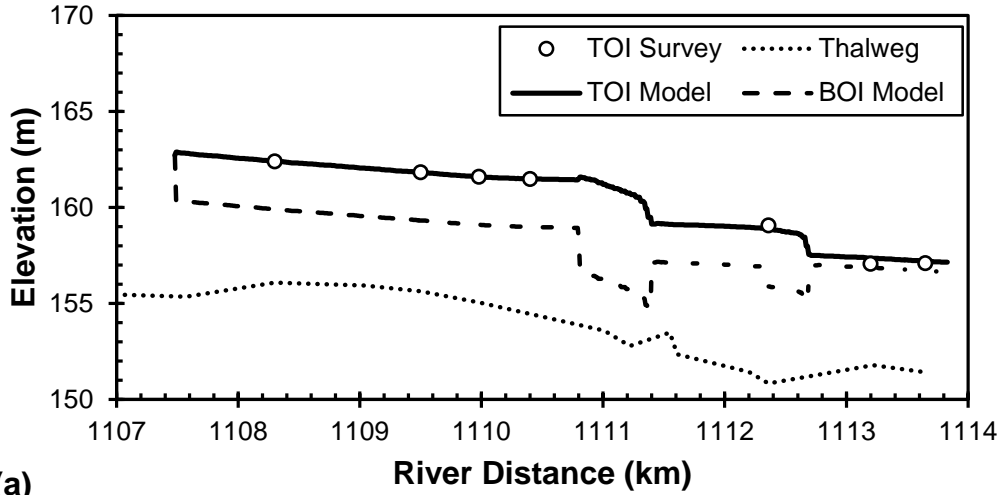


(b)

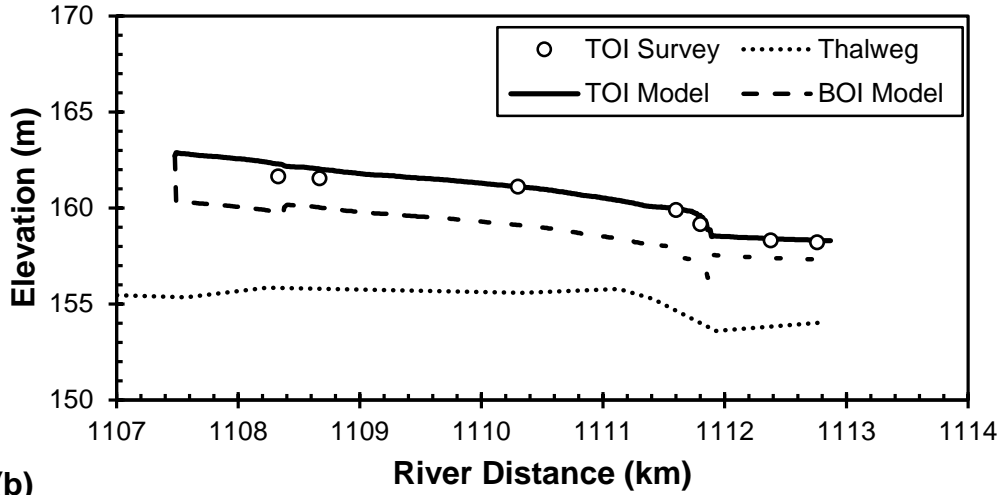


(c)

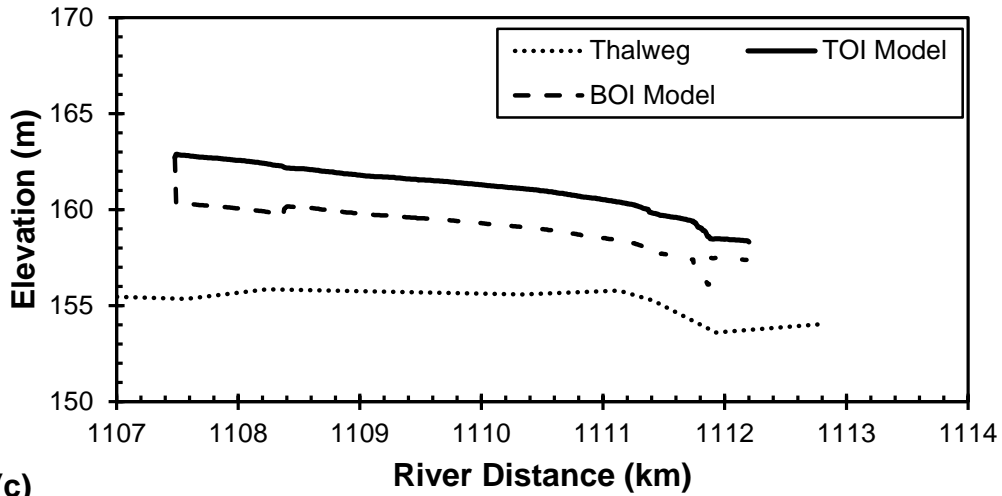
Figure 4.27 A comparison of the surveyed top of ice profiles from 1990 and the River 2-D model ice jam profile results in the (a) East, (b) Fishing Village and (c) Rudd Channels.



(a)



(b)



(c)

Figure 4.28 A comparison of the surveyed top of ice profiles from 1992 and the River 2-D model ice jam profile results in the (a) East, (b) Fishing Village and (c) Rudd Channels.

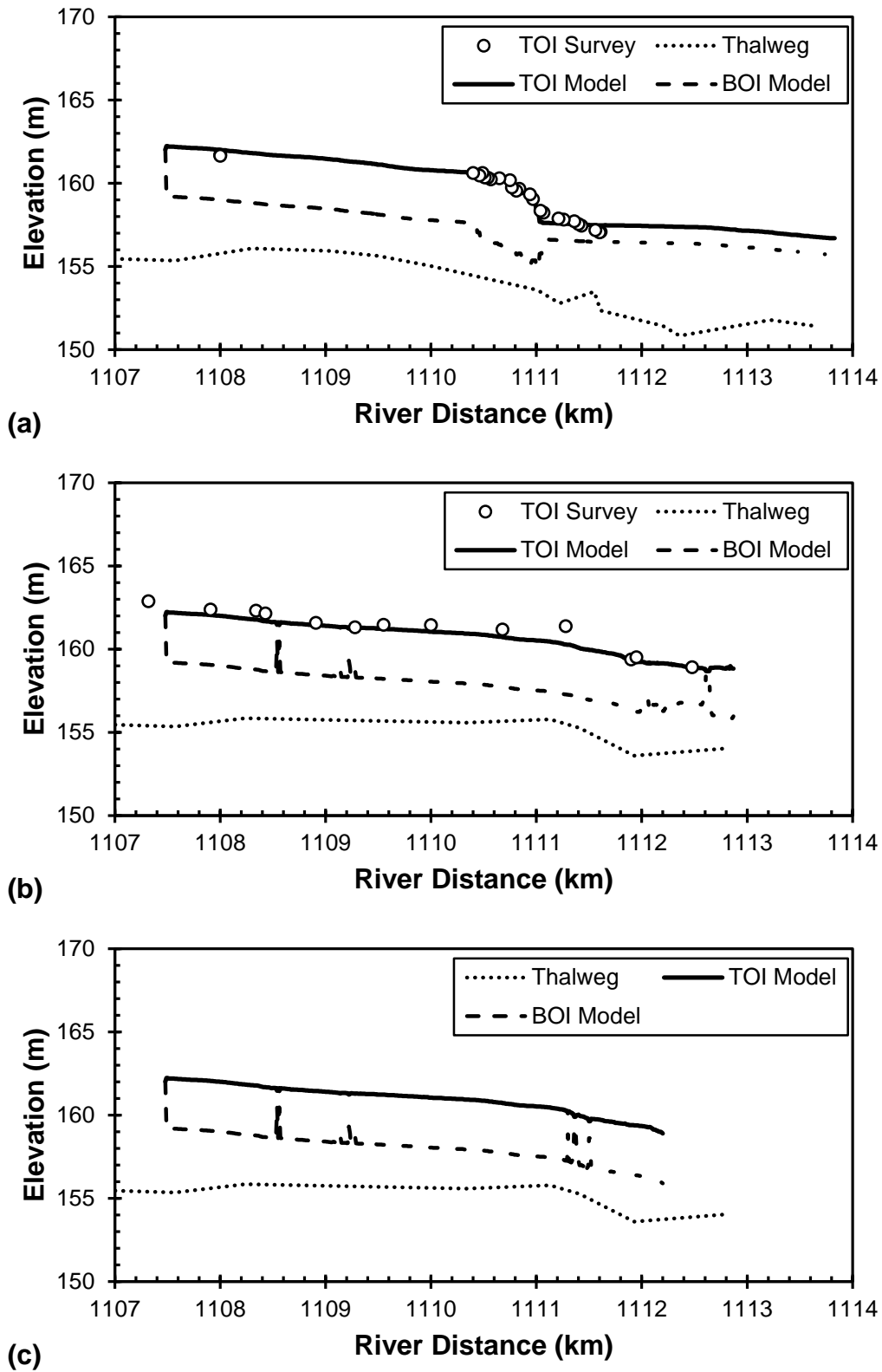


Figure 4.29 A comparison of the surveyed top of ice profiles from 5-May-08 and the River 2-D model ice jam profile results in the (a) East, (b) Fishing Village and (c) Rudd Channels.

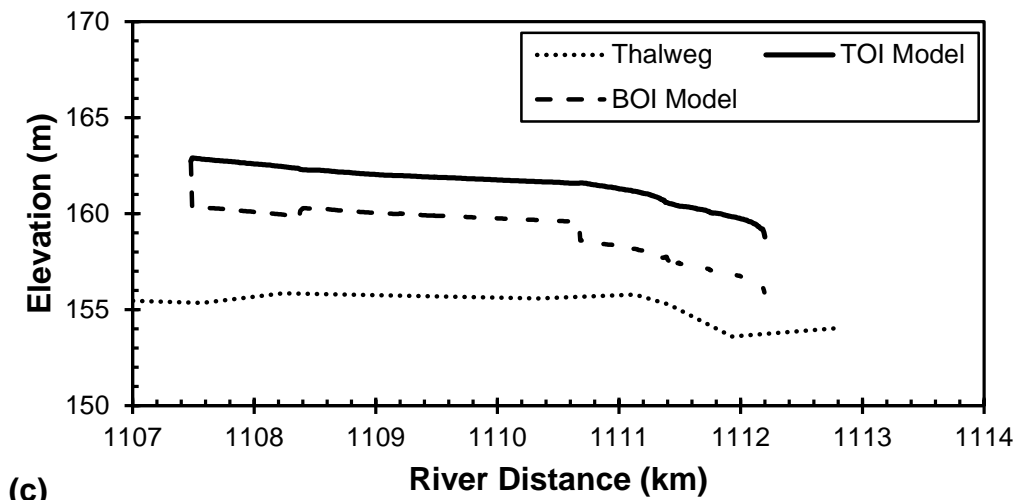
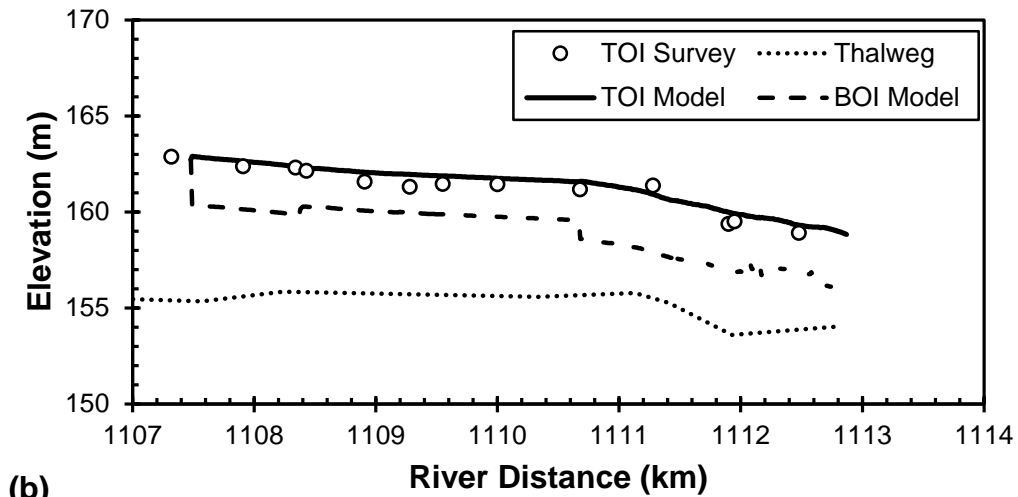
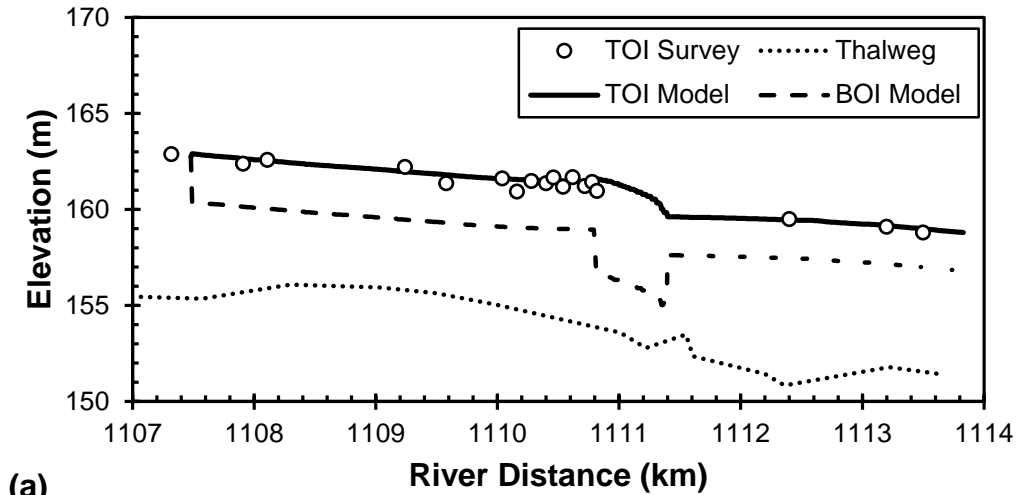


Figure 4.30 A comparison of the surveyed top of ice profiles from 6-May-08 and the River 2-D model ice jam profile results in the (a) East, (b) Fishing Village and (c) Rudd Channels.

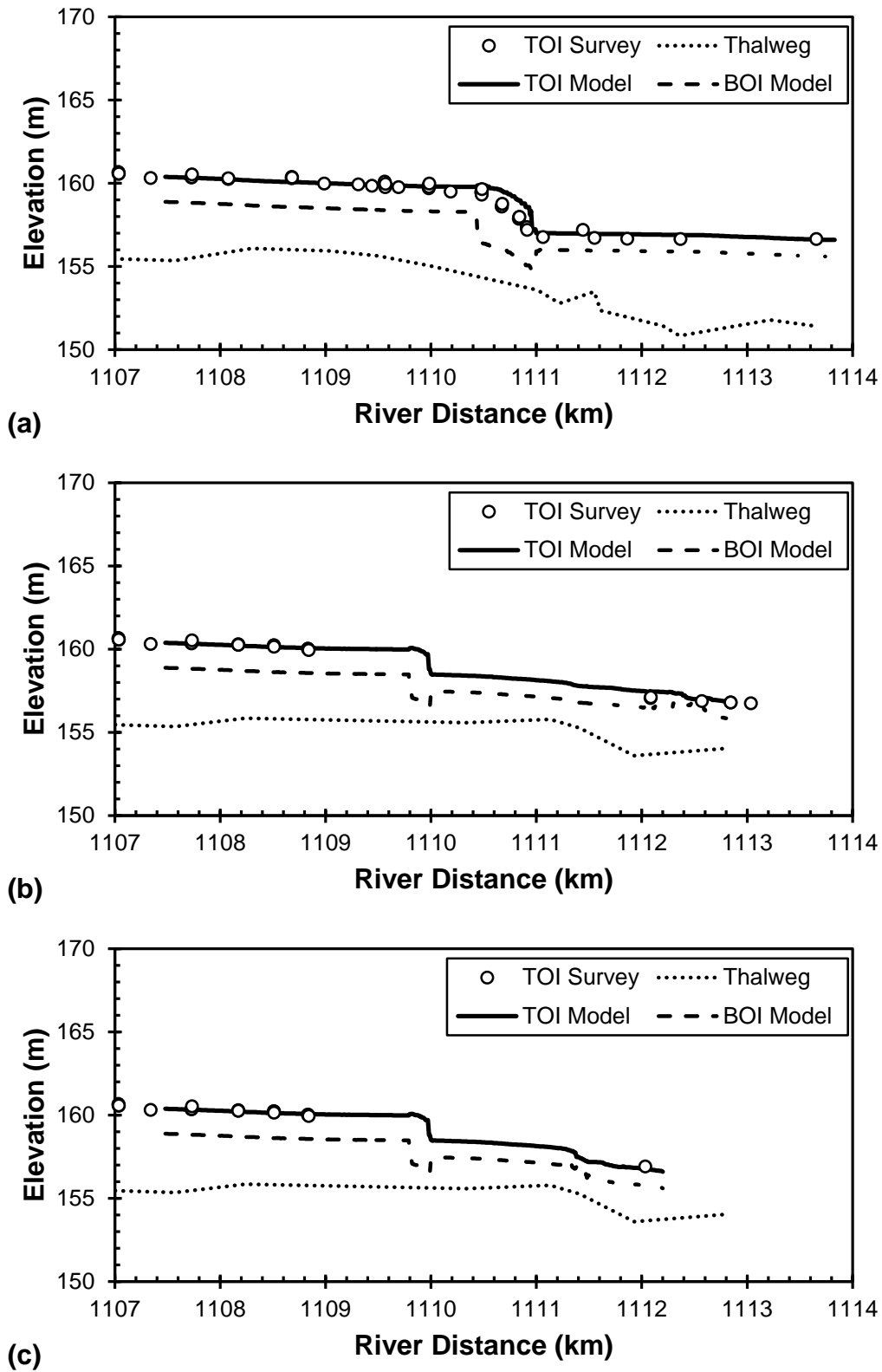


Figure 4.31 A comparison of the surveyed top of ice profiles from 3-May-09 and the River 2-D model ice jam profile results in the (a) East, (b) Fishing Village and (c) Rudd Channels.

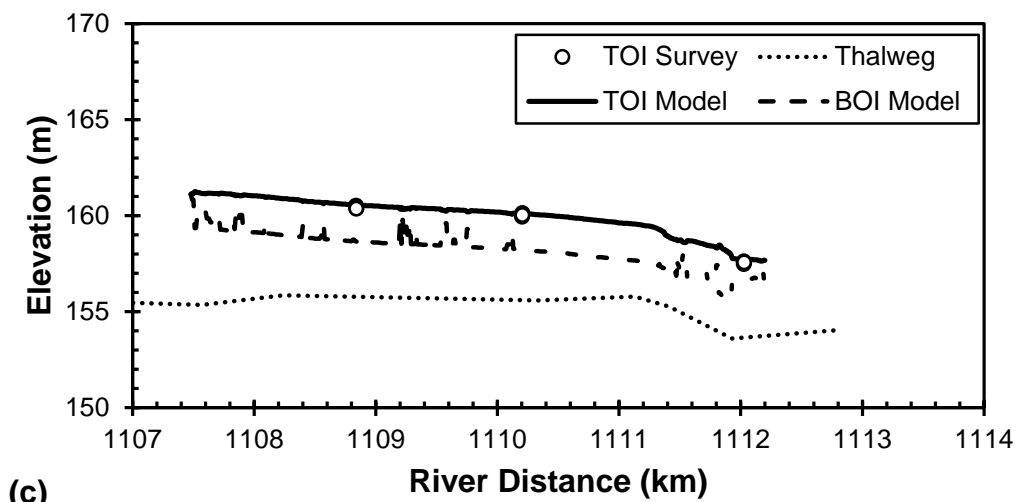
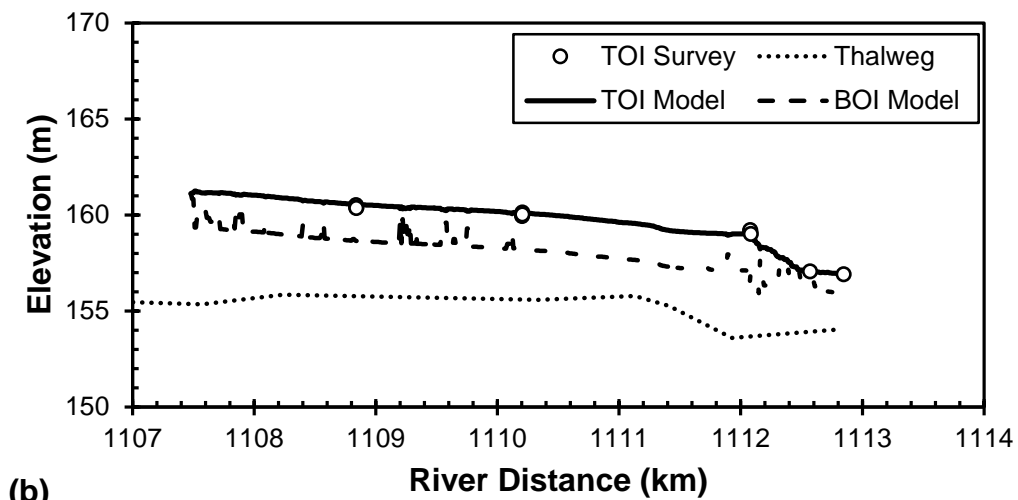
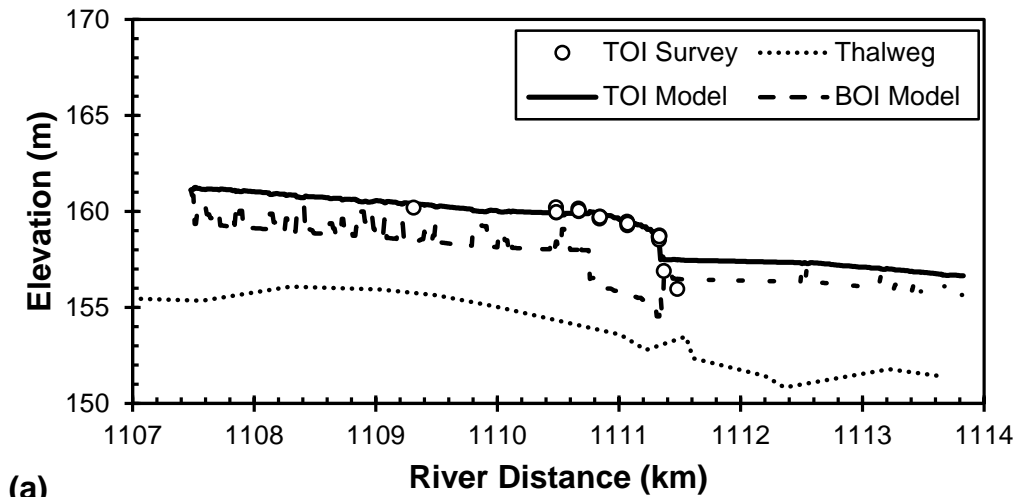


Figure 4.32 A comparison of the surveyed top of ice profiles from 4-May-09 and the River 2-D model ice jam profile results in the (a) East, (b) Fishing Village and (c) Rudd Channels.

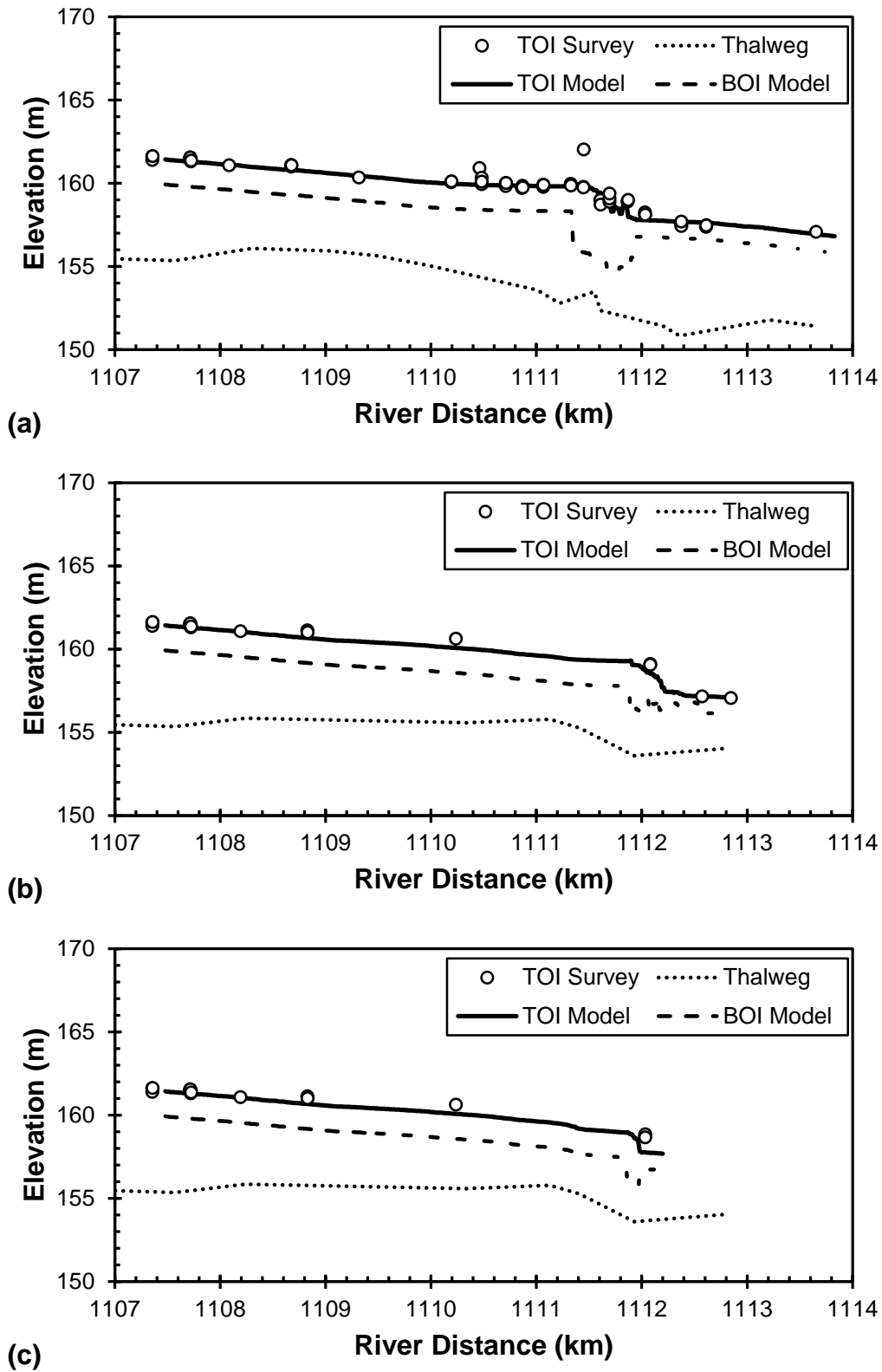
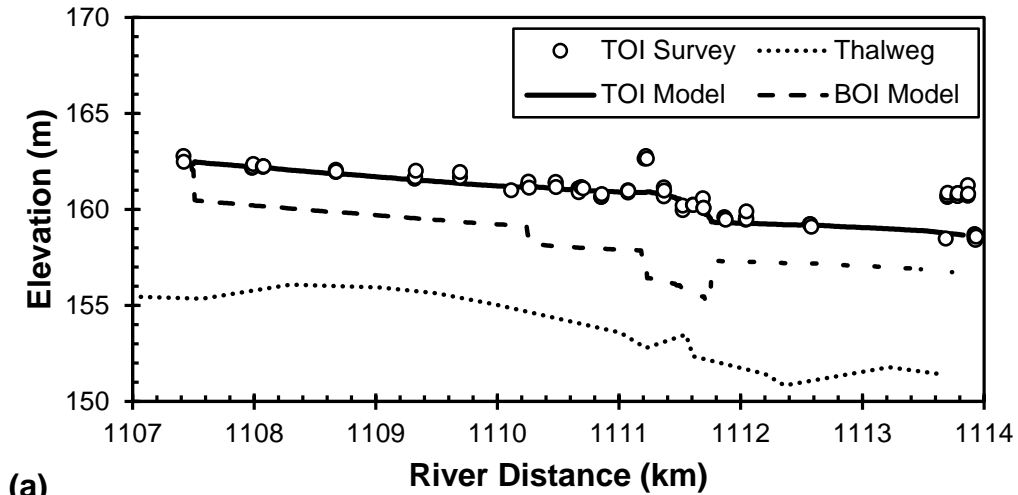
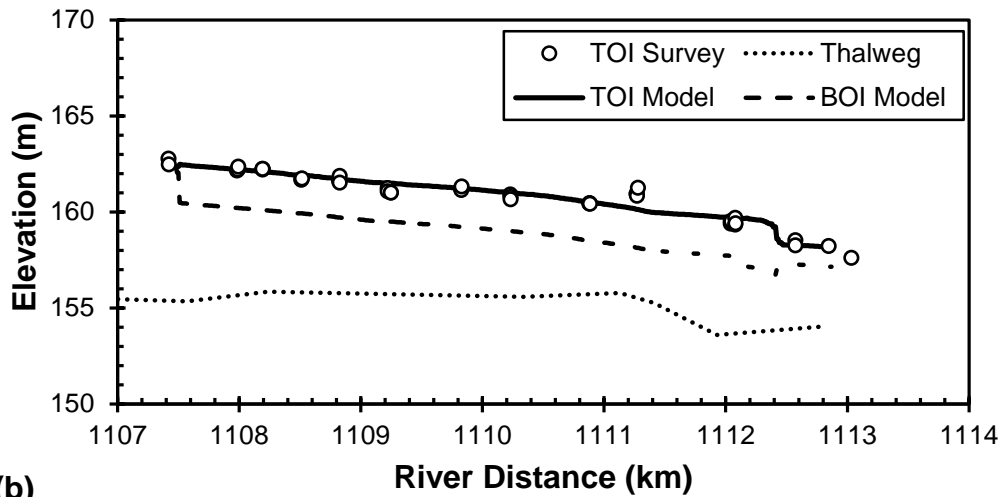


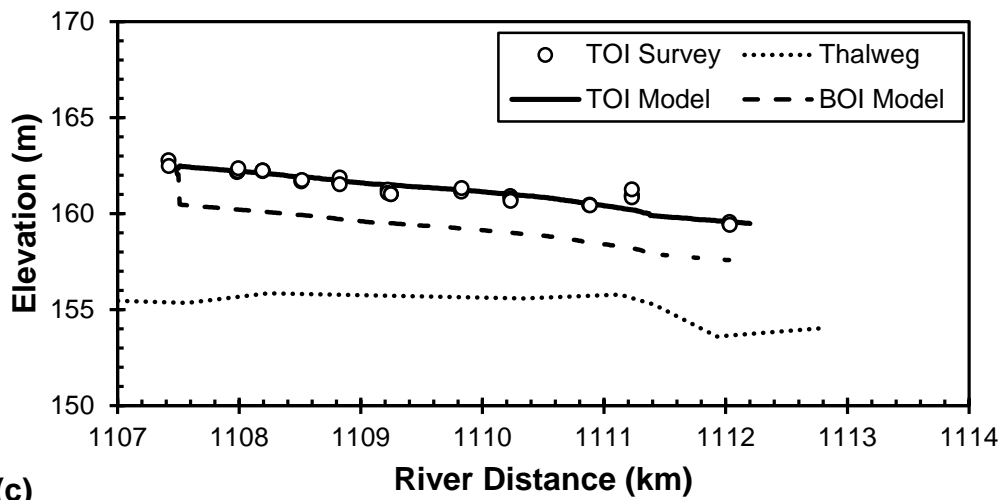
Figure 4.33 A comparison of the surveyed top of ice profiles from 5-May-09 and the River 2-D model ice jam profile results in the (a) East, (b) Fishing Village and (c) Rudd Channels.



(a)



(b)



(c)

Figure 4.34 A comparison of the surveyed top of ice profiles from 7-May-09 and the River 2-D model ice jam profile results in the (a) East, (b) Fishing Village and (c) Rudd Channels.

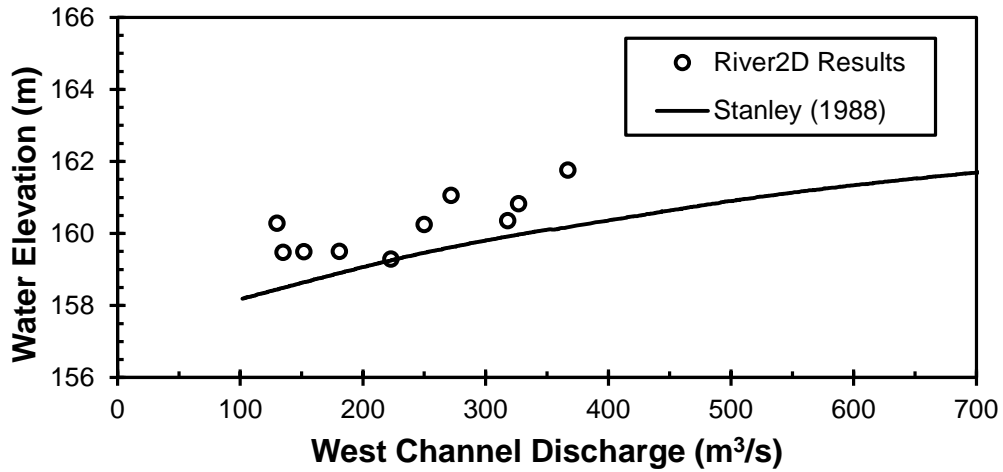


Figure 4.35 Comparison of the rating curve in Stanley (1988) at the West Channel split (river km 1111.0) and the River2D model results.

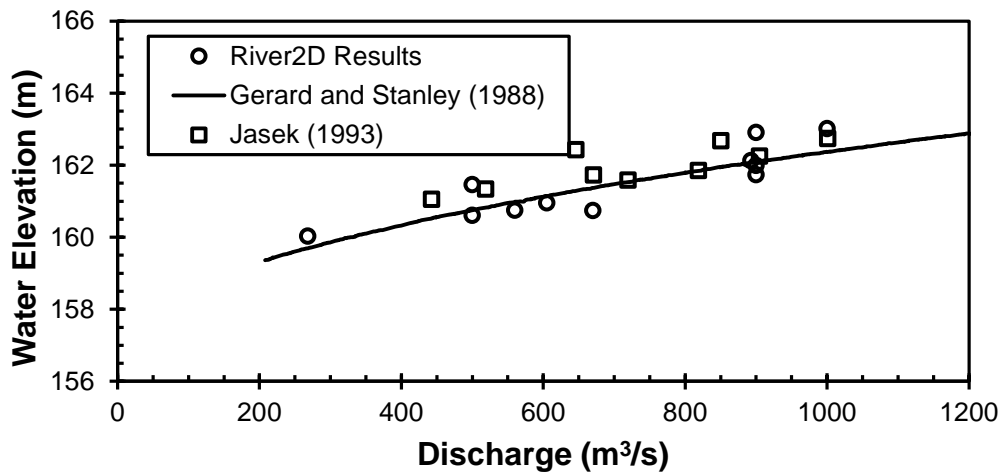


Figure 4.36 Comparison of the rating curve in Gerard and Stanley (1988) and discharge measurements in Jasek (1993) to the River2D model results.

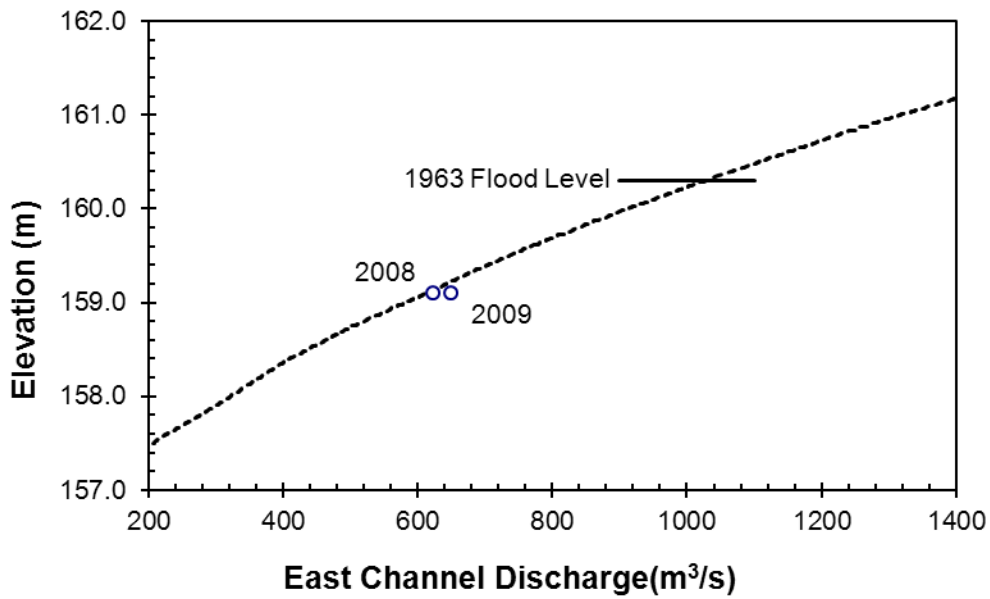


Figure 4.37 Comparisons of rating curve at Island A (river km 1113) from Stanley (1988) for an ice jam at the East Channel mouth and the 2008 and 2009 final ice elevations.

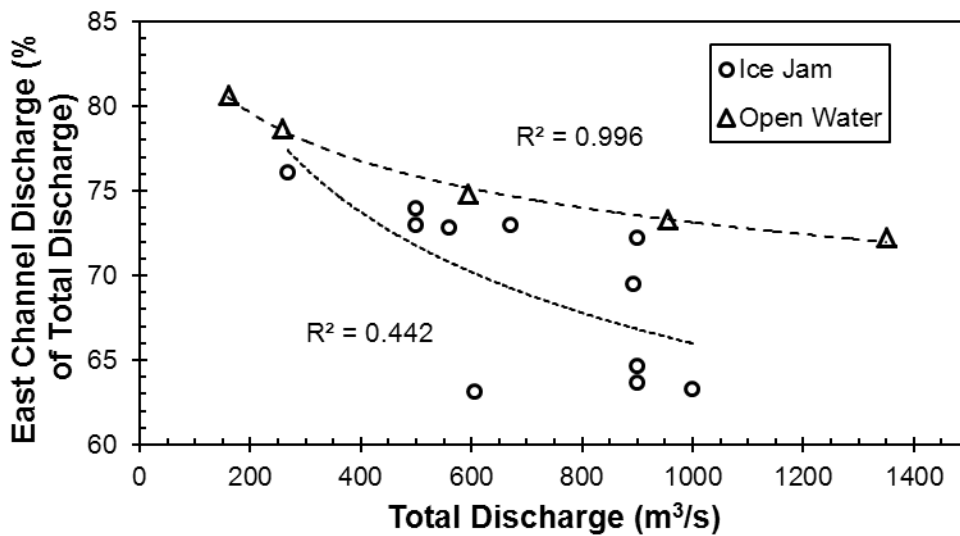


Figure 4.38 Relationship between the total discharge and the percentage going down the East Channel under open water and ice jam conditions.

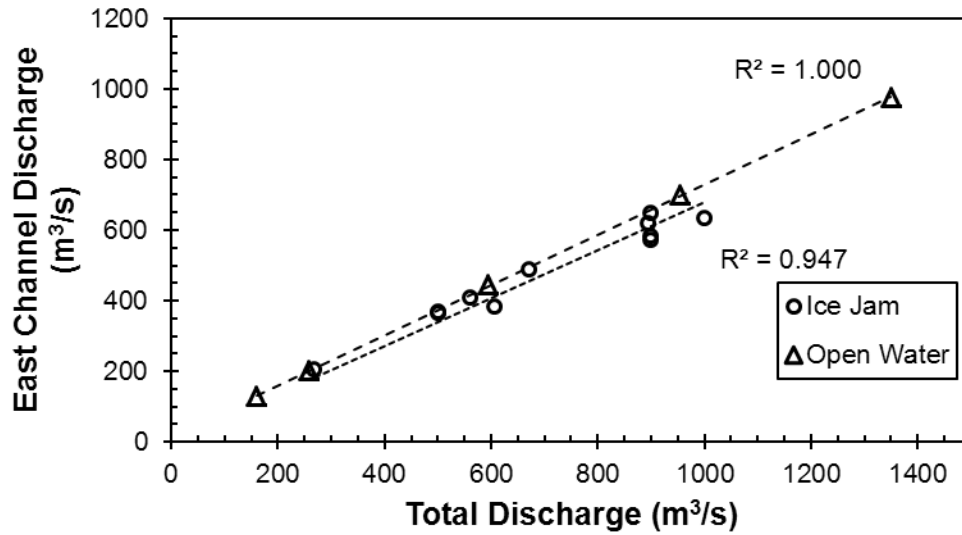


Figure 4.39 Relationship between the total discharge and the East Channel discharge under open water and ice jam conditions.

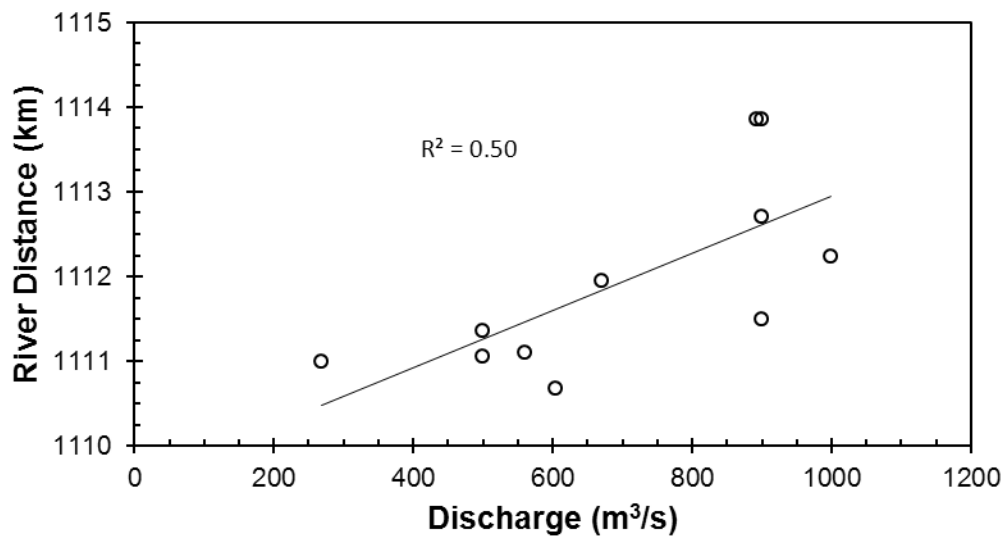


Figure 4.40 Relationship between the discharge and the most downstream extent of ice movement in the East Channel.

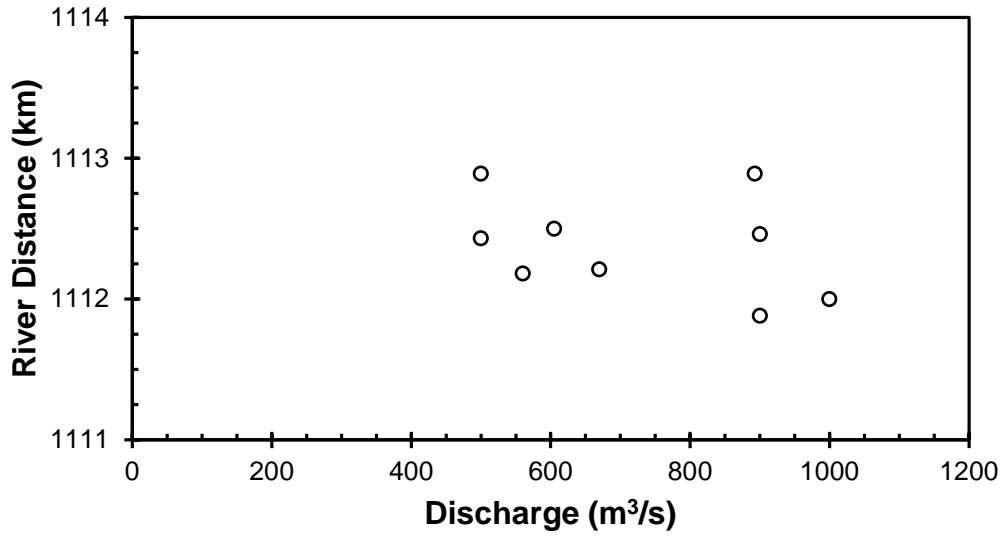


Figure 4.41 Relationship between the discharge and the most downstream extent of ice movement in the West Channel.

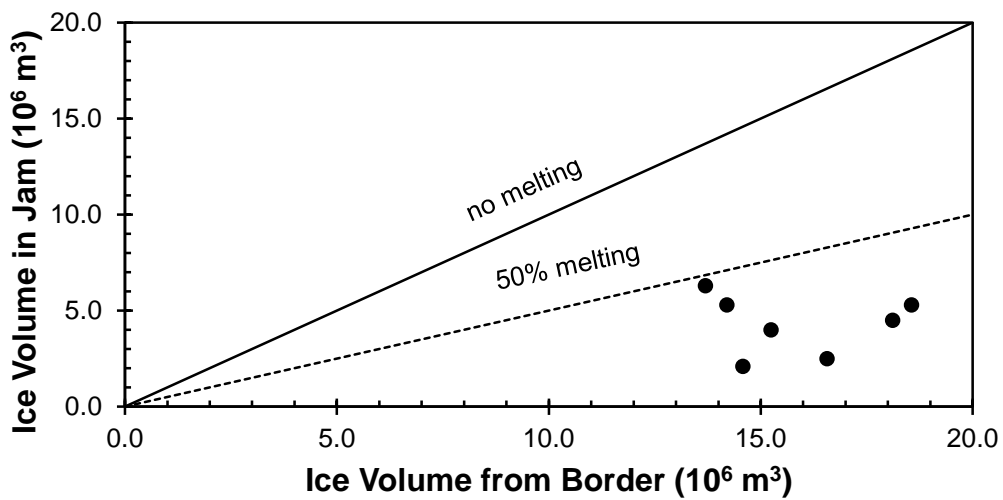


Figure 4.42 Comparison of ice volume estimates on the Hay River before breakup and the ice volume in the final ice jam configuration.



Figure 4.43 An example of stranded ice on an Island from the 2009 breakup of the Hay River.

5.0 Ice Jam Profile Generator

To assist the town of Hay River with predicting future ice jam levels, the River2D ice jam model data was used to develop an Ice Jam Profile Generator (IJPG). The IJPG used the modeled top of ice profiles to generate an average ice profile based on the discharge. It also provided error bars based on historical measured ice jam profiles. The IJPG was used to match several known ice surface profiles and the error is discussed.

Eleven ice jams were modeled with input discharges ranging from 268 m³/s to 1000 m³/s. The model results facilitated the development of ice jam rating curves at regular intervals along the East and West Channels. The rating curves were combined together to develop an Ice Jam Profile Generator (IJPG) which ‘predicts’ the expected ice jam profile for a user specified input discharge. The results of the IJPG were compared against three selected top of ice profiles.

Top of ice levels were extracted from the computed top of ice profile for each of the modeled historical events at 0.5 km intervals along both the East and West Channels. Half kilometer spacing between data points was selected because it provided enough data to illustrate changes in the profile without providing a cumbersome amount of data to process. River km 1107.5 and 1108.0 were in the main channel upstream of the split and were common to both the East and West Channel profiles. The modeled ice levels and the rating curves are shown in Figure 5.1 and Figure 5.2. For the East Channel profile, a total of eleven rating curves were developed from river km 1108.5 to 1113.5. These rating curves are shown in Figure 5.3 to Figure 5.13, respectively. Finally, nine rating curves were

made in the West Channel and go from river km 1108.5 to 1112.5. It must be noted that the rating curves were only done down the Fishing Village Channel in the West Channel delta. The same curves were not developed for the Rudd Channel because flooding does not affect people and property when it occurs in the Rudd Channel. The West Channel rating curves are shown in Figure 5.14 to Figure 5.22.

It was important to look at how the rating curves over and under predicted the modeled ice levels. In the East Channel the maximum over prediction was 1.8 m at river km 1111.0 and the maximum under prediction was 1.6 m at river km 1111.5. Overall, the worst curve fits occurred between river km 1110.5 and 1111.5 in the East Channel. This reach of the river is the typical location for ice jam toes to develop and have a rapid change in top of ice elevation. In the West Channel the maximum over prediction was 1.1 m at river km 1112.0 and the maximum under prediction was 1.4 m at river km 1112.5. Appendix B documents the error of each rating curve relative to the modeled results down the East and West Channels.

The over and under prediction error of each rating curve is not constant with discharge. Error envelope curves as a function of discharge were generated for the over and under prediction of each rating curve. The errors in the top of ice prediction are present in the model because the ice jam toe location is function of many variables, not just discharge. The major variables are the discharge, the rate of change of discharge, the water surface slope, the ice thickness and the degree

of ice deterioration. Discharge was used in the model because it was available as a model input.

Three profile events were selected to illustrate the effectiveness of the IJPG.

They were from 1985, 6-May-08 and 1990. The event from 1985 was selected because the discharge was high and the flooding in that year was severe in the West Channel. The 6-May-08 profile was selected because the high discharge and the fact that the ice movement in the East Channel extended to the mouth.

This scenario is important because historically it causes the most severe flooding in the East Channel. Finally, the 1990 profile was selected because it showed the results at a lower discharge.

Figure 5.23 compares the modeled and surveyed ice surface profiles from 1985 in the East and Fishing Village Channels. In the East Channel, the surveyed ice jam toe is approximately 0.5 km further downstream than the modeled toe. As well, the model generally under predicts the ice level upstream of the ice jam toe. Downstream of the ice jam toe, the model over predicts the ice levels. No data was available in the upstream reach of the West Channel. In the downstream reach, the model under predicts the surveyed ice level by as much as 1.5 m. The error bars envelope the modeled error quite well in both channels.

Figure 5.24 compares the modeled and surveyed ice surface profiles from 1990 in the East and Fishing Village Channels. In the East Channel, the modeled ice jam toe location matches quite well at approximately river km 1110.5. The modeled ice surface profile upstream of the ice jam toe also matches the surveyed ice

surface profile very well. Downstream of the ice jam toe the model over predicts by around 1.0 m. This error decreases further downstream from the ice jam. In the West Channel, the model matches the points in the upstream reach very well. In the downstream reach though, the ice jam toe formed between river km 1111.8 and 1112.4, but the model over predicts in this reach by approximately 0.5 m. The error bars do a good job of capturing the model error in the downstream reach of the West Channel. In the East Channel though, the negative error bars are above the measured ice profile by approximately 0.3 m.

Figure 5.25 compare the modeled and surveyed ice surface profiles from 6-May-08 in the East and Fishing Village Channels. In Figure 5.25 (a), the modeled ice surface profile matches the surveyed profile quite well upstream of the ice jam toe at around river km 1111.0. Downstream of the ice jam toe, the model under predicts the surveyed profile by around 1.0 m. In the West Channel, the model matches the surveyed profile very well but misses the ice jam toe at river km 1111.3. The error bars do a good job of capturing discrepancies between the modeled and surveyed profiles.

To make the IJPG more informative to the town of Hay River, key elevations were added in both the East and West Channels. In the East Channel, the elevations that were added were the NTCL berm, the East Channel docks, the KFN road and three avenue elevations in the Old Town adjacent to the river. The East Channel features are shown in Figure 5.26(a). It is difficult to distinguish the difference between the key elevations in Figure 5.26(a) at the East Channel mouth. Figure 5.27 shows the key elevations in better detail. In the West

Channel the elevation of the airport runway and the Fishing Village berm were included and are shown in Figure 5.26 (b). Both Figure 5.26 (a) and (b) and Figure 5.27 are plotted against the predicted ice surface profile for a discharge of $600 \text{ m}^3/\text{s}$.

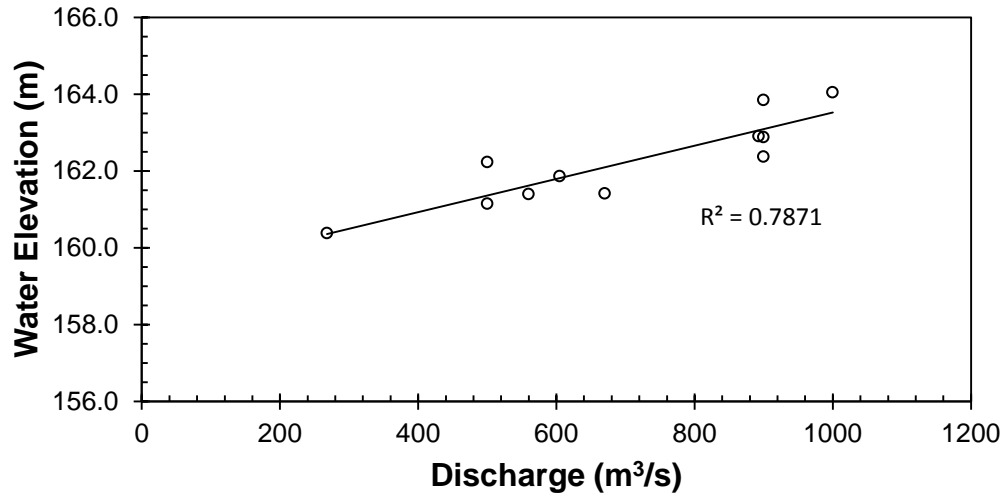


Figure 5.1 An ice jam rating curve developed from River 2-D modeling results at river km 1107.5.

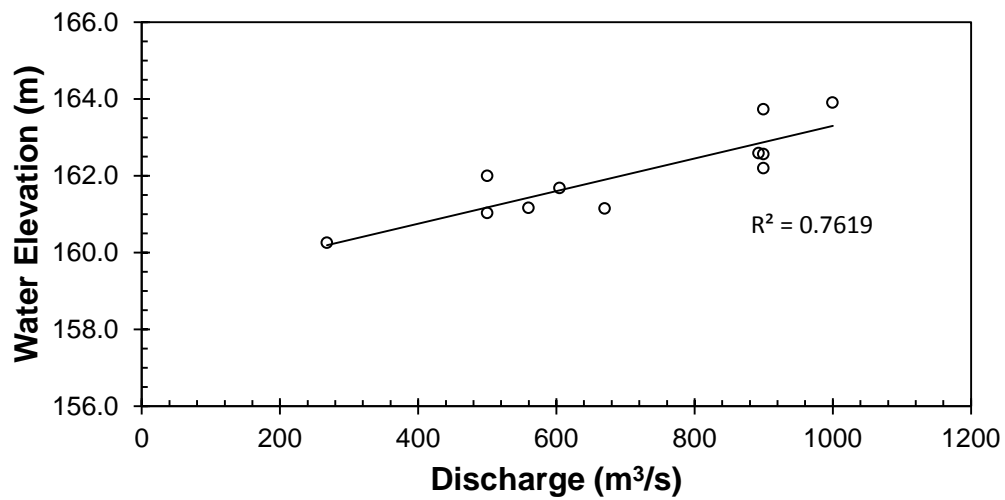


Figure 5.2 An ice jam rating curve developed from River 2-D modeling results at river km 1108.0.

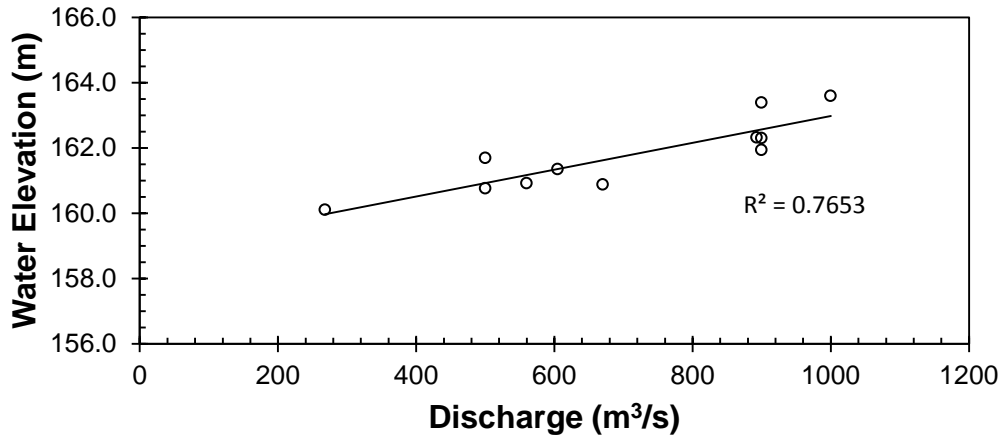


Figure 5.3 An ice jam rating curve developed from River 2-D modeling results at river km 1108.5 in the East Channel.

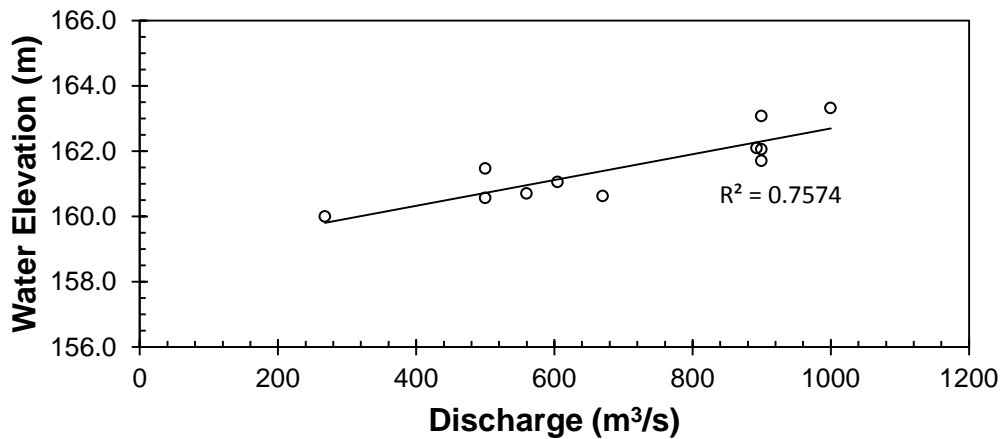


Figure 5.4 An ice jam rating curve developed from River 2-D modeling results at river km 1109.0 in the East Channel.

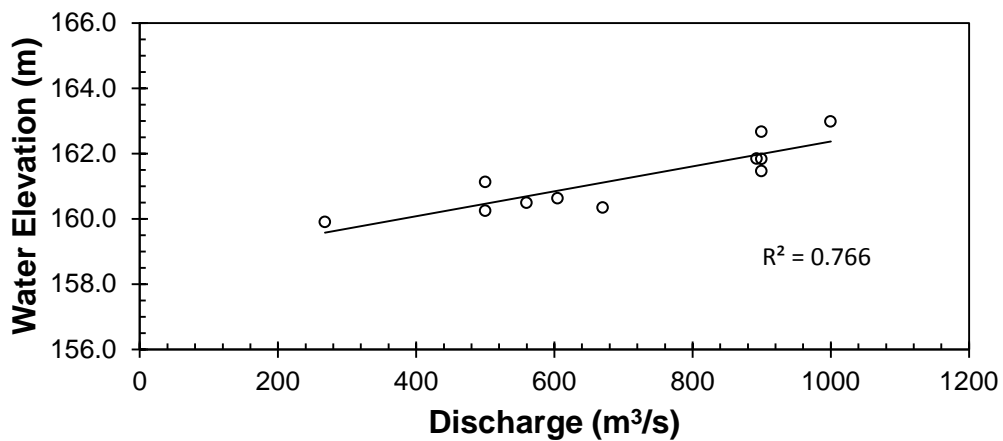


Figure 5.5 An ice jam rating curve developed from River 2-D modeling results at river km 1109.5 in the East Channel.

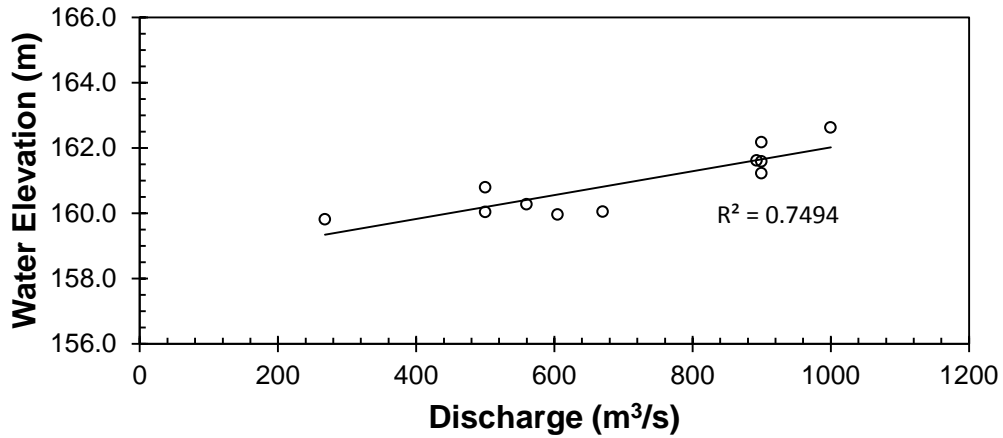


Figure 5.6 An ice jam rating curve developed from River 2-D modeling results at river km 1110.0 in the East Channel.

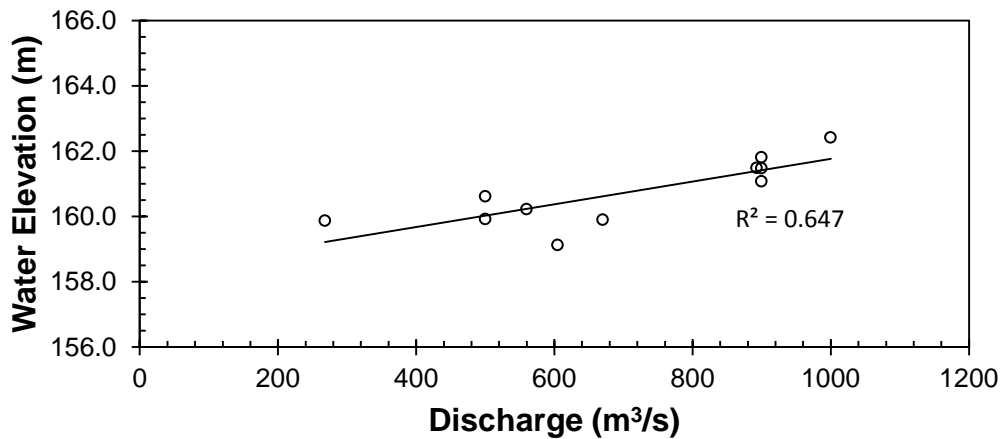


Figure 5.7 An ice jam rating curve developed from River 2-D modeling results at river km 1110.5 in the East Channel.

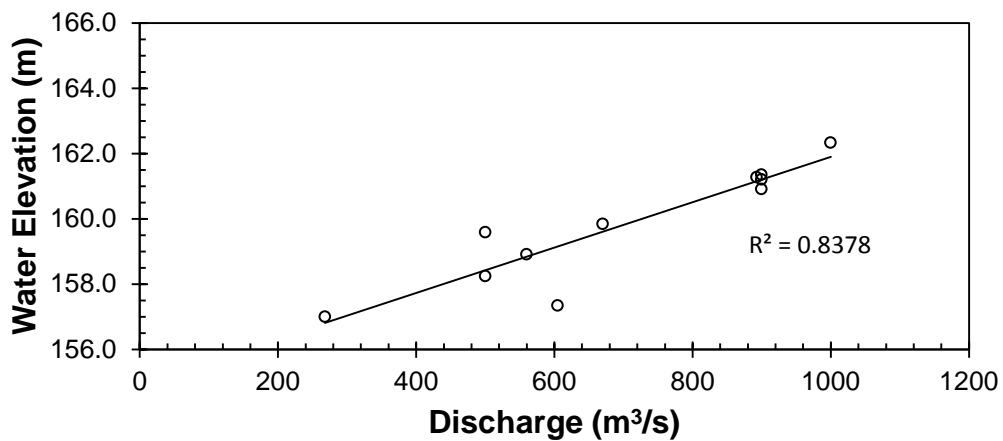


Figure 5.8 An ice jam rating curve developed from River 2-D modeling results at river km 1111.0 in the East Channel.

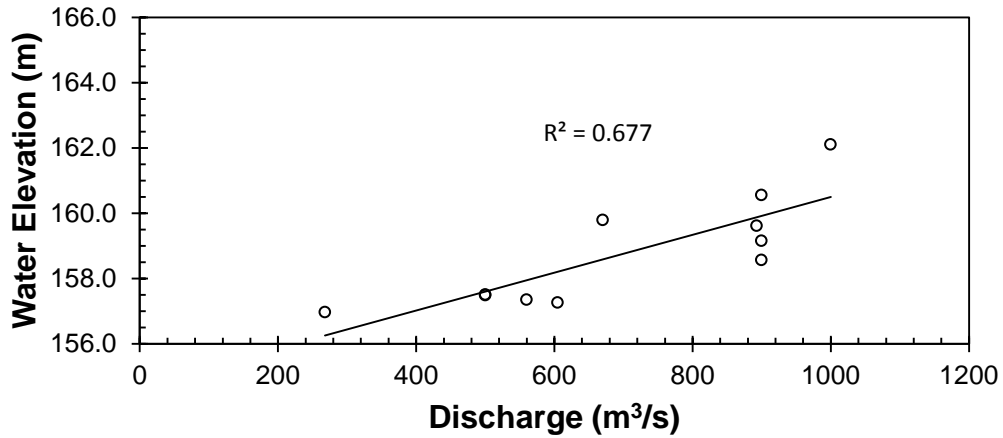


Figure 5.9 An ice jam rating curve developed from River 2-D modeling results at river km 1111.5 in the East Channel.

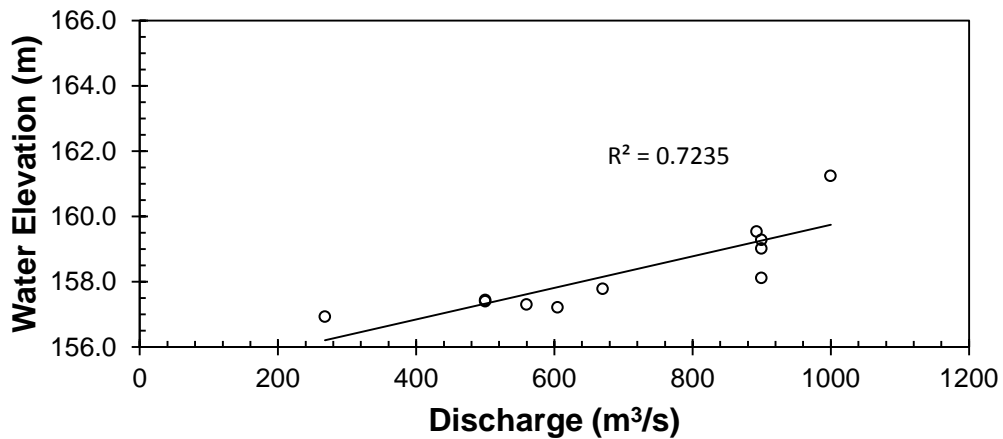


Figure 5.10 An ice jam rating curve developed from River 2-D modeling results at river km 1112.0 in the East Channel.

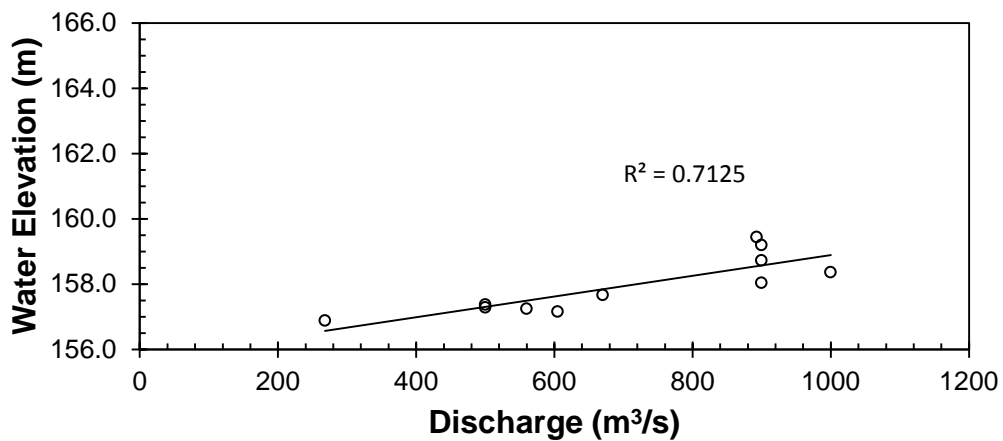


Figure 5.11 An ice jam rating curve developed from River 2-D modeling results at river km 1112.5 in the East Channel.

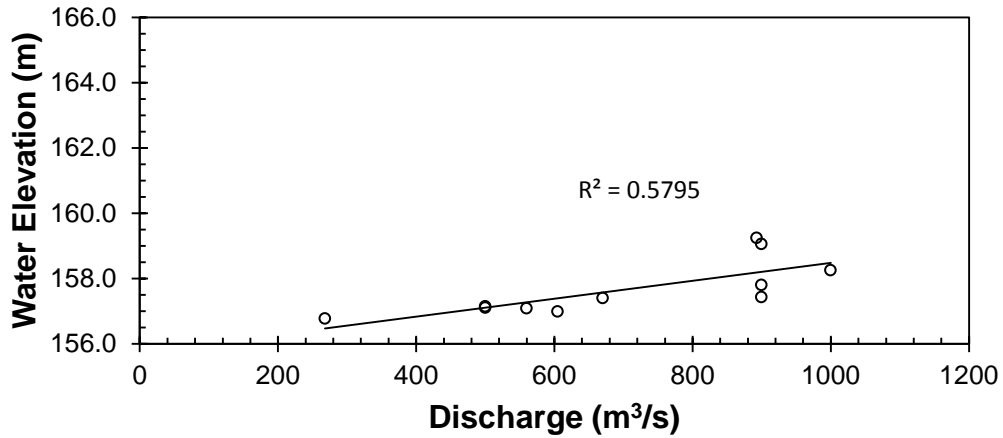


Figure 5.12 An ice jam rating curve developed from River 2-D modeling results at river km 1113.0 in the East Channel.

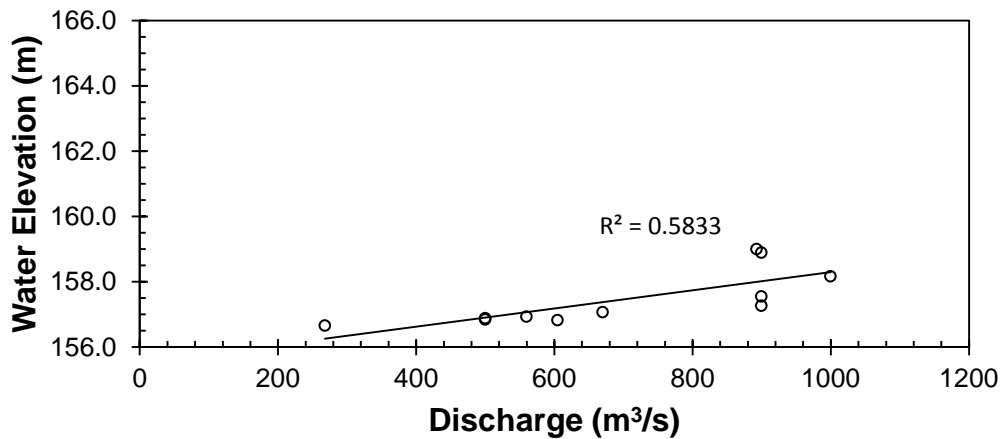


Figure 5.13 An ice jam rating curve developed from River 2-D modeling results at river km 1113.5 in the East Channel.

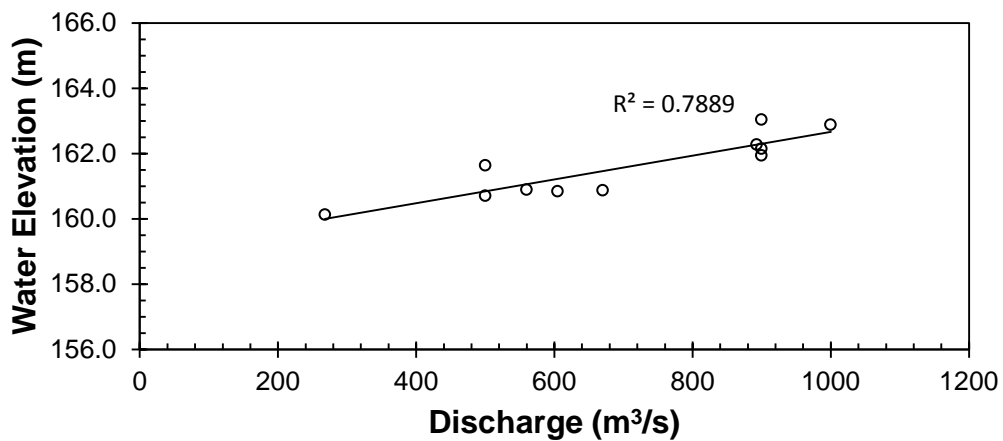


Figure 5.14 An ice jam rating curve developed from River 2-D modeling results at river km 1108.5 in the West Channel.

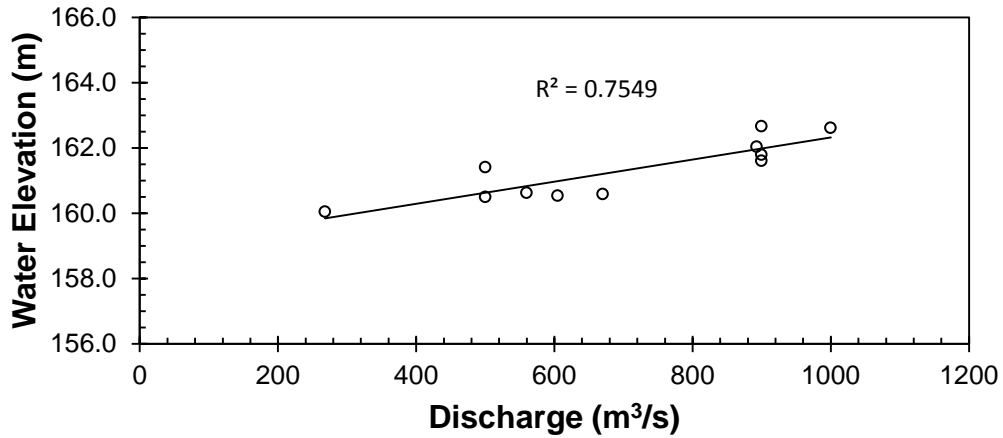


Figure 5.15 An ice jam rating curve developed from River 2-D modeling results at river km 1109.0 in the West Channel.

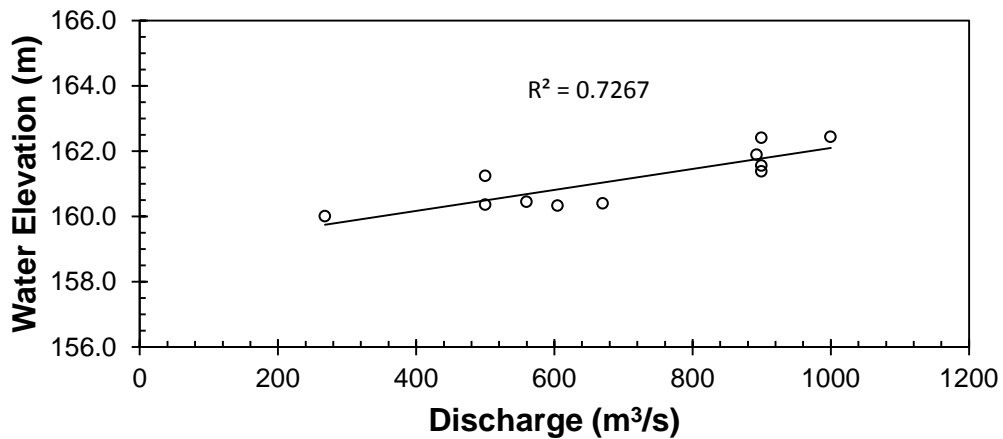


Figure 5.16 An ice jam rating curve developed from River 2-D modeling results at river km 1109.5 in the West Channel.

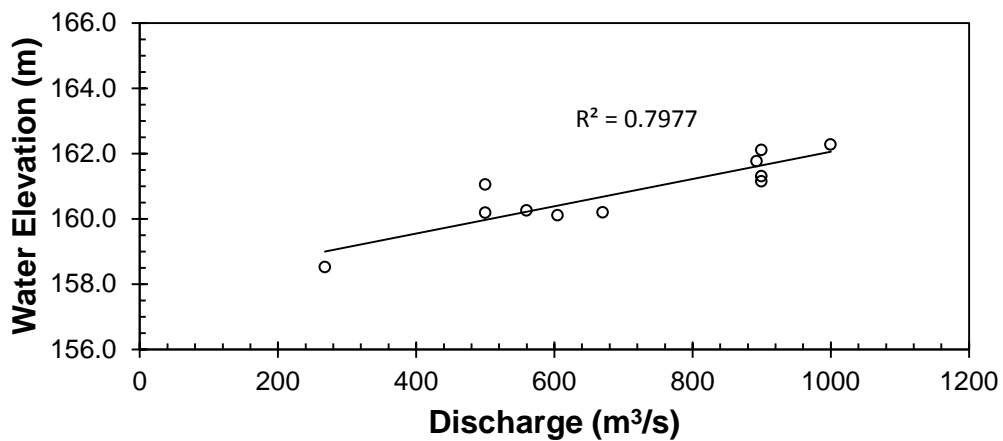


Figure 5.17 An ice jam rating curve developed from River 2-D modeling results at river km 1110.0 in the West Channel.

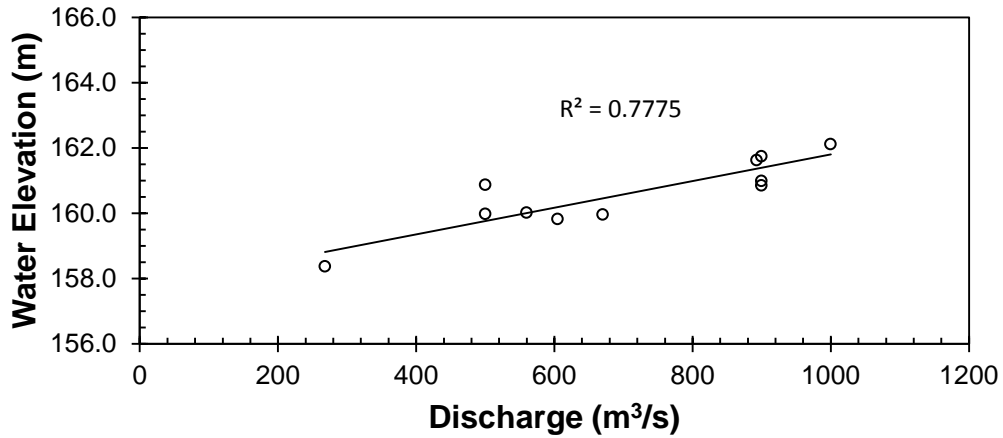


Figure 5.18 An ice jam rating curve developed from River 2-D modeling results at river km 1110.5 in the West Channel.

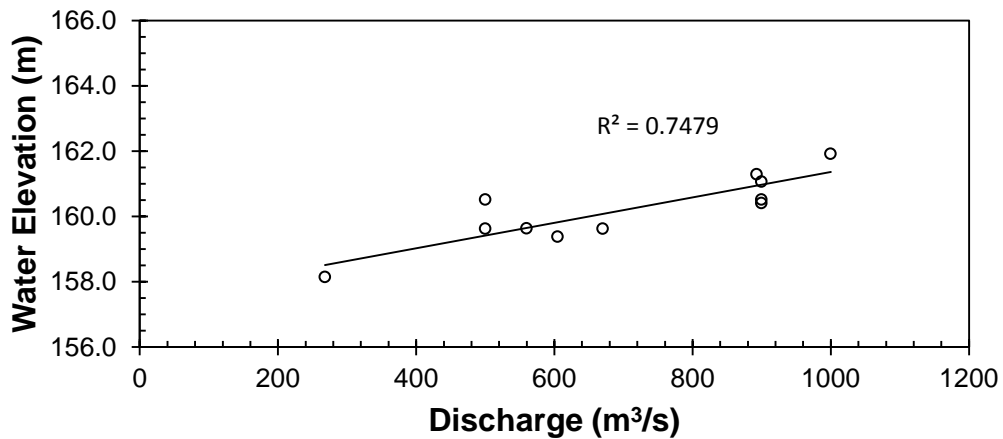


Figure 5.19 An ice jam rating curve developed from River 2-D modeling results at river km 1111.0 in the West Channel.

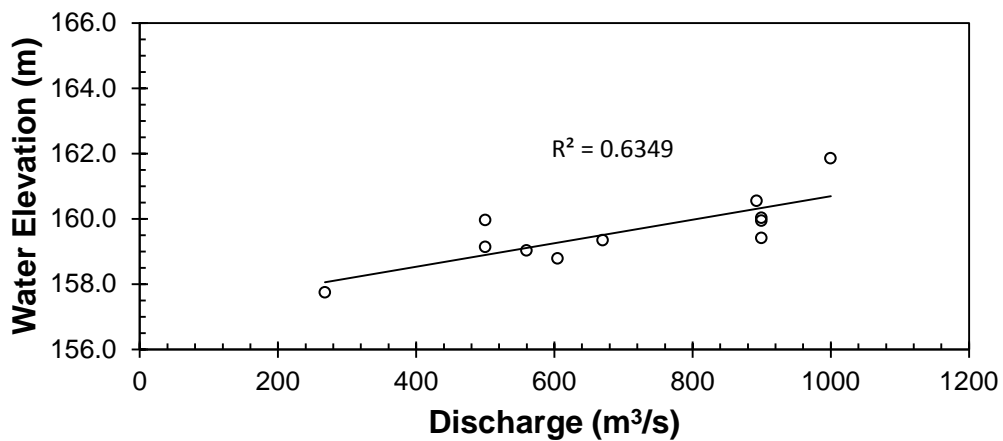


Figure 5.20 An ice jam rating curve developed from River 2-D modeling results at river km 1111.5 in the West Channel.

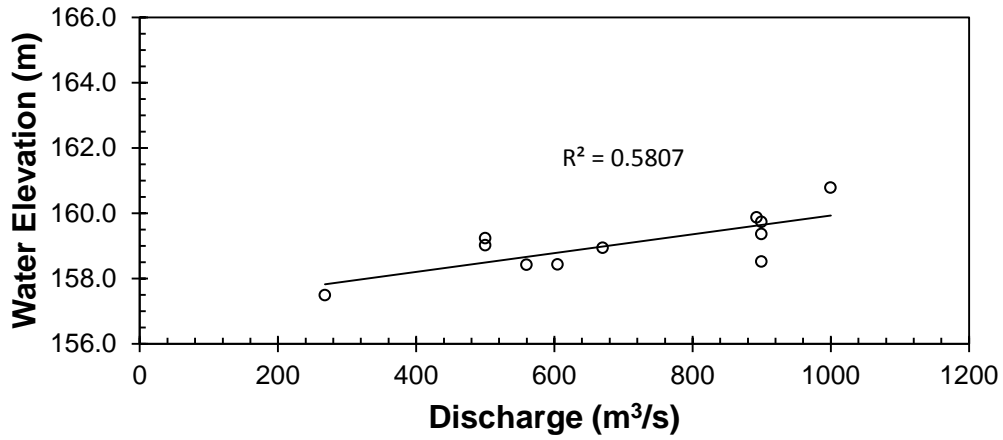


Figure 5.21 An ice jam rating curve developed from River 2-D modeling results at river km 1112.0 in the West Channel.

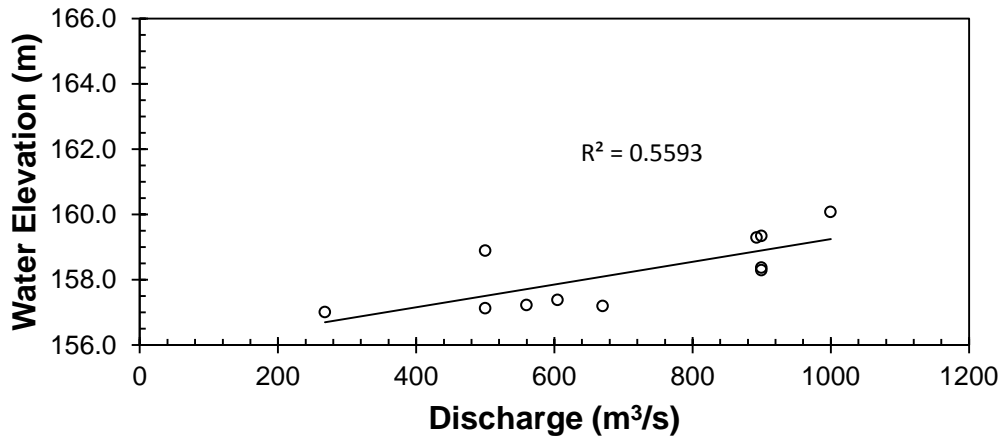


Figure 5.22 An ice jam rating curve developed from River 2-D modeling results at river km 1112.5 in the West Channel.

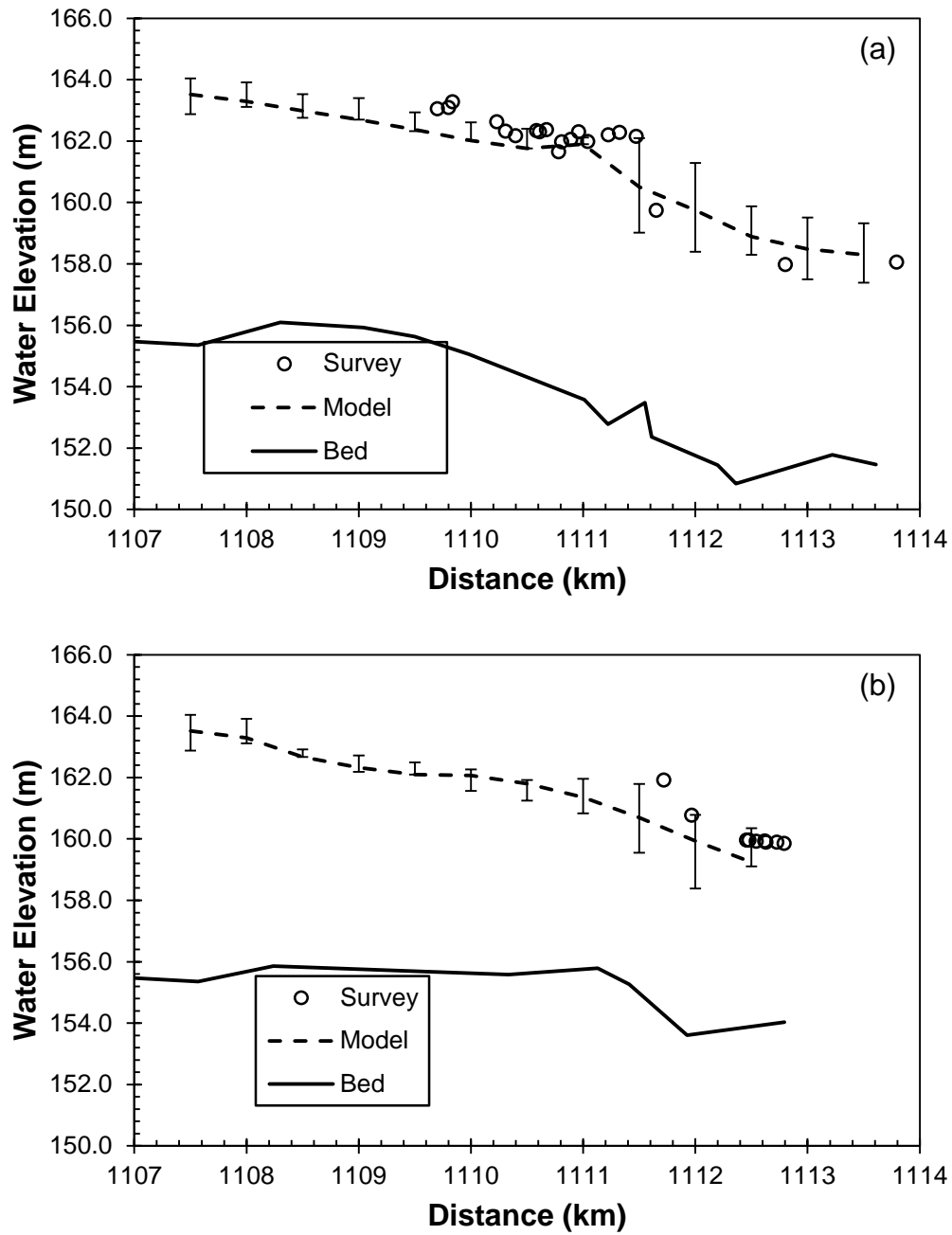


Figure 5.23 Comparison of ice jam survey data from 1985 and the ice surface profile from the Ice Jam Profile Generator in the (a) East and (b) West Channels.

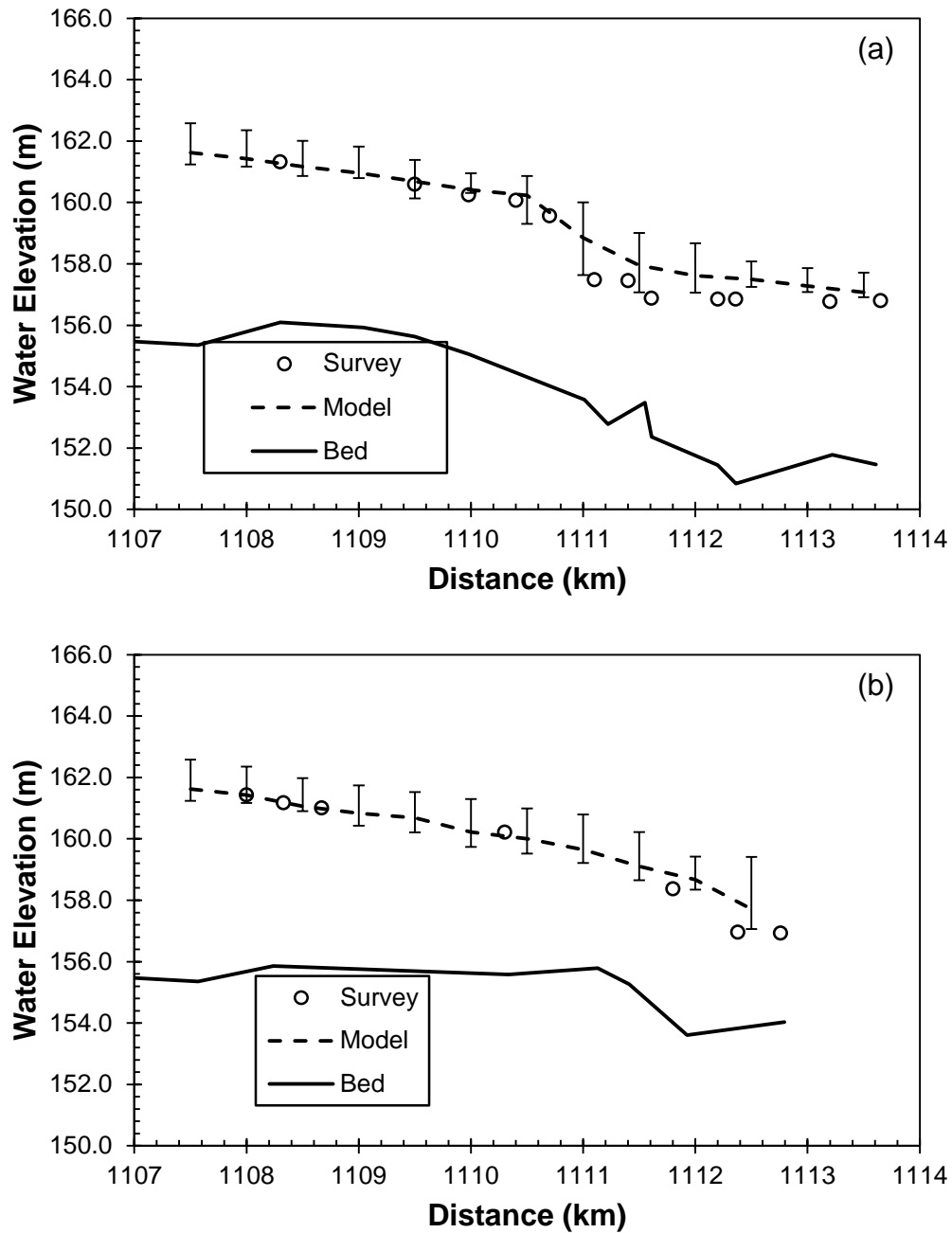


Figure 5.24 Comparison of ice jam survey data from 1990 and the ice surface profile from the Ice Jam Profile Generator in the (a) East and (b) West Channels.

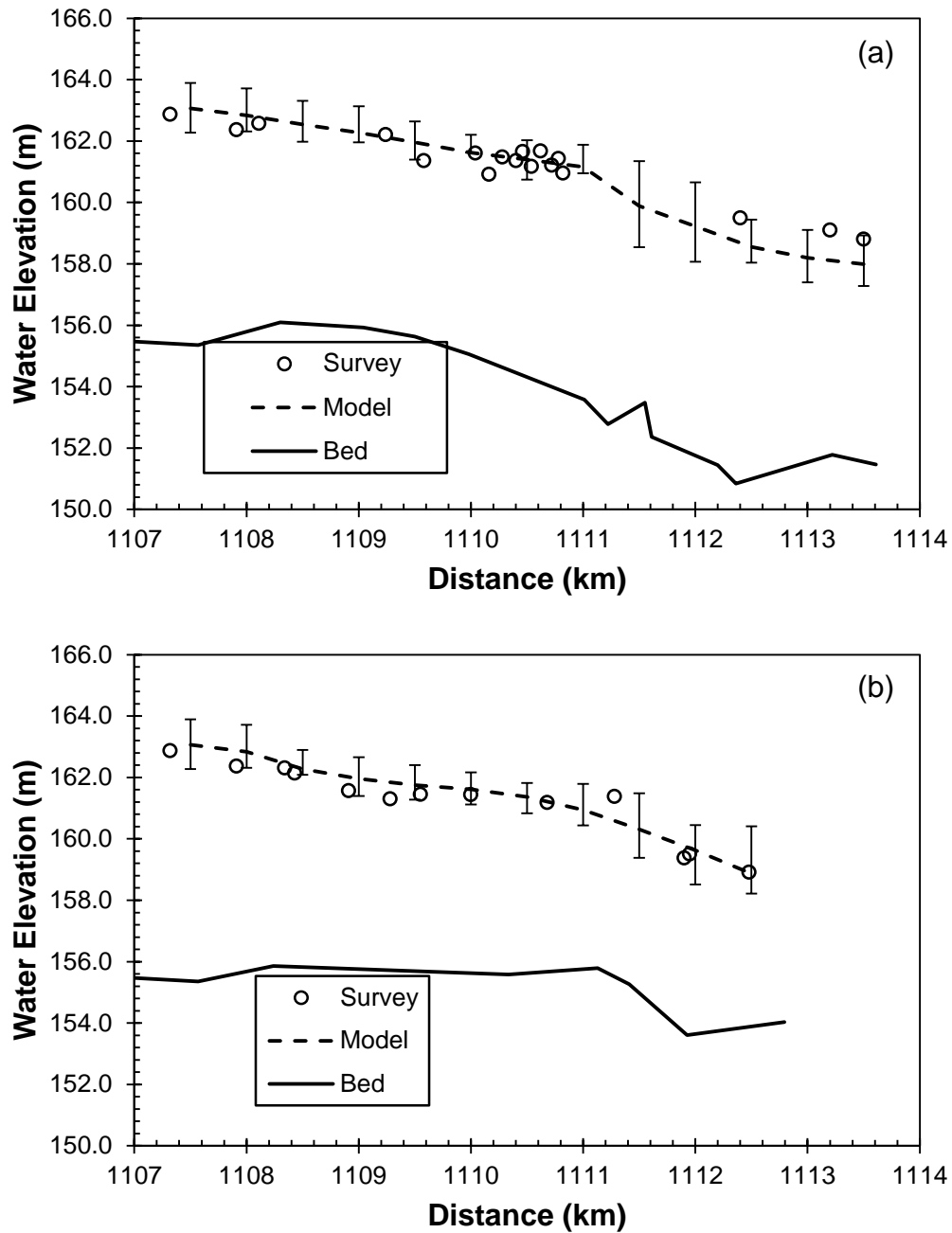


Figure 5.25 Comparison of ice jam survey data from 6-May-08 and the ice surface profile from the Ice Jam Profile Generator in the (a) East and (b) West Channels.

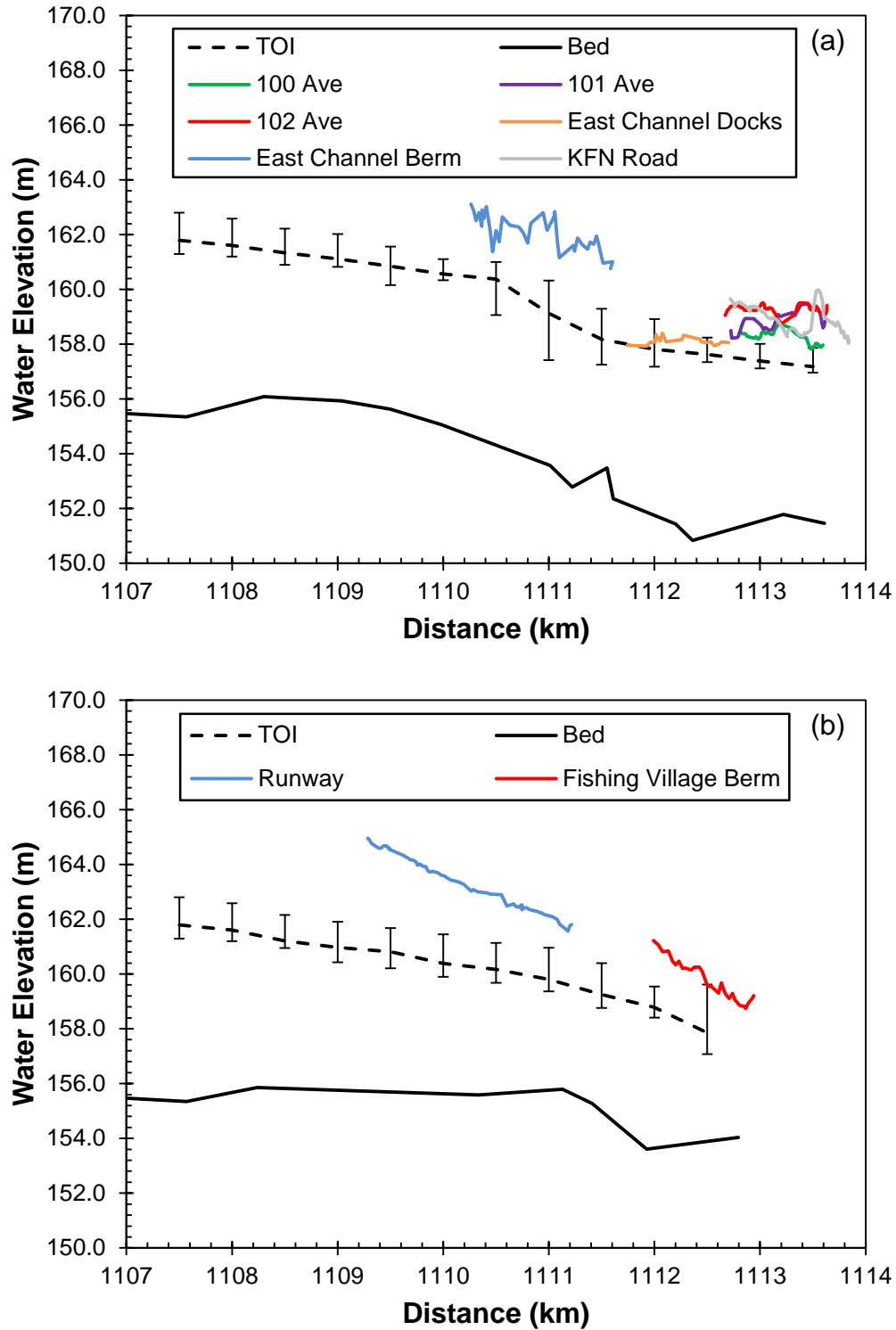


Figure 5.26 Ice jam profile plot at a discharge of $600 \text{ m}^3/\text{s}$ highlighting key elevations in the (a) East and (b) West Channels.

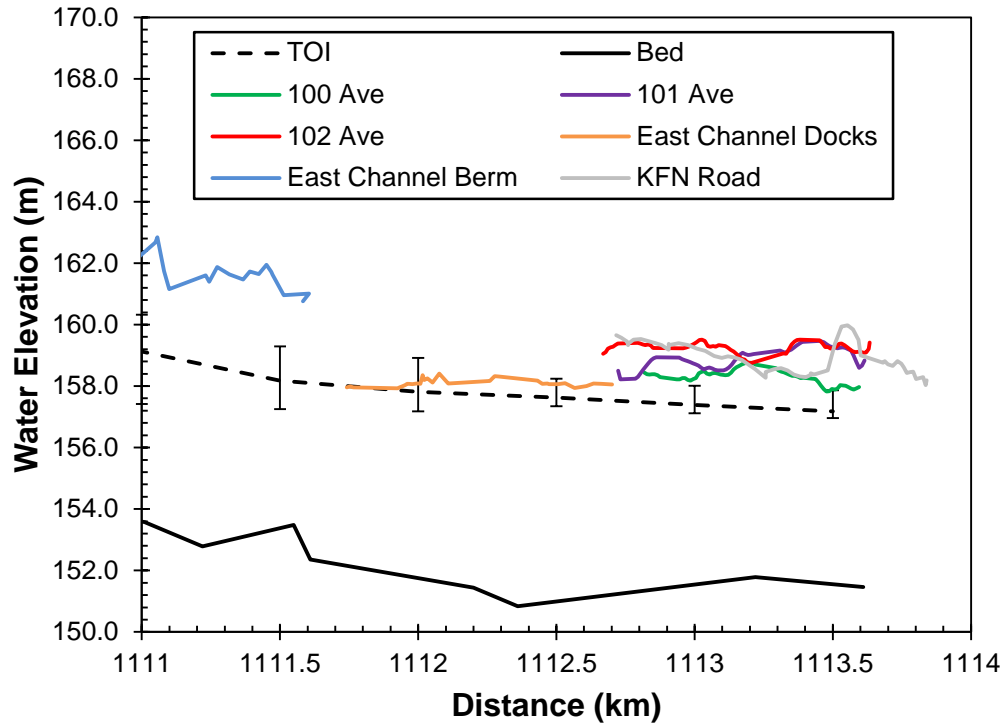


Figure 5.27 Ice jam profile plot at a discharge of 600 m³/s highlighting key elevations in the mouth of the East Channel.

6.0 Summary and Recommendations

This study was undertaken to determine whether two dimensional numerical models could accurately model break up ice jams and be used as an evacuation planning tool for the Town of Hay River. The models were tested for their ability to predict ice jam formation, ice movement and subsequent water elevations in the Hay River delta. It was part of a larger study aimed at developing an updated flood forecasting system for the town of Hay River.

A two dimensional numerical model requires a large quantity of data to develop and calibrate. Bathymetry data was collected in three phases and was used to create the model domain. Field work trips were conducted during river freeze-up and during the winter to get a better understanding of the ice and flow regimes. Breakup monitoring was done in 2008 and 2009 to document the breakup timeline and to measure ice jam profiles. Discharge and water surface profile data collected in the field were used to calibrate the models.

The two models tested were CRISSP2D and River2D. Both models are finite element models capable of simulating open water and ice affected scenarios. CRISSP2D is capable of modeling dynamic ice conditions while River2D can only handle specified, stationary ice conditions. River2D had a large amount of available documentation in the public domain while CRISSP2D is a proprietary product with only limited documentation. For that reason, preliminary testing was done with CRISSP2D to get an understanding of the model inputs and how the output results were affected.

The extensive field work program allowed for the creation of models under open water, freeze-up, winter and breakup conditions. Open water modeling compared the hydrodynamic capabilities of both models and calibrated the bed roughness in each model. Both models were able to match surveyed water surface profiles and agreed with measured velocity profiles. An open water rating curve at the East-West Channel split was created with River 2D and was found to be different than previous research. The open water modeling also provided a relationship between the discharge split in the East and West Channels and the total discharge. Winter ice modeling was done to calibrate the intact ice roughness. Freeze-up modeling was done with CRISSP2D to test the ice dynamic capabilities and to better understand the progression of ice formation. The CRISSP2D results matched the field observation quite well. A detailed sensitivity analysis of the model input parameters was not done but would be effective for improving the model results.

Breakup modeling was done with both models to test whether either could be used as a flood forecasting tool. CRISSP2D models were developed to test the models' ability to create an ice jam without additional user inputs and to see if CRISSP2D could match observed water surface profiles. Extensive testing was done but CRISSP2D was unable to generate an ice jam without a user instigated jam toe. Four surveyed ice jam profiles were modeled with CRISSP2D in which the ice jam toe location was specified. The results were quite poor with the model being unable to consolidate the ice sheet thick enough to match the observed ice elevations. Several input parameters were tested to improve the results with little or no improvement.

Several limitations were encountered during the CRISSP2D modeling. The first was that the model has a limit on the number of nodes and elements in the finite element mesh. This limits the size and the accuracy of the model geometry. The second limitation was the computational time required by the model. The fastest model runs took in the order of one day to complete and the slowest took several days. This means CRISSP2D could not be used as a forecasting tool when evacuation plans are changing on an hourly basis.

River2D was the second model used to model ice jam events. Eleven ice jam models were developed based on surveyed top of ice profiles from past research. Though no measured ice thickness data were available, each model was an analog of each ice jam and was useful for studying each event. A relationship between the total discharge and the East-West Channel split was produced from the model results and compared to the open water curve. The documented breakup events in 2008 and 2009 were unique years because ice jams developed at the mouth of the East Channel. Historically, this is when the worst flooding is experienced. Both events were compared to the rating curve at Island A developed by Stanley (1988) and agreed very well.

Two additional relationships were investigated. The first was the correlation in the East and West Channels between the maximum downstream extent of ice movement and the maximum discharge was explored. No correlation was found in the West Channel. A weak correlation was found in the East Channel ($R^2 = 0.50$) and showed that a high discharge equated to further downstream movement. The second relationship that was investigated was how the volume of ice in each

modeled ice jam compared to the expected ice volume from upstream. The results suggest that over 50% of the ice from upstream had melted or become stranded before it reaches the delta.

The River2D model results enabled the development of an ice jam profile predictor to be used by the town of Hay River. Rating curves were constructed at half kilometer intervals down the East and West Channels and used to develop the relationship between the ice jam profile and the channel discharge. The correlation between the maximum error and discharge was also developed for each rating curve to quantify the maximum error of the predicted ice jam profile. The ice jam profile predictor was compared to three surveyed ice jams and performed reasonably well. Road and key feature elevations in the East and West Channels were added to increase the utility of the IJPG.

The ice jam predictor results showed that River2D could be a useful model for estimating ice jam flooding. Several limitations still exist though. Predicting ice jams in the Hay River delta is only possible because of the extensive record of ice jam events. For sites with little or no breakup records, River2D is unable to predict the formation of an ice jam and the subsequent water levels. Additional work is still required concerning the stopping and release of intact ice jams to assist the town of Hay River to predict when an ice jam will form at the mouth of the East Channel.

Future research should focus on studying what causes an established ice jam in the East Channel to slide down towards the channel mouth. The 2008 and 2009

breakup years were the first since 1963 in which an East Channel ice jam formed downstream of river km 1111.0 and suggests that it may become a more common occurrence. The major cause is believed to be surge waves from the release of upstream ice jams. Measurement of the amplitude and period of ice jam surge waves in the delta would be valuable information for predicting an ice jam at the East Channel mouth. Research is continuing on dynamic ice modeling software and hopefully in the future a model will be developed that can predict when and where ice jams will form on the Hay River.

7.0 References

Ashton, G. D. (1986). *River and Lake Ice Engineering*. Littleton, Colorado: Water Resources Publications.

Beltaos, S., Ford, J. S., and Burrell, B. C. (1996). Remote Measurements of Ice Jam Thickness Profiles. *Proceedings of the 13th IAHR Ice Symposium*, (pp. 577-584). Beijing.

Flato, G., and Gerard, R. (1986). Calculation of Ice Jam Thickness Profiles. *4th Workshop on the Hydraulics of Ice Covered Rivers* (pp. C3.1 - C3.18). Montreal: CRIPE.

Gerard, R., and Jasek, M. (1990). *Breakup observations and ice jam flood forecast algorithm evaluation, Hay River, N.W.T.* Edmonton: University of Alberta.

Gerard, R., and Stanley, S. (1988). *Ice jams and flood forecasting, Hay River, N.W.T.: Phase 1 - Final Report*. Edmonton: University of Alberta.

Gerard, R., Hicks, F., and Jasek, M. (1990). *Ice jams and flood forecasting, Hay River, N.W.T. - Phase 2: surges and interactive computer program*.

Gingold, R. A., and Monaghan, J. J. (1977). Smoothed particle hydrodynamics: theory and applications to non-spherical stars. *Monthly Notices of the Royal Astronomical Society*, 181, 375-389.

- Hanes, D. M., and Inman, D. L. (1985). Observations of Rapidly Flowing Granular-Fluid Materials. *Journal of Fluid Mechanics [0022-1120]* , 150, 357-380.
- Hicks, F. E., Steffler, P. M., and Gerard, R. (1992). Finite element modeling of surge propagation and an application to the Hay River, N.W.T. *Canadian Journal of Civil Engineering* , 19, 454-462.
- Hutchison, T., Hicks, F. (2007). Observations of ice jam release events on the Athabasca River, AB. *Canadian Journal of Civil Engineering* , 473-484.
- Jasek, M. (1993). *Hay River flood control: Hay River, N.W.T.* The Town of Hay River, N.W.T.
- Jasek, M., Stanley, S., and Gerard, R. (1993). *Update of ice jam flood database, Hay River, N.W.T.* Yellowknife, N.W.T., Indian and Northern Affairs.
- Jasper, J. N. (1983). *Hay RiverL historical flood review.* Yellowknife: Indian and Northern Affaris Canada.
- Ji, S., Shen, H. T., Wang, Z., Shen, H., and Yue, Q. (2004). Ice Dynamic Model with a Viscoelastic-Plastic Constitutive Law. *Proceedings from 17th International Ice Symposium*, (pp. 274-281). Saint Petersburg.
- Liu, L., Shen, H. T., and Tuthill, A. M. (1998). A numerical model for rive ice jam evolution. *Proceedings of the 14th international symposium on ice*, V2. Potsdam.

Lucy, L. B. (1977). A numerical approach to the testing of the fission hypothesis. *The Astronomical Journal* , 82 (12), 1013-1024.

Meliefste, C., Hicks, F. (2006). *Bathymetric Survey of the Hay River Delta, 2005*. University of Alberta, Department of Civil and Environmental Engineering, Edmonton.

Saad, Y., and Schultz, M. H. (1986). GMRES: A generalized minimal residual algorithm for solving nonsymmetric linear systems. *SIAM J. Sci. Stat. Comp.* , 7 (3), 856-869.

Shen, H. (2005b). *CRISSP2D Programmer's Manual. CEATI Report No. T012700-0401*. Montreal: CEA Technologies Inc.

Shen, H. (2005a). *CRISSP2D User's Manual. CEATI Report No. T012700-0401*. Montreal: CEA Technologies Inc.

Shen, H. T., and Chen, Y. C. (1992). *Lagrangian discrete parcel simulation of two-dimensional river ice dynamics, CEE Reprot 92-9*. Clarkson University, Potsdam.

Shen, H. T., Chen, Y. C., Wake, A., and Crissman, R. D. (1993). Lagrangian discrete parcel simulation of river ice dynamics. *International Journal of Offshore and Polar Engineering* , 3 (4), 328-332.

Shen, H. T., Shen, H., and Tsai, S. M. (1990). Dynamic Transport of River Ice. *Journal of Hydraulic Research* , 28 (9), 659-671.

- Stanley, R., and Dusel, F. J. (1963). *Engineering Report of Flood Protection at Hay River, N.W.T.* Edmonton: The Department of Public Works Canada.
- Stanley, S. J. (1988). *Ice Jam Analysis in a Complex Reach: A Case Study*. MSc Thesis, Univeristy of Alberta, Civil Engineering, Edmonton.
- Steffler, P., and Blackburn, J. (2002). *Introduction to Depth Averaged Modeling and User's Manual*. Univeristy of Alberta, Edmonton.
- UMA. (1978). *Flood risk mapping for the Hay River, Northwest Territories*. Winnipeg: Underwood McLellan.
- Watson, D. (2011). *Observations and modeling of ice jam release events on the Hay River, N.W.T.* Edmonton: University of Alberta.
- Wedel, J. H. (1985). *1985 Hay River Flood Report, N.W.T.* Yellowknife, N.W.T., Water Planning and Managment.
- Wiens, L. H. (1983). *Hay River Flood Risk Study*. Environment Canada.
- Wojtowicz, A. (2010). *2-D Modeling of Freeze-up Processes on the Athabasca River downstream of Fort McMurray, Alberta*. University of Alberta, Civil and Environmental Engineering. Edmonton: University of Alberta.

Appendix A : CRISSP2D Default Model Inputs

| Input File | Input Parameter | Abreviation | Default Value | Unit |
|-----------------------------|---|--------------------|----------------------|-------------------|
| Time Control | hydrodynamic simulation time step based on the CFL condition | deltath | 5 | s |
| .tim | ice dynamic simulation time step | deltati | 1 | s |
| | coupling time step between the hydrodynamics and the ice dynamics | tintvl | 900 | s |
| Geometry Information | bed Manning's roughness coefficient | cnn(i) | 0.025 | |
| .geo | boundary roughness modifier | cnnbdr(i) | 1.0 | |
| | x-x component of eddy viscosity | exx(i) | 1.0 | m ² /s |
| | y-y component of eddy viscosity | eyy(i) | 1.0 | m ² /s |
| | x-y component of eddy viscosity | exy(i) | 1.0 | m ² /s |
| | smoothing coefficient | smn(i) | 1.0 | |
| | upwind weight coefficient | wupwind(i) | 0.25 | |
| | diameter of bed particles | dsnb(i) | 0.01 | m |
| Ice Flux information | Manning's roughness of ice islands or border ice | cnisld | 0.02 | |
| .iqb | Darcy's coefficient for seepage flow in ice islands | darcyild | 0.02 | |
| | Darcy's coefficient for seepage flow in rubble ice | darcyrub | 1.0 | |
| | maximum concentration of ice parcels | anmax | 0.6 | |
| | initial concentration of each parcel | an0 | 0.6 | |
| | initial surface ice thickness of each parcel | thi0 | 0.2 | m |
| | initial frazil ice thickness of each parcel | thi0f | 0 | m |
| | initial ice parcel edge length | hpi0 | 10 | m |
| | friction coefficient between ice and river bank | fric1 | 1.04 | |
| | friction coefficient between ice and bed | fric2 | 1.04 | |
| | wind-ice stress coefficient | ca | 0.0015 | |
| | Manning's roughness coefficient of single ice layer | cni | 0.02 | |
| | maximum roughness coefficient for ice jams | cnimax | 0.06 | |
| | internal friction angle of ice | phi | 46 | |
| | empirical constant | pj | 15 | |

| Input File | Input Parameter | Abreviation | Default Value | Unit |
|----------------------------|--|-------------|---------------|------------------|
| Physical Parameters | solar radiation parameters | | | |
| .par | geographic latitude | phid | 44.73 | |
| | height of wind data measurement | z1 | 4.5 | m |
| | elevation from sea level | z2 | 80 | m |
| | sun exit angle, 180 for horizontal | alphsd | 180 | |
| | sun emission angle, 0 for horizontal | alphrd | 0 | |
| | solar constant | sio | 1380 | W/m ² |
| | standard longitude | alsm | 75 | |
| | local longitude | allm | 75.43 | |
| | albedo of ice | alberdo | 0.2 | |
| | water temperature, thermal growth and ice decay parameters | | | |
| | coefficient of linear heat flux between water and air | hwa | 20 | |
| | coefficient of linear heat flux between ice and air | hia | 12.189 | |
| | coefficient of linear heat flux between ice and air | alp | 32.547 | |
| | coefficient for calculating heat transfer between ice and water for turbulent flow | cwi1 | 1477.25 | |
| | coefficient for calculating heat transfer between ice and water for supercooled turbulent flow | ciw1 | 1433.45 | |
| | Nuselt number for calculating heat transfer coefficient between ice and water for laminar flow | ata | 2.47 | |
| | thermal conductivity of black ice | xki | 2.24 | W/m/C |
| | thermal conductivity of white ice | xkw | 1.12 | W/m/C |
| | thermal conductivity of snow | xks | 0.3 | W/m/C |
| | heat transfer coefficient from water to ice | cwi | 900 | |

| Input File | Input Parameter | Abreviation | Default Value | Unit |
|----------------------------|---|--------------------|----------------------|-------------|
| Physical Parameters | border ice formation parameters | | | |
| .par | critical water surface temperature for border ice formation | tc | -0.5 | C |
| | critical velocity above which skim ice will not form | vcrskm | 0.25 | m/s |
| | critical average flow velocity above which shore ice accumulation does not form | vcrbom | 1.3 | m/s |
| | maximum concentration for border ice formation | anmaxborder | 1 | |
| | skim ice formation parameters | | | |
| | intial skim ice thickness | hi0 | 0.001 | m |
| | maximum concentration of skim ice | anmaxskim | 1 | |
| | mass exchange parameters between suspended layer, surface layer and anchor ice | | | |
| | probablity of deposition of frazil particles reaching the surface layer for open water | theta0 | 1 | |
| | probablity of deposition of frazil particles reaching the surface layer under ice cover | theta1 | 1 | |
| | coefficient quantifying the rate of re-entrainment of surface ice into suspension per unit area | beta1 | 0 | |
| | average rise velocity of frazil ice in turbulent river flow | vcc | 0.001 | m/s |
| | initial thickness of frazil part of ice floes | hf0 | 0.01 | m |
| | maximum concentration of frazil ice parcel from suspended layer to surface layer | anmaxfra | 0.9 | |
| | minimum concentration for frazil ice parcel from suspended layer to surface layer | anminfra | 0.0001 | |
| | porosity of frazil ice | ef | 0.4 | |

| Input File | Input Parameter | Abreviation | Default Value | Unit |
|----------------------------|--|--------------------|----------------------|-------------------|
| Physical Parameters | supercooling parameters | | | |
| .par | Nusselt number | vnu | 4 | |
| | length of a-axis of frazil crystal | df | 0.002 | m |
| | frazil crystal thickness | de | 0.0003 | m |
| | nucleation temperature | tun | 0 | C |
| | initial surface ice concentration | ca0 | 0.0001 | |
| | initial suspended frazil concentration | cv0 | 0.00001 | |
| | thermal conductivity between water and suspended frazil | xkwp | 0.56594 | W/m/C |
| | anchor ice formation parameters | | | |
| | porosity of anchor ice | poran | 0.4 | |
| | coefficient quantifying the rate of accretion to the bed per unit area | gama | 0.001 | |
| | initial anchor ice thickness | han0 | 0.001 | m |
| | density of bed material | rob | 2650 | kg/m ³ |
| | maximum anchor ice concentration | anmaxanchor | 0.8 | |
| | undercover transport parameters | | | |
| | nominal diameter of ice particles | unpsize | 0.01 | m |
| | critical flow strength below which there is no ice transport | unthetac | 0.041 | m/s |
| | maximum concentration of undercover load | unmaxanp | 0.6 | |
| | the ratio of undercover load transportation velocity to flow velocity | unalphav | 1 | |
| | hydrodynamic parameters | | | |
| | minimum water depth | htmin | 0.5 | m |
| | ice cover formation parameters | | | |
| | ice parcel stoppage criterion | stp _v | 0 | m/s |
| | critical froude number for ice parcel to submerge | crifr | 0.09 | |
| | erosion velocity of ice parcels | ueros | 1.5 | m/s |
| | critical velocity for freezeing calculations | vcrfrz | 0 | m/s |

Appendix B : Ice Jam Profile Predictor Error Results

The difference between the rating curves and the modeled top of ice profiles in the East Channel.

| Discharge | Difference Between the Rating Curve and the Modeled Top of Ice Elevation at output river kilometers (m) | | | | | | | | | | | | |
|-----------|---|--------|--------|--------|--------|--------|--------|--------|--------|--------|--------|--------|--------|
| | 1107.5 | 1108.0 | 1108.5 | 1109.0 | 1109.5 | 1110.0 | 1110.5 | 1111.0 | 1111.5 | 1112.0 | 1112.5 | 1113.0 | 1113.5 |
| 900 | -0.21 | -0.31 | -0.28 | -0.25 | -0.16 | -0.06 | 0.05 | 0.00 | -0.77 | -0.25 | 0.15 | -0.79 | -0.75 |
| 900 | 0.75 | 0.86 | 0.82 | 0.77 | 0.67 | 0.52 | 0.39 | 0.14 | -1.36 | -1.15 | -0.54 | -0.41 | -0.47 |
| 605 | 0.05 | 0.05 | -0.01 | -0.09 | -0.24 | -0.62 | -1.26 | -1.82 | -0.94 | -0.62 | -0.48 | -0.41 | -0.38 |
| 670 | -0.68 | -0.75 | -0.75 | -0.78 | -0.77 | -0.77 | -0.72 | 0.23 | 1.21 | -0.36 | -0.18 | -0.18 | -0.31 |
| 560 | -0.22 | -0.27 | -0.25 | -0.25 | -0.21 | -0.14 | -0.01 | 0.07 | -0.60 | -0.32 | -0.25 | -0.19 | -0.14 |
| 1000 | 0.52 | 0.61 | 0.61 | 0.62 | 0.60 | 0.61 | 0.65 | 0.43 | 1.60 | 1.49 | -0.54 | -0.24 | -0.13 |
| 500 | -0.22 | -0.15 | -0.17 | -0.16 | -0.22 | -0.15 | -0.11 | 1.16 | -0.11 | 0.07 | -0.02 | -0.01 | -0.07 |
| 500 | 0.87 | 0.82 | 0.76 | 0.74 | 0.66 | 0.59 | 0.59 | -0.19 | -0.10 | 0.11 | 0.06 | 0.03 | -0.02 |
| 268 | 0.02 | 0.07 | 0.14 | 0.19 | 0.32 | 0.46 | 0.65 | 0.18 | 0.71 | 0.72 | 0.31 | 0.30 | 0.39 |
| 900 | -0.72 | -0.67 | -0.64 | -0.61 | -0.53 | -0.43 | -0.34 | -0.30 | 0.63 | 0.02 | 0.62 | 0.84 | 0.88 |
| 893 | -0.16 | -0.26 | -0.22 | -0.18 | -0.12 | -0.01 | 0.10 | 0.11 | -0.27 | 0.30 | 0.89 | 1.05 | 1.00 |

The difference between the rating curves and the modeled top of ice profiles in the West Channel.

| Discharge | Difference Between the Rating Curve and the Modeled Top of Ice Elevation at output river distances (m) | | | | | | | | | | |
|-----------|--|-------|--------|-------|--------|-------|--------|-------|--------|-------|--------|
| | 1107.5 | 1108 | 1108.5 | 1109 | 1109.5 | 1110 | 1110.5 | 1111 | 1111.5 | 1112 | 1112.5 |
| 670 | -0.68 | -0.75 | -0.60 | -0.63 | -0.64 | -0.49 | -0.50 | -0.45 | -0.16 | -0.05 | -0.91 |
| 900 | -0.72 | -0.67 | -0.37 | -0.38 | -0.39 | -0.50 | -0.54 | -0.57 | -0.40 | 0.08 | -0.61 |
| 900 | -0.21 | -0.31 | -0.16 | -0.19 | -0.22 | -0.35 | -0.40 | -0.46 | -0.31 | -1.13 | -0.52 |
| 560 | -0.22 | -0.27 | -0.18 | -0.22 | -0.24 | 0.03 | 0.01 | -0.01 | -0.08 | -0.25 | -0.49 |
| 605 | 0.05 | 0.05 | -0.39 | -0.45 | -0.50 | -0.30 | -0.37 | -0.44 | -0.50 | -0.37 | -0.49 |
| 500 | -0.22 | -0.15 | -0.14 | -0.13 | -0.14 | 0.22 | 0.21 | 0.21 | 0.24 | 0.52 | -0.38 |
| 268 | 0.02 | 0.07 | 0.12 | 0.19 | 0.26 | -0.48 | -0.45 | -0.37 | -0.31 | -0.34 | 0.31 |
| 893 | -0.16 | -0.26 | -0.01 | 0.07 | 0.14 | 0.14 | 0.26 | 0.35 | 0.23 | 0.24 | 0.42 |
| 900 | 0.75 | 0.86 | 0.73 | 0.67 | 0.64 | 0.46 | 0.35 | 0.09 | -0.93 | -0.29 | 0.45 |
| 1000 | 0.52 | 0.61 | 0.21 | 0.29 | 0.34 | 0.20 | 0.31 | 0.56 | 1.15 | 0.84 | 0.83 |
| 500 | 0.87 | 0.82 | 0.78 | 0.77 | 0.75 | 1.07 | 1.11 | 1.11 | 1.06 | 0.73 | 1.39 |